



POLITECNICO DI TORINO  
DAUIN - Dipartimento di Automatica e Informatica  
Collegio di Ingegneria Informatica, del Cinema e Meccatronica

**A flexible demonstrator composed of  
a printed integrated circuit based on OFETs,  
a flexible battery and an electrochromic display,  
as a precursor of a fully-printed  
smart label for metered-dose inhalers**

by

*Ariel Esteban Seisdedos Alvarado*

Thesis submitted as one of the requirements to qualify  
for the Master of Science in Mechatronic Engineering

*Supervisors :* Prof. Maurizio Martina  
Prof. Marcello Chiaberge

July, 2019  
*Turin, Italy*

*A mi familia*

# Abstract

Printed electronics is a promising candidate to seamlessly integrate electronics in everyday devices, with low-cost achievement. Despite the current limitations of printed logic circuits, they are now ready for low-end applications such as smart labels. This is particularly interesting in the metered-dose inhalers market, in order to compete with all-plastic mechanical dose counting mechanisms. In this context, a demonstrator composed of (1) a fully-printed organic four-bit complementary-logic counter manufactured at Istituto Italiano di Tecnologia, (2) an electrochromic display provided by RISE Acreo, and (3) a printed battery from Imprint Energy was developed. Additionally, a rigid non-form-factor board was designed in order to test the printed circuits, which allows to make them work down to 3 V. It also incorporates an NFC, to show how these technologies can be merged with off-the-shelf connectivity devices. Both the non-form-factor and the flexible boards worked as expected, and some printed counters showed correct operation at 3 V supply voltage.

# Preface

This thesis is an original work by the author, A. Seisdedos. However, this research is part of a multidisciplinary project, which involves:

- Flex Milan.
- Printed and Molecular Electronics team (PME), Istituto Italiano di Tecnologia (IIT).
- To a certain extent, RISE Acreo and Imprint Energy.

The author actively contributed to the development of this project during an internship at Flex Milan, from October 2018 to June 2019. Therefore, some of the information available to the author is classified as Company Confidential, and was not published. Every reference to a Company Confidential document is stated as such within this thesis.

# Acknowledgements

Quisiera agradecer a todas las personas que fueron parte del proceso de desarrollar una tesis en el extranjero. ¡Pero es que son tantas! Si describiera la importancia de cada una sería demasiado largo, por lo que convenientemente las resumiré en tres grupos:

1. Todo el equipo de Flex Milano, particularmente a los teams de HR y NPI, y a quienes aportaron directamente para el proyecto: Tommaso Borghi, Marco Ferrari, Ennio Bandera, Emanuele Pozzi, Fabio Bragonzi y Ruben Gandus. Desde el lado IIT, agradecimientos especiales a Paolo Colpani y Giorgio dell'Erba.
2. A mis amigos en Torino y Milano, quienes fueron cruciales durante mi estadía en Italia, y se convirtieron en mi familia provisoria. Nuevamente, aquí hay muchos nombres, y para no dejar fuera a nadie, ¡prefiero no nombrar explícitamente a ninguno!
3. A mi familia, polola, y amigos en Chile, quienes siempre acogieron de buena forma mi decisión de participar en el programa de doble título, y me apoyaron desde la distancia. Ha sido un periodo largo, pero cada día se acerca más el momento en que nos reencontraremos.

# Contents

Acronyms . . . . .	vii
Glossary . . . . .	viii
List of Figures . . . . .	ix
List of Tables . . . . .	xi
<b>1 Introduction</b>	<b>1</b>
1.1 Why smart data labels for inhalers? . . . . .	1
1.2 Why printed electronics? . . . . .	3
1.3 Current phase goals . . . . .	5
<b>2 Flexible electronics</b>	<b>7</b>
2.1 Overview . . . . .	7
2.2 Batteries . . . . .	8
2.3 Displays . . . . .	12
2.3.1 Thermochromic displays . . . . .	12
2.3.2 Electrochromic displays . . . . .	13
2.4 Transistors and logic circuits . . . . .	15
2.4.1 Complementary logic circuits at PME - IIT . . . . .	17
<b>3 SDL project: initial state</b>	<b>20</b>
3.1 Design review . . . . .	21
3.1.1 Board schematics . . . . .	21
3.1.2 PCB layout . . . . .	24
3.2 Current measurement tests . . . . .	25
<b>4 Non-form factor board design</b>	<b>28</b>
4.1 Requirements . . . . .	28
4.1.1 Mandatory . . . . .	28
4.1.2 Desirable features . . . . .	28
4.2 Design process . . . . .	29
4.2.1 Components benchmark . . . . .	29
4.2.2 Schematics . . . . .	34
4.2.3 PCB layout . . . . .	36
4.2.4 Firmware . . . . .	37

<b>5</b>	<b>NFF board characterization</b>	<b>40</b>
5.1	Electrochromic display . . . . .	40
5.1.1	RISE Acreo . . . . .	40
5.1.2	Ynvisible . . . . .	41
5.1.3	ECD Comparison . . . . .	41
5.1.4	Custom display . . . . .	41
5.2	NFF board . . . . .	43
5.2.1	Power budget . . . . .	43
5.2.2	Initial tests . . . . .	46
5.2.3	Tests with previous 2-bit printed counter . . . . .	47
5.2.4	Tests with new 4-bit printed counter . . . . .	48
5.2.5	Oscillator output . . . . .	49
5.2.6	Digital potentiometers . . . . .	50
5.2.7	NFC . . . . .	50
5.3	Flexible battery . . . . .	54
5.3.1	Current extracted from the battery . . . . .	55
<b>6</b>	<b>Flexible board</b>	<b>58</b>
6.1	Implications of the NFF tests . . . . .	58
6.2	Design process . . . . .	59
6.2.1	Design decisions . . . . .	59
6.2.2	Schematic . . . . .	60
6.2.3	PCB layout . . . . .	61
6.2.4	Demonstrator Showcase . . . . .	62
6.3	Testing and results . . . . .	62
<b>7</b>	<b>Conclusion and remarks</b>	<b>66</b>
	<b>Bibliography</b>	<b>69</b>
	<b>Datasheets</b>	<b>73</b>
	<b>News and other online resources</b>	<b>75</b>
<b>A</b>	<b>NFF main schematic</b>	<b>77</b>
<b>B</b>	<b>FPC schematic</b>	<b>84</b>
	<b>Index</b>	<b>90</b>

# Acronyms

- a-Si** amorphous silicon.
- ADC** analog-to-digital converter.
- BLE** Bluetooth low-energy.
- CVD** chemical vapor deposition.
- ECD** electrochromic display.
- EPD** electrophoretic display.
- FDA** Food and Drug Administration.
- FHE** flexible-hybrid electronics.
- FPC** flexible printed circuit.
- GPIO** general purpose input/output.
- I2C** inter-integrated circuit.
- IC** integrated circuit.
- IDE** integrated development environment.
- IIT** Istituto Italiano di Tecnologia.
- ILO** internal low-speed oscillator.
- IME** in-mold electronics.
- IoT** Internet of Things.
- LED** light emitting diode.
- LIB** lithium-ion battery.
- LiPo** lithium-polymer.
- LTPS** low-temperature polycrystalline silicon.
- MCU** microcontroller unit.

**MDI** metered-dose inhaler.

**NDEF** NFC Data Exchange Format.

**NFC** near field communication.

**NFF** non-form factor.

**NTAG** NFC tag.

**OEET** organic electrochemical transistor.

**OFET** organic field-effect transistor.

**OLED** organic light-emitting diode.

**OTFT** organic thin-film transistor.

**PCB** printed circuit board.

**PDPS** printed dopant polysilicon.

**PEC** printed electronic circuit.

**PEDOT** poly(3,4-ethylenedioxythiophene).

**PFM** pulse-frequency-modulation.

**PME** Printed and Molecular Electronics.

**POR** power on reset.

**PSoC** programmable system-on-chip<sup>®</sup>.

**PSS** poly(styrene sulfonic acid).

**R2R** roll-to-roll.

**RF** radio frequency.

**RFID** radio-frequency identification.

**S2S** sheet-to-sheet.

**SDL** Smart Data Label.

**TCD** thermochromic display.

**TFT** thin-film transistor.

# Glossary

**Electrochromic display** Display based on the color-changing property of some materials when they experiment REDOX reactions.

**Electrophoretic display** Display based on the displacement of electrically-charged pigments. Widely used in electronic paper applications.

**Flexible-hybrid electronics** Refers to boards composed of one or more silicon-based chips, mounted on a flexible polymer substrate which contains the required electrical connections.

**In-mold electronics** A process consisting on printing conductive inks into 2D surfaces, and then molding them to form custom 3D shapes.

**Poly(3,4-ethylenedioxythiophene)** A conductive polymer widely used in printed electronics research and applications, due to its versatility.

**Poly(styrene sulfonic acid)** A polymer used to increase PEDOT solubility by combining both materials to form PEDOT:PSS.

**Programmable system-on-chip<sup>®</sup>** A family of microcontroller integrated circuits, by Cypress semiconductors.

**Thermochromic display** Display based on the color change of some materials, due to temperature variations.

# List of Figures

1.1	MDIs with counters . . . . .	2
1.2	Smart Data Label project concept . . . . .	3
1.3	FleX™ Silicon-on-Polymer™ . . . . .	4
1.4	Flexible Arduino, NextFlex . . . . .	4
2.1	Printing techniques . . . . .	8
2.2	Lithium-ion battery diagram (example) . . . . .	9
2.3	Energy density comparison for different flexible battery technologies . . . . .	9
2.4	Batteries with novel form factors . . . . .	10
2.5	Typical layered architecture of thin-film batteries . . . . .	10
2.6	Some flexible batteries on the market . . . . .	12
2.7	7-segment thermochromic display (TCD) . . . . .	13
2.8	Thermochromic displays and applications . . . . .	14
2.9	Electrochromic device structure . . . . .	14
2.10	A matrix addressable electrochromic display . . . . .	15
2.11	ECD examples . . . . .	15
2.12	Organic field-effect carrier mobility values over time . . . . .	16
2.13	Flexible ICs benchmark . . . . .	18
2.14	IIT manufacturing diagram . . . . .	18
2.15	D flip-flop at IIT . . . . .	19
3.1	Initial prototype . . . . .	20
3.2	Initial printed circuit . . . . .	21
3.3	Board Block Diagram . . . . .	22
3.4	LT1615 Block Diagram . . . . .	22
3.5	Schmitt trigger configuration . . . . .	23
3.6	Main board layout . . . . .	25
3.7	Breakout board layout . . . . .	25
3.8	Current consumption distribution . . . . .	26
4.1	TPS61096A block diagram . . . . .	32
4.2	MAX17220 block diagram . . . . .	33
4.3	NFF Board Block Diagram . . . . .	35
4.4	NFF Board Power Diagram . . . . .	35
4.5	NFF Main Board Layout . . . . .	37
4.6	NFF Breakout Board Layout . . . . .	38

4.7	Firmware Block Diagram . . . . .	39
5.1	Electrochromic display samples . . . . .	40
5.2	RISE Acreo display design layout . . . . .	42
5.3	Acreo display: custom version . . . . .	43
5.4	NFF board with previous printed circuit . . . . .	47
5.5	NFF board with new 4-bits counter . . . . .	48
5.6	Oscillator output . . . . .	49
5.7	NFC matching network schematic . . . . .	51
5.8	NFC resonance frequency . . . . .	52
5.9	NTAG I2C Demo app . . . . .	53
5.10	Flexible battery from Imprint Energy . . . . .	54
5.11	Startup current . . . . .	55
5.12	Deep sleep current . . . . .	56
5.13	ECD update current . . . . .	57
6.1	Flexible board Block diagram . . . . .	61
6.2	Flexible board layout . . . . .	62
6.3	Demonstrator showcase . . . . .	62
6.4	Vias in pad . . . . .	63
6.5	Delaminated display . . . . .	64
6.6	Flexible demonstrator . . . . .	65

# List of Tables

4.1	Components' current consumption . . . . .	31
4.2	Digital potentiometers' consumption . . . . .	34
5.1	ECD comparison . . . . .	42
5.2	Power budget, worst case scenario . . . . .	45
5.3	Power budget, more realistic scenario . . . . .	46
5.4	Internal capacitance of the NFC . . . . .	51

# Chapter 1

## Introduction

The Smart Data Label (SDL) is an R&D project born at Flex Milan, and developed in collaboration with the Printed and Molecular Electronics (PME) team of Istituto Italiano di Tecnologia (IIT). Its aim is to design a fully-printed smart label for displaying the remaining doses inside an metered-dose inhaler (MDI), as an alternative to mechanical dose counters.

In the first phase of the project, which ended on May 2018, the PME team designed a printed electronic circuit (PEC) composed of two 2-bit counters, while Flex developed a rigid printed circuit board (PCB) for testing it. Now, in this second phase, a flexible demonstrator was designed and successfully tested.

This chapter describes the importance of counting mechanisms for inhalers, why printed electronics is a promising candidate to tackle the development of smart labels, and ends with the objectives that were set for this phase of the project.

### 1.1 Why smart data labels for inhalers?

A metered-dose inhaler is a device intended for delivering medicine to a patient through inhalation. They have been available on the market for nearly 60 years, and are now an important delivery method for drugs which treat obstructive airway diseases. Nowadays, MDIs are produced in tens of millions of units, as more and more patients around the globe rely on them during asthma attacks.

Many of these devices don't have counting mechanisms and often patients must perform unreliable methods to check the filling status of their devices (e.g. shaking, weigh inspection, or usage of notes). Moreover, MDIs usually contain more medicine than what is strictly required to expel the indicated number of actuations. For instance, an MDI labelled to deliver 120 doses may seem to be working for 20 additional actuations, while delivering a lesser amount of drug per spray [1].

A study published in the July 2006 volume of the "Annals of Allergy, Asthma and Immunology", found that 25% of the people who used bronchodilators (a common type of MDI) had reached their MDI during an acute asthmatic episode only to find that it was empty. In 2003, the Food and Drug Administration (FDA) released a guidance [2] that provides some general indications on how to address this issue. Even though following this guidance is not mandatory, it provides useful hints on how the next generation devices should be designed.



Figure 1.1: MDIs with counters.

Available at <sup>a</sup>EMC Mobi, <sup>b</sup>Presspart, <sup>c</sup>Aptar pharma, <sup>d</sup>iMedicalApps.

All the images are property of their respective owners.

A confidential report at Flex [1] summarizes said guidance in three main ideas (textual):

1. Dose counters should provide, either through a direct numeric count or colour coding, a clear indication when an MDI is approaching the end of its recommended number of actuations, as well as when it has reached or exceeded that number.
2. Dose counters should be engineered to reliably track actuations and should be designed to be as close to 100 percent reliable as possible. However, if some low frequency of error is unavoidable, the device should be designed to specifically avoid undercounting.
3. A lock-out mechanism to prevent doses beyond the labelled number of actuations would be an optional feature of dose counters.

After its release, some devices with incorporated dose-counting systems, both using fully-mechanical and electro-mechanical approaches, started to appear on the market (figure 1.1). While the fully-mechanical designs proved to be simple and cheap, in the two-thousands a number of patents were issued, which started to represent an entry barrier for new players: digital counters started to be used instead.

The presence of digital counters makes easier to expand the functionality of the inhaler, adding, for instance, logging capabilities or reminders (figure 1.1d). Nevertheless, using off-the-shelf electronics requires, at least, the following components:

- A printed circuit board or flexible printed circuit
- A microcontroller
- A display
- A battery

Each of the above items contributes to the size of the final device, which is crucial since it may compromise its usability, especially for patients with limited dexterity.

Moreover, the all-plastic mechanical counters are clearly cheaper than the digital ones, which sets a target cost that is very hard to achieve with conventional electronics.

In fact, some digital counters on the market are put in the main body of the inhaler, and are intended to be used with more than one canister (the disposable part of the inhaler), in order to make it a competitive alternative to mechanical solutions. In this context, Flex proposed the presence of a smart label pasted on the canister itself (see figure 1.2), which would have several advantages [1]:

- Each canister would have its own counting mechanism, inseparable from the drug canister. This avoids the usage of different canisters with the same counter.
- Due to its intrinsically thin form factor, the increase in size would be almost negligible.
- Would allow to easily migrate from a traditional inhaler to a dose counting one, just by replacing the canister.
- Combined with proper printed indications, the display mechanism can be very easy to understand.

This gave birth to Smart Data Label, an internal R&D project. In order to accomplish the ultimate objective, flexible electronic technologies need to be investigated, so Flex partnered with IIT for this purpose.

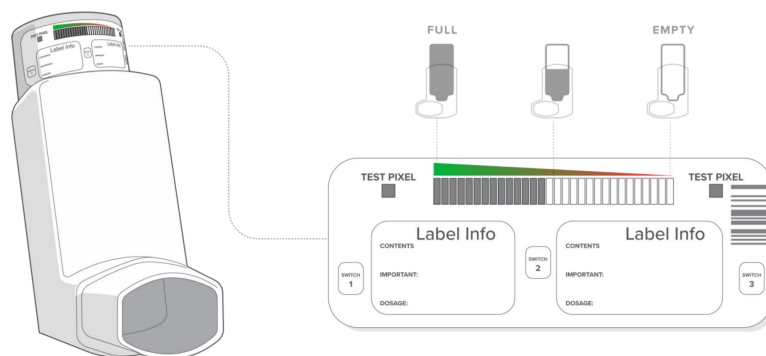


Figure 1.2: Smart Data Label project concept.

## 1.2 Why printed electronics?

Printed electronics refers to a set of technologies aimed to print electronic components, born as a combination of different engineering disciplines: from chemistry and material sciences to solid-state physics. To the date, a number of devices have been successfully developed: displays, transistors, batteries, radio-frequency identification (RFID) devices, and sensors, some of which are going to be detailed in the next chapter.

In the previous section, we already established there's a niche on *flexible* technologies for integration of intelligence into smart labels. As a matter of fact, *printed* electronics is a subset of flexible electronics, so here the particular advantages of printed electronics with respect to other solutions are exposed (in particular, concerning logic circuits).

In the first place, one could think about using a flexible-hybrid electronics (FHE) board. However, by definition, an FHE still has rigid components over the board, which could make it difficult to integrate in a printed label (depending on their size). And also, the cost of silicon components may be just too high.

In order to solve the rigidity problem, some have tackled it by modifying the silicon process (specifically the thickness of the wafers) to be flexible. For instance, American Semiconductors has recently manufactured flexible silicon circuits [62]: their so-called FleX™ Silicon-on-Polymer™ (figure 1.3).

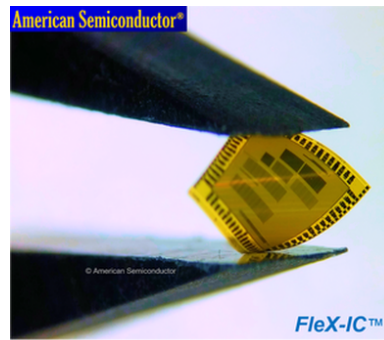


Figure 1.3: FleX™ Silicon-on-Polymer™. Property of [American Semiconductors](#).

Similarly, NextFlex<sup>1</sup> developed the so called Flexible Arduino prototype (figure 1.4), which was produced by directly attaching the thin bare die on the flexible substrate. With respect to conventional electronics, the amount of process steps was reduced by almost two-thirds [63].

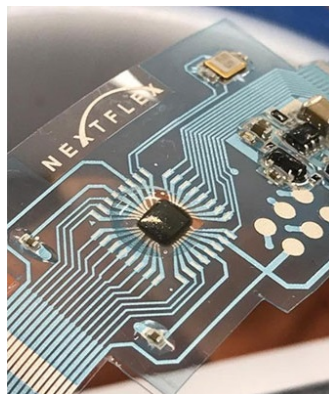


Figure 1.4: Flexible Arduino. Property of [NextFlex](#).

The above mentioned technologies are likely to be successful and become a suitable option for flexible electronics applications, as no significant performance reduction has

<sup>1</sup>A consortium, of which Flex is part.

been observed with respect to standard integrated circuits (ICs). But the result is always a silicon-based chip, which process involves wafer manufacturing and high-resolution deposition and lithography. This makes them inherently expensive.

On the other side, printed electronics logical circuits are much less mature than conventional silicon solutions, and their performance can hardly be compared (at least for now). But, for simple applications (such as counting events), they have proven to be enough, and they promise a highly scalable cost. After all, the marginal cost of a device would basically be the cost of the conductive inks and the encapsulation material.

Furthermore, knowledge in printed electronics allows not only to replace a microcontroller by a flexible version, but also to print other components, that can be shape-customized for each application (for instance, batteries and displays with personalized designs, merging the electronic and visual design phases)<sup>2</sup>. In the future, it may be possible to integrate a fully-printed system into a single manufacturing process (composed, obviously, of several printing steps), reducing even more the cost of a smart label.

Finally, investing in printed electronics research is also an opportunity for Flex to acquire the know-how to develop other medical products<sup>3</sup>, such as skin patches or textile electronics, or adding intelligence to all sort of product labels. The development of digital PECs is precisely the missing stone required to build fully-printed applications.

### 1.3 Current phase goals

The (confidential) report that closed the first phase of the project [3] concluded three possible short-term improvements:

- Device yield and operating voltage can be improved by a better control of dielectric deposition.
- Flexible barriers can be used to encapsulate the final device.
- A flexible fixture can be designed to show the counter behaviour in air during bending.

Based on the former as guidelines, the goals that were set up for the current phase of the project were:

- Integrate the prototype into a single flexible printed circuit (FPC), using:
  - Flexible batteries.
  - A flexible display.
  - An updated 4-bit version of the printed electronic counter, using flexible encapsulation.

---

<sup>2</sup>In fact, Flex has already customized electrochromic displays.

<sup>3</sup>The Milan design center is focused on biomedical applications.

- In particular, the PEC shall contain not only the counter itself, but also an oscillator, and ideally should work at 3 V<sup>4</sup>.
- Desirable features should be evaluated:
  - Variable supply voltage of the printed electronic circuit, through a digital potentiometer.
  - Addition of near field communication (NFC) technologies, and possibly energy harvesting integration.

The author of this thesis was the main developer of this phase, from the Flex side.

---

<sup>4</sup>In the previous phase of the project, the counters were tested from 6 V.

## Chapter 2

# Flexible electronics

### 2.1 Overview

With the synthesis of conductive polymers in the second half of the twentieth century [4], different possibilities started to open for electronic devices. Even though the development process has been complex and long, flexible electronics applications are now becoming a reality:

- In the medical sector, wearables and monitoring skin patches are starting to use flexible electronics. For instance, Blue Spark created TempTraq<sup>®</sup>, which incorporates a temperature sensor, a Bluetooth module and a printed zinc-carbon battery, especially designed for temperature monitoring of babies and children [64].
- Concerning retail products, flexible electronics (and, in particular, electronic textiles or e-textiles) will enable intelligence incorporation in clothes. For example, NFC-enabled jackets have been on the market for a couple of years [65], and Loomia already released a self-heating jacket on March 2019 [66].
- Printed electronics is particularly attractive for novel packaging and transport or cold-chain monitoring. Smart labels with integrated WiFi connectivity could apply the Internet of Things (IoT) concept to a whole new level<sup>1</sup>. Some examples of smart labels are Ynvisible's Integrity Smart Label<sup>2</sup>, or the smart wine bottle recently presented by American Semiconductors [67].
- In the automotive sector, original user interfaces can be designed. Moreover, textile electronics could allow the incorporation of pressure sensors or heaters in the seats, while in-mold electronics (IME) makes possible to embed electronics in 3D surfaces (for instance, the center console).
- Even Airbus has identified potential in the aviation industry and presented a demo at the LOPEC 2019 conference<sup>3</sup>. Printed electronics allows to customize the furnishings and cabin, which is hard to do for aircraft manufacturers since they provide aircrafts to different aviation companies [68].

---

<sup>1</sup>The so-called "Internet of Everything".

<sup>2</sup>[https://www.cm-equity.de/wp-content/uploads/20171004\\_Ynvisible\\_CM-Equity\\_Presentation.pdf](https://www.cm-equity.de/wp-content/uploads/20171004_Ynvisible_CM-Equity_Presentation.pdf)

<sup>3</sup>The annual trade fair and conference for printed electronics, which was held in Munich, and in which the author was fortunately able to participate.

Regarding the materials used, in the past decade poly(3,4-ethylenedioxythiophene) (PEDOT) has been widely investigated. Its main advantage is the versatility, which directly leads to lower manufacturing costs: it can serve as a dielectric material, conductive traces, or n-type and p-type semiconductor, depending on doping. Even electrochromism have been exploited (details in section 2.3.2). Moreover, combined with poly(styrene sulfonic acid) (PSS), its solubility is high enough to produce inks that are compatible with conventional printing processes.

Printed electronics is a particular case of flexible electronics. Different printing techniques have been studied in the past years (figure 2.1). A number of flexible electronic components are manufactured by screen, flexographic, gravure or inkjet printing. The printing process may be roll-to-roll (R2R) or sheet-to-sheet (S2S). The former is done by rotation of rollers, and this allows more continuous operation and scalable production. On the other hand, S2S processes are more suitable at prototyping or laboratory scales.

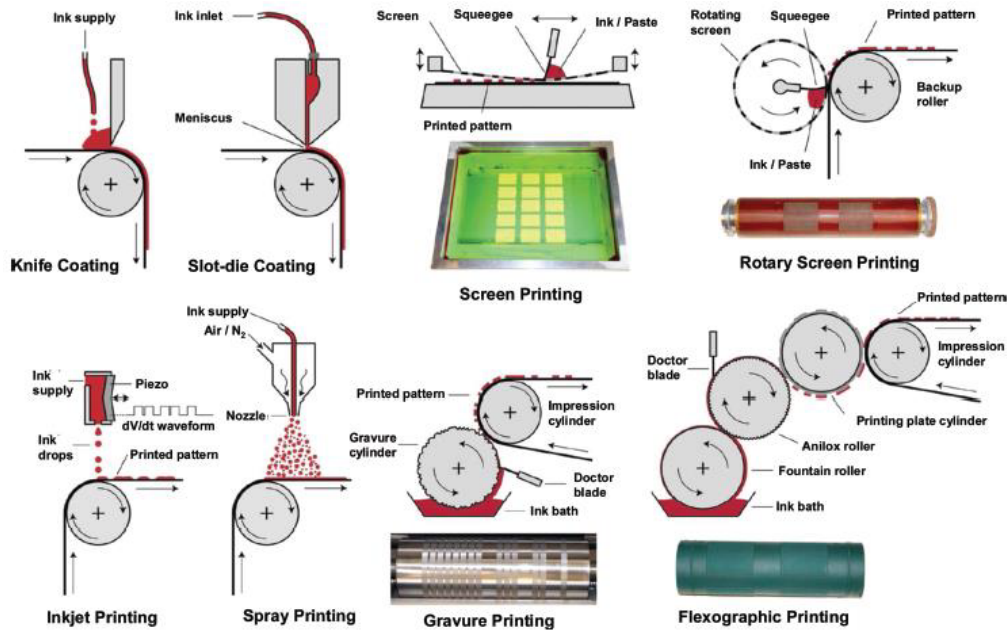


Figure 2.1: Printing techniques. Source: [5].

## 2.2 Batteries

If flexible electronics technologies are to become the commercial success they have promised, efficient power sources need to be incorporated. These could consist on supercapacitors and/or batteries. The first rely on electrostatics and, as such, are able to deliver high current peaks, but their self-discharge performance can be poor. Hence, this section will focus on battery alternatives.

Batteries rely on REDOX reactions to store energy. They are composed of electrodes (anode and cathode), and an electrolyte for ion conductivity between the two. Practical applications also require current collectors (for instance, metal foils) to get the most

out of the electrodes (figure 2.2). Primary cells are single-use, while secondary cells are rechargeable. Flexible batteries contain the very same components, but arranged in a different manner or using novel materials, to achieve new form factors.

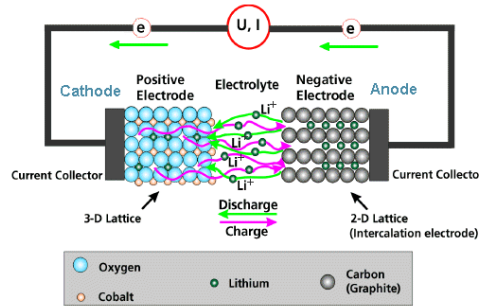


Figure 2.2: Lithium-ion battery diagram (example)<sup>a</sup>.

<sup>a</sup>© H. Föll. [https://www.tf.uni-kiel.de/matwis/amat/elmat\\_en/kap\\_2/advanced/t2\\_1\\_3.html](https://www.tf.uni-kiel.de/matwis/amat/elmat_en/kap_2/advanced/t2_1_3.html)

The first natural choice is to power up a flexible system using conventional batteries, for instance, tiny (but rigid) NiMH button cells. Nevertheless, none of the available button cells on the market are in the sub-millimeter range. That's not likely to change, since the packaging leaves less and less space for the active chemistry while reducing the thickness of the cells, thus reducing their volumetric energy density.

A similar problem occurs with lithium-polymer (LiPo) pouches. Since the chemistry is sensitive to air, volatile and often toxic, the encapsulation requirements are very high, and foil barriers that add some hundreds of microns at each side of the battery need to be used [6]. This reduces the volumetric energy density when approaching the sub-millimeter thicknesses (figure 2.3). Zinc-carbon pouches also suffer from this issue.

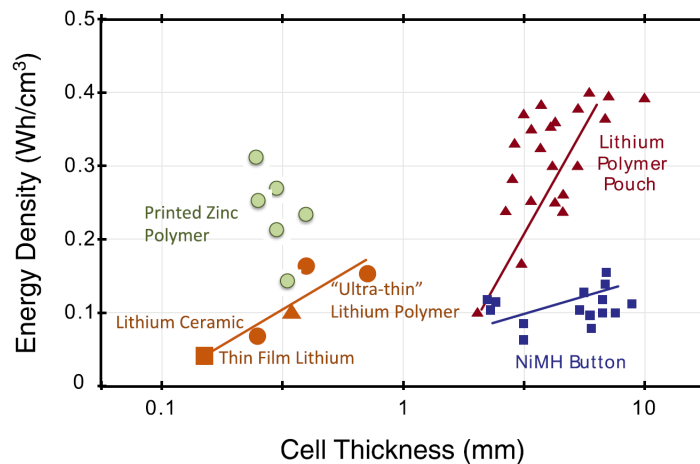


Figure 2.3: Energy density comparison for different flexible battery technologies. Source: [6].

However, some companies are commercializing pouches, such as LionRock<sup>4</sup> (figure 2.6a). Their LiPo batteries provide a rated capacity of 80 mAh with low impedance (0.26

<sup>4</sup><https://lionrockbatteries.com/product/>

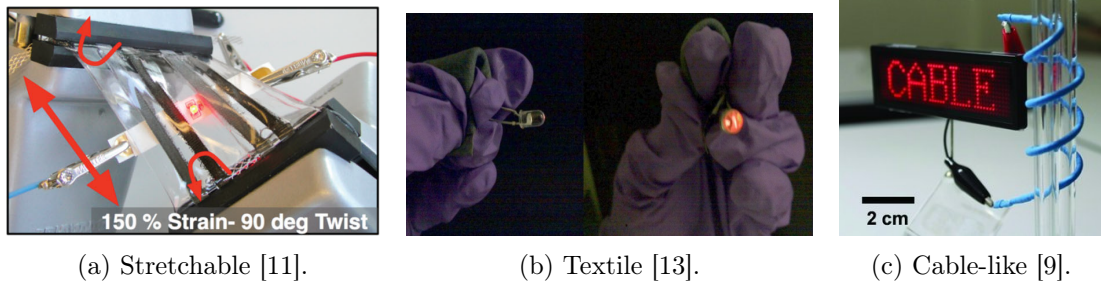


Figure 2.4: Batteries with novel form factors.

$\pm 0.1 \Omega$ ), but are still quite thick (1.35 mm). The need of novel battery technologies is crucial for truly flexible applications.

One of the first thin-film micro-batteries was produced in 1993, based on a lithium anode [7], i.e., it's a lithium-ion battery (LIB). Since then, a lot of effort has been made in improving the flexibility and performance of LIBs, mainly focusing on two approaches: new materials<sup>5</sup>, and novel cell designs [8]. The latter has led to interesting configurations, such as co-planar LIBs, or cable-like batteries [9] (figure 2.4c).

Other novel form factors or different value propositions (figure 2.4) include transparent [10], stretchable [11][12] and textile [13] batteries. Even biobatteries [14], or batteries based on nanocomposite paper [15] have already been produced (at laboratory scale). As the reader may have already noticed, flexible batteries is a huge and interesting topic<sup>6</sup>, with a high potential to revolutionize energy storage in seamlessly integrated electronics.

Having said the above, flexible batteries' classification is not simple, as many different characteristics need to be treated separately. For instance, flexibility is often related to thickness, but a thinner battery is not necessarily more flexible. Regarding manufacturing, thin-film batteries are produced by layer deposition (figure 2.5), while printed batteries can be obtained with standard printing processes. Even stencil-printing batteries which electrodes can be "painted" have already been developed [16].

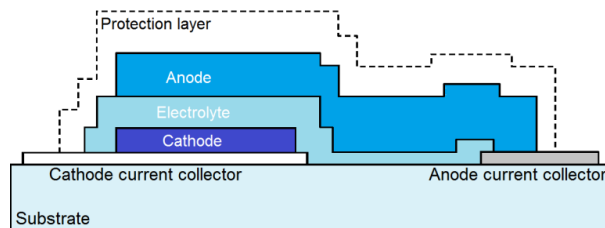


Figure 2.5: Typical layered architecture of thin-film batteries. Source: [69].

Moreover, solid-state batteries are the ones in which all the components (including the electrolyte<sup>7</sup>) are solid, and micro-batteries are intended for very low-power applica-

<sup>5</sup>Carbon nanotubes, carbon textiles and graphene derivatives have been investigated for current collectors, while polymeric substrates enhance the binding property with electrode materials [8].

<sup>6</sup>And, as such, this thesis only provides a very summarized overview.

<sup>7</sup>LIPON (lithium phosphorous oxynitride, not a polymer) is a commonly used solid-state electrolyte.

tions (micro Watts). The chemistry may be based on (just as a brief example) lithium-polymer, zinc [17], lithium glass-ceramic [18], or alkaline [19] cells. And, obviously, these are not exclusive classifications, meaning that a solid-state thin-film micro-battery could be based on lithium chemistry, using LIPON as electrolyte (for instance, the MEC202 from Thinergy [41]), with different responses to dynamic bending.

Despite the storm of different kinds of flexible batteries, further work needs to be done to improve the performance, especially to allow connectivity technologies such as Bluetooth low-energy (BLE) or WiFi, which require significant peak currents above 10 mA [6]. A possible workaround is to combine energy storage (batteries and supercapacitors) with energy harvesting, such as solar cells or thermoelectric devices. Secondary (or rechargeable) cells are necessary in order to adopt this approach.

For better-performing batteries, the nature of the electrolyte is especially important. For instance, conventional LIBs use liquid or polymer electrolytes with high ion conductivity. As a result, small series resistances (ergo, better efficiency) and higher peak currents can be got. On the other hand, solid-state electrolytes such as LIPON are less conductive, while showing better mechanical properties [8].

Some interesting companies that can be found on the market are listed below:

- BrightVolt<sup>8</sup>, has designed their own Polymer Matrix Electrolyte, which allows to produce a solid-state LiPo battery and reduce the thickness of the cell to 0.45 mm (figure 2.6b), with high reported conductivity of the electrolyte ( $1 \times 10^{-3}$  S/cm at  $-30^\circ\text{C}$ , and between  $3.3 \times 10^{-3}$  S/cm and  $4 \times 10^{-3}$  S/cm at room temperature).
- Blue Spark<sup>9</sup> (fig. 2.6d) uses a printed zinc-carbon approach. While benefiting of the advantages of printing, a drawback is that the cells are only primary (non-rechargeable). Also, the peak drain current is only about 1 mA to 2 mA (as stated in the datasheet [42]).
- SoftBattery<sup>®</sup> from Enfucell<sup>10</sup> (fig. 2.6c) also produces primary cells based on zinc-manganese dioxide chemistry (datasheet: [43]). They reach higher peak currents (up to 20 mA), but the initial internal resistance (at least  $25 \Omega$ ) may be a bit high for connectivity applications.
- Imprint Energy<sup>11</sup> has developed their ZincPoly<sup>™</sup> technology, which started by creating the "high conductivity polymer gel electrolyte" presented in [20] in 2010. The chemistry is always based on zinc-manganese oxide, but secondary cells can be produced, and current peaks of up to 45 mA have been obtained, making it a promising fully-printed candidate (figure 2.6e).

---

<sup>8</sup><https://www.brightvolt.com/our-technology/>

<sup>9</sup><https://www.bluesparktechnologies.com/>

<sup>10</sup><https://www.enfucell.com/softbattery>

<sup>11</sup><http://www.imprintenergy.com/>

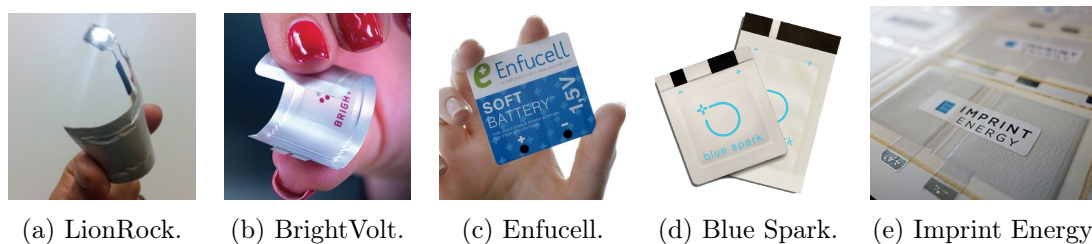


Figure 2.6: Some flexible batteries on the market.

Available at <sup>a</sup>LionRock, <sup>b</sup>Printed Electronics Now, <sup>c</sup>Printed Electronics World, <sup>d</sup>Twitter, <sup>e</sup>IoT business. All the images are property of their respective owners.

## 2.3 Displays

Regarding flexible displays, a number of different alternatives have been developed. The most commercially successful technologies in the last decade have been electrophoretic displays (EPDs) and organic light-emitting diodes (OLEDs). Flexible inorganic LEDs are under development as well [21].

The main drawback of the above technologies is that they are often "manufactured in a complex production flow [... and] there's still a huge technical barrier to carry out an entire manufacturing process using standard sheet-based or roll-to-roll printing" [22], which obviously has repercussions on the final cost. Combined with the fact that their performance is higher than what is actually required in the smart labels sector, cheaper solutions more suitable for low-end applications would be preferred.

Moreover, considering the limitations of the printed batteries, the power consumption shall be a major concern. Two low-power (order of  $100\ \mu\text{W}$  or less) technologies were identified and analyzed at Flex: TCDs and electrochromic displays (ECDs).

### 2.3.1 Thermochromic displays

#### Operating principle

Thermochromism is a property of some materials, which consists on a change of color as a function of temperature. Thermochromic materials can be inorganic or organic (either monomers or polymers), and their change in color may be either reversible or irreversible [23]. A nice feature is that they have been successfully implemented on paper [24][25].

The displays are often made by using a thermochromic composite, combined with a conductive wiring that works as resistive heater, as reported by [24]. When a voltage is applied, the Joule losses in the wiring heat up the thermochromic layer, thus modifying the resulting color.

#### Applications

Seven-segment displays were fabricated in laboratory scale at the Harvard University in 2007 [25]. Even though the dimensions were in the cm scale (figure 2.7), the study

shows the potential that these kind of technologies could bring in the future.

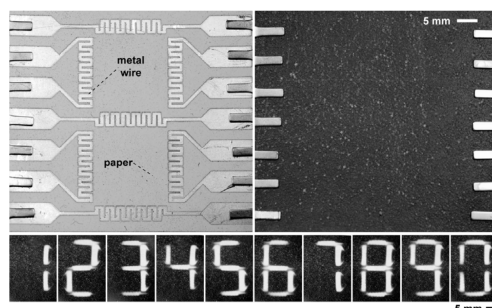


Figure 2.7: 7-segment TCD

Perhaps the most clear commercial application available nowadays is Duracell's PowerCheck™, which indicates the remaining charge in a battery using thermochromic materials<sup>12</sup>, as shown in figure 2.8b. Other applications include thermometers, foodstuff class pointers, and papers [70].

An advantage of TCDs with respect to ECDs is the wide variety of colors already available. This makes thermochromic pigments especially attractive for revolutionizing the color industry (even thermochromic nail polishes can be found in the market). Also, their driving protocol is very simple: only an on/off current is required.

### 2.3.2 Electrochromic displays

#### Operating principle

ECDs operate in a totally different manner: they're based on the property of some materials which color change when exposed to REDOX reactions. In practice, electrochromism occurs whenever a material has oxidized and reduced state with different optical absorption spectrums.

In order to fabricate a stacked ECD, three layers are required:

1. The pixel electrode or active electrochromic layer, which contains the electrochromic material.
2. The counter electrode or ion storage layer.
3. An electrolyte layer in between, which allows the flux of ions from the pixel electrode to the counter electrode and vice versa.

Figure 2.9 illustrates this internal structure. The working principle is:

1. An external voltage stimulates the displacement of the ions.
2. The presence of ions in the electrochromic layer alters the equilibrium of the REDOX reaction.

<sup>12</sup><https://www.duracell.ng/technology/get-the-most-from-duracell-batteries/>

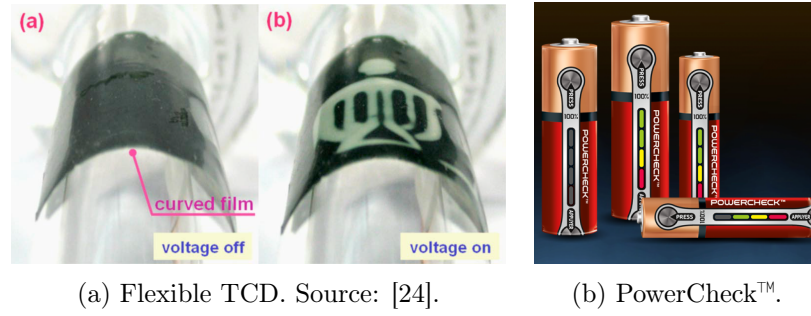
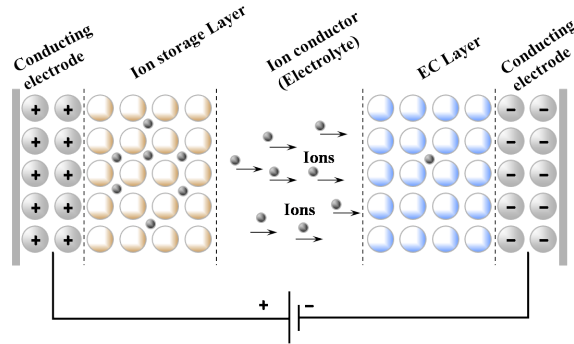


Figure 2.8: Thermochromic displays and applications.

<sup>b</sup>Property of Duracell.

- The proportions of oxidized and reduced material change, thus modifying the color of the pixel electrode.

Figure 2.9: Electrochromic device structure<sup>a</sup>.<sup>a</sup>By Keyur.tithal - Own work, CC BY-SA 3.0,<https://commons.wikimedia.org/w/index.php?curid=40874975>

### PEDOT:PSS as an electrochromic material

Early research in ECDs was mainly based in inorganic oxides (such as tungsten trioxide), or organic materials, e.g. viologen or prussian blue [26]. With the discovery of conducting polymers with different properties depending on doping agents, PEDOT:PSS started to be used as electrochromic material as well.

In the case of PEDOT:PSS, the chemical reaction involved in the process (where  $M^+$  denotes a generic ion) is [27]:



The oxidized  $\text{PEDOT}^+\text{PSS}^-$  state, or idle state, is color gray/transparent, while the reduced state color ranges from light blue to dark blue, depending on the pixel electrode thickness. Fine color tuning may be achieved by adding electrochromically inert pigments [28].

PEDOT:PSS can be processed as water dispersion using traditional printing (e.g. inkjet) and coating tools, allowing to print electrochromic displays using scalable R2R

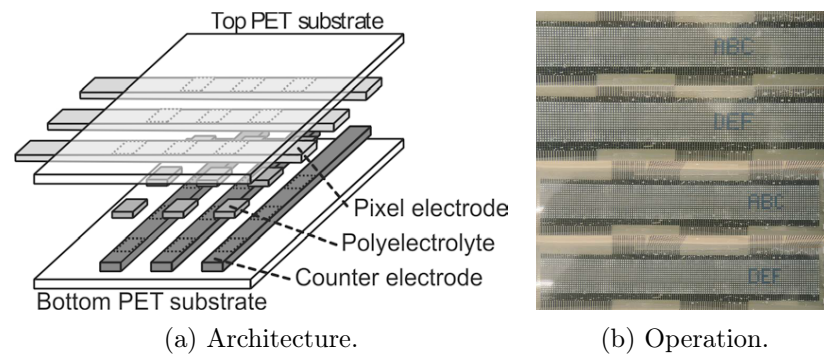


Figure 2.10: A matrix addressable electrochromic display. Source: [22].

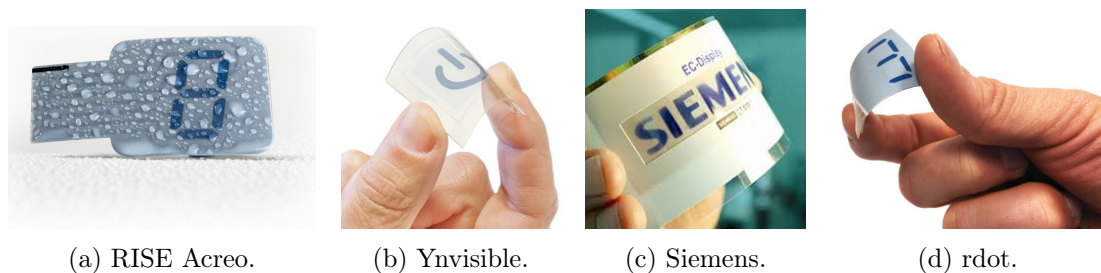


Figure 2.11: ECD examples.

Available at <sup>a</sup>[Acreo](#), <sup>b</sup>[Twitter](#), <sup>c</sup>[Researt Gate](#), <sup>d</sup>[Electronics Weekly](#).

All the images are property of their respective owners.

processes. Another key advantage is that it can also be used as counter electrode, as well as the electrical connections between different components [27], which is crucial for low-cost achievement.

### Some examples and companies of interest

In the past decade, matrix addressable displays have also been manufactured [22], by using the simple architecture shown in figure 2.10a. This particular example is a *passive* matrix (without driving transistors). It avoids crosstalk by designing displays with a given threshold, which was achieved by changing the counter electrode material.

Some companies that commercialize electrochromic displays are rdot<sup>13</sup>, RISE Acreo<sup>14</sup> or Ynvisible<sup>15</sup>. A number of other companies have invested in research projects, being able to produce their own ECDs, e.g. Siemens, RICOH, and Prelonic Technologies. Some of these displays are illustrated in figure 2.11.

## 2.4 Transistors and logic circuits

TFTs have been used for switching in liquid-crystal displays at least for three decades. The mainstream thin-film transistor (TFT) technologies available in the mar-

<sup>13</sup><https://rdotdisplays.com/>

<sup>14</sup><https://www.acreo.se/expertise/acreo-display>

<sup>15</sup><https://www.ynvisible.com/>

ket are amorphous silicon (a-Si), low-temperature polycrystalline silicon (LTPS) and amorphous metal-oxide semiconductors [29]. In 1986, Tsumura *et al.* [30] reported the first working organic field-effect transistor (OFET). Since then, organic transistors offer a huge potential for flexible electronics, despite their current limitations.

Myny [29] compares these alternatives. While LTPS transistors offer high performance (CMOS technology), their manufacturing cost is just too high to be incorporated in low-end flexible applications. On the other hand, a-Si TFTs can be produced with simpler processes, but their carrier mobility<sup>16</sup> is low (in the order of  $1 \text{ cm}^2\text{V}^{-1}\text{s}^{-1}$  [29]), and only n-type semiconductors can be obtained. Oxide semiconductors, which carrier mobility than can reach up to  $40 \text{ cm}^2\text{V}^{-1}\text{s}^{-1}$  [29]), also suffer from the lack of p-type semiconductors.

The development of flexible complementary-logic<sup>17</sup> circuits requires both n-type and p-type materials, and is therefore intrinsically tied to organic thin-film transistors (OTFTs)<sup>18</sup>: the only of the four, apart from LTPS, in which p-type semiconductors are possible. They still lack of competitive mobility with respect to LTPS, especially in the case of n-type semiconductors (see chart in figure 2.12).

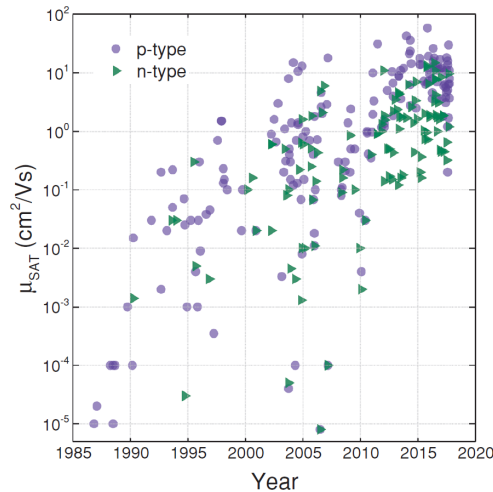


Figure 2.12: Organic field-effect carrier mobility values over time. Source: [31].

Even though OTFTs are mature enough for switching applications<sup>19</sup>, complex all-polymer digital circuits are still under development. Research on how to improve the complexity and performance (e.g. frequency of operation) of digital circuits has led to high voltage devices. For instance, in 2000, Crone *et al.* reported an 864-transistors complementary-logic organic shifting register [33]. The clock frequency went up to

<sup>16</sup>The mobility  $\mu$  is a measure of how quickly the charges can move through a semiconductor.

<sup>17</sup>The complementary-logic requirement offers advantages in power consumption and area usage (with respect to exclusively n-type or p-type logic gates).

<sup>18</sup>Or OFETs. "Thin-film" refers to the manufacturing process, while "field-effect" to the operating principle. However, in most cases the transistors are, at the same time, OTFTs and OFETs, so the two terms are often used interchangeably with each other.

<sup>19</sup>In 2007, Sony presented an all-plastic OLED display, using OTFTs, and in 2010, they even made them rollable. Part of their manufacturing process was published in [32].

1 kHz, but the operating voltage was 80 V.

In 2012, an 8-bit organic microcontroller unit (MCU) was reported [34]. Its supply voltage was quite low (10 V), but the back-gate voltage was 50 V and the frequency of operation was only 40 instructions per second. Two years later [35], the same authors showed another microcontroller, working up to 2.1 kHz at 6.5 V. However, it wasn't fully organic<sup>20</sup>, but an hybrid combination of organic p-type and soluble oxide n-type transistors.

Other approaches to design organic logic circuits include the usage of organic electrochemical transistors (OECTs) and other organic transistors (not all-solid-state), which are especially promising for biosensor applications [36]. Even though n-type OECTs are rare in the literature, complementary-logic circuits have recently been reported [37] in aqueous media. Inorganic components have also been explored in the form of 2D semiconductors with atomic scale thickness [38].

Finally, some companies of interest in flexible electronics are briefly described:

- PragmatIC<sup>21</sup> has developed flexible electronic circuits. Even though they're only based on n-type logic gates, they have reduced the scale of their circuits, developing, for instance, RFID circuits<sup>22</sup>. They are commercializing their FlexLogIC<sup>®</sup> Fab-in-a-box system, which enables quick prototyping.
- FlexEnable<sup>23</sup> started by designing single transistors for switching in flexible OLED and OLCD applications. They have now moved into smart systems as well (flexible sensors, analog and digital logic).
- ThinFilm<sup>24</sup> developed its R2R printed non-volatile ThinFilm Memory<sup>™</sup>. They are now designing flexible electronic circuits using their printed dopant polysilicon (PDPS) technology [71], for instance, NFC tags.
- Fleep Technologies<sup>25</sup> is a recently born start-up. The IIT is transferring the knowledge in organic circuits to this spin-off company. It's aiming for a fully-printed approach.

#### 2.4.1 Complementary logic circuits at PME - IIT

In 2015, Mandal *et al.* reported the first<sup>26</sup> fully-printed complementary-logic circuit (a 7-stage ring oscillator) [39], which was designed and manufactured at IIT. The stage delay was 246  $\mu$ s at 30 V, and 31  $\mu$ s at 100 V.

<sup>20</sup>The organic feature would be a plus for printing recyclable circuits.

<sup>21</sup><https://www.pragmatic.tech/>

<sup>22</sup>ConnectIC<sup>®</sup>.

[pragmatic.tech/assets/media/connectic-pragmatic-pr1101-product-brief.pdf](https://www.pragmatic.tech/assets/media/connectic-pragmatic-pr1101-product-brief.pdf)

<sup>23</sup><https://www.flexenable.com/technology/smart-systems/>

<sup>24</sup>[thinfilm-multi-kai.sfi.tytlab.com/](http://thinfilm-multi-kai.sfi.tytlab.com/)

<sup>25</sup><https://www.fleeptech.com/>

<sup>26</sup>To the authors' knowledge.

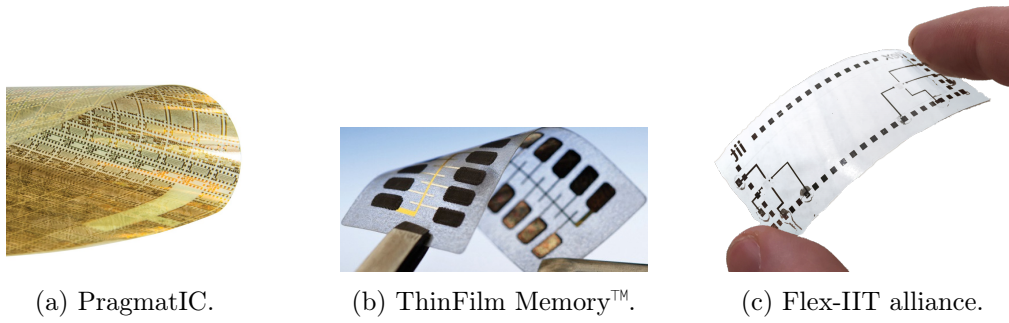


Figure 2.13: Flexible ICs benchmark.

Available at <sup>a</sup>[Electronics Weekly](#), <sup>b</sup>[ThinFilm](#). All the images are property of their respective owners.

Further research has been performed in order to reduce the operating voltage of the transistors. In particular, they developed a parylene-C based bilayer dielectric that enables not only to increase the device yield, but also to lower the supply voltage and manufacture inverters, 7-stage ring oscillators and D flip-flops that operate down to 2 V [40].

Figure 2.14 illustrates the layers of the resulting circuits. Fabrication is carried out through printed techniques (inkjet, bar coating) with the presence of a vacuum-based chemical vapor deposition (CVD) process. All the processes involved are performed at temperatures below 100 °C.

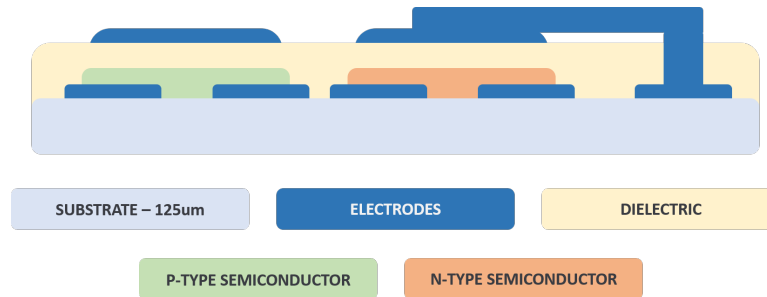


Figure 2.14: IIT manufacturing diagram.

The 2-bit counter that was tested in the first phase of the project was designed by connecting two D flip-flops in chain, that is, the output of the first one is the clock of the other<sup>27</sup>. Each D flip-flop was designed by using a pass-transistor approach (figure 2.15). The current phase of the project is an opportunity to test a slightly more complex 4-bit counter composed of four D flip-flops in chain configuration.

In this section, it has been clearly said that many different candidates for flexible and/or organic electronic circuits have been explored. The main advantages of fully-printed complementary-logic organic electronics with respect to other alternatives are:

- Printing techniques enable low-cost and scalable manufacturing, as well as highly customised layouts.

<sup>27</sup>The input of the second flip-flop is its own negated output, so that is toggles on each clock cycle.

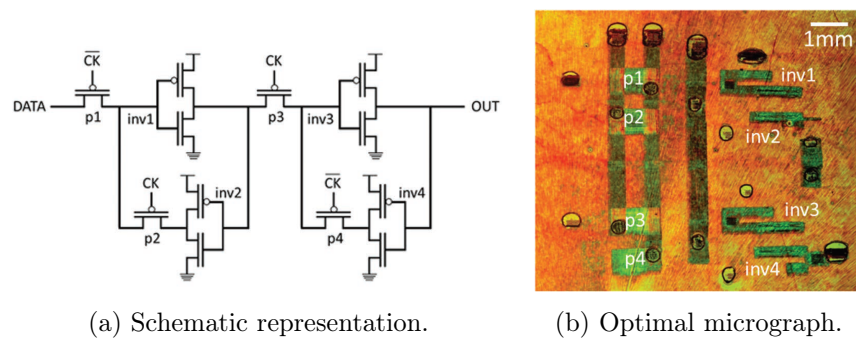


Figure 2.15: D flip-flop at IIT. Source: [40].

- Complementary-logic would allow to minimize the power consumption and area, as well as designing simple and efficient complementary pass-transistor logic gates.
- Being fully-polymeric, they are environmentally friendly and can be recycled as plastic.
- Their decreasing low-voltage operation has already reached the levels of conventional electronics (for simple designs).
- Being organic, they require low-temperature manufacturing processes, below  $100^{\circ}\text{C}$ .

As it has been said, the (for now) low frequency of operation is not a problem at all, since the purpose of the Smart Data Label project is precisely to find technologies suitable for simple low-end applications.

## Chapter 3

### SDL project: initial state

In this chapter, the state of the SDL project when the author started to work at Flex Milan is summarized. In this first stage, the circuit designed by the IIT was a two-bit counter, with supply voltage from 6 V to 10 V. It was tested by using two PCBs:

- One for mounting and encapsulating the printed circuit (known as fixture or break-out board).
- A main board for generating the counter inputs (clocks) and displaying its outputs on some light emitting diodes (LEDs).

A picture of the prototype is shown in figure 3.1. Both the fixture and the main board can be seen.



Figure 3.1: Initial prototype (source: [3]).

Figure 3.2 shows a picture of the printed circuit used in this stage. Each device is composed of:

- Two instances of a two-bit counter.
- Two instances of a single complementary logic inverter (which in the end weren't used in the firmware).

Each counter is composed of two D flip-flops connected in chain (that is, the input of each flip-flop is equal to its inverted output, and the clock is the output of the previous

flip-flop), and the inverter is done by using a simple complementary logic inverter. Even though the single inverters' functionality wasn't shown by the demo, it was useful for characterizing them at IIT.

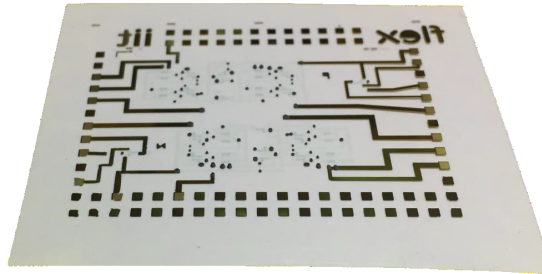


Figure 3.2: Initial printed circuit (source: [3]).

## 3.1 Design review

### 3.1.1 Board schematics

This version of the board was developed by Fabio Bragonzi at Flex Milan. A simple description of it is provided by the author in this subsection. To summarize, the board has the following modules:

- Power module.
- Printed circuit front-end.
- Microcontroller.
- Human interface.

Figure 3.3 shows a simplified diagram of the board, in which the different modules can be identified.

#### Power module

The whole circuit was supplied by a single coin cell battery (the commonly used CR2032). The standard for CR2032 states a nominal voltage of 3 V and an end-point voltage of 2 V. Hence, the MCU was directly fed with the battery<sup>1</sup>.

Nevertheless, since the printed circuit worked at relatively high voltages (from 6 V to 10 V), a DC converter was needed in order to generate the printed circuit supply voltage. The chosen converter was the LT1615 from Linear Technology<sup>2</sup> ([datasheet: \[44\]](#)), which block diagram is shown in figure 3.4. The approach of turning on and off a transistor connected to an inductor is widely found among commercially available micropower step-up DC/DC converters.

<sup>1</sup>The supply voltage of the chosen MCU ranges from 1.71 V to 5.5 V

<sup>2</sup>Now part of Analog Devices.

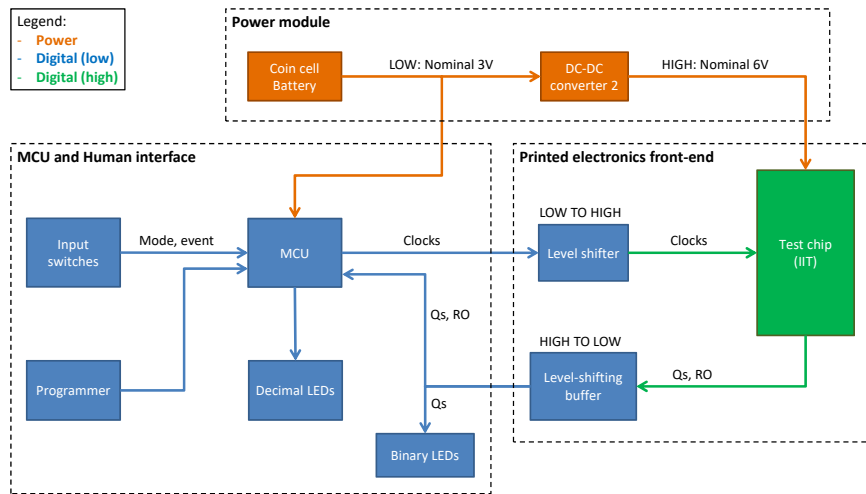
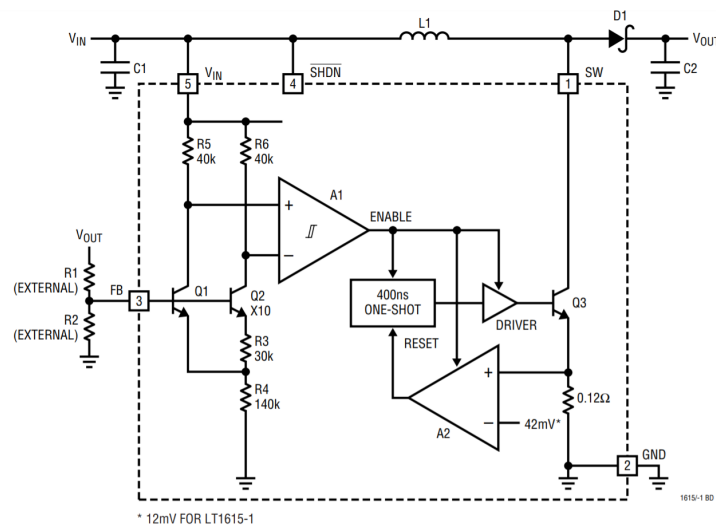


Figure 3.3: Board Block Diagram.

Figure 3.4: LT1615 Block Diagram (source: [datasheet](#) [44]).

Its working principle is quite simple: if the FB pin voltage is above a certain voltage threshold (1.23 V), the comparator A1 disables Q3 and the current at the output pin is provided by the capacitor C2, which gradually discharges until the FB pin voltage goes below its threshold. Q3 is turned on and the inductor L1 starts charging. When the inductor current surpasses a current threshold (350 mA), the comparator A2 resets the ONE-SHOT, thus turning off Q3 for 400 ms (during this period, the inductor current is delivered to the load through D1 while ramping down). The cycle of turning on and off Q3 is repeated until the FB pin voltage is again above its threshold.

The values selected for the board were (using the nomenclature in figure 4.2):

- L1: 47  $\mu$ H.
- R1: 180 k $\Omega$ .

- R2: 47 k $\Omega$ .

The value of L1 is quite high, which improves the load capability while lowering the switching frequency (and increasing the output voltage ripple). The values of R1 and R2 provide a fixed 6 V nominal output. In order to change the output voltage, the resistors were manually replaced by Fabio in a few boards (sometimes also using a trimmer potentiometer).

### Printed circuit front-end

Since the printed circuit outputs can manage a low amount of current, a high impedance load must be connected to them. Comparators configured as (inverting) Schmitt triggers were used for this purpose (see figure 3.5). This circuits are represented in the block "Level-shifting buffer" in figure 3.3. The selected comparator was the TS391 from STMicroelectronics ([datasheet](#): [45]). Since it's a single comparator, one chip was placed per each output of the printed circuit.

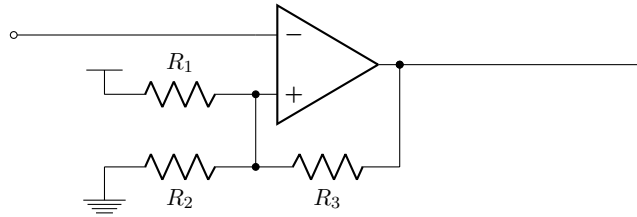


Figure 3.5: Schmitt trigger configuration.

In particular:

- The comparators were, naturally, supplied with the same voltage as the printed circuit (i.e., the output of the previously mentioned DC converter).
- The resistor values were  $R_1 = R_2 = 1 \text{ M}\Omega$ ,  $R_3 = 5.1 \text{ M}\Omega$ .
- The above implies that the theoretical threshold values of the Schmitt trigger (assuming an ideal comparator) are given by:

$$V_1^{th} = \frac{R_2 // R_3}{R_1 + (R_2 // R_3)} \approx 45.5\% \quad V_2^{th} = \frac{R_2}{R_2 + (R_1 // R_3)} \approx 54.5\%$$

These comparators are open-collector. Therefore, a simple pull-up resistor (connected to the supply voltage of the MCU) was used for translating the logic voltage level from the printed circuit to the microcontroller. No external resistors were connected, as the general purpose input/outputs (GPIOs) were configured as pull-up by firmware.

In addition, a low-to-high level shifter was needed. The circuit chosen for this purpose was the CD4504B from Texas Instruments ([datasheet](#): [46]). It was configured in CMOS-to-CMOS operation, with input voltage given by the battery, and output voltage equal to the printed electronics supply voltage.

## Microcontroller

The chosen MCU was a programmable system-on-chip<sup>®</sup> (PSoC), specifically the CY8C4247AZI-M485 from PSoC 4200M family ([datasheet](#): [47]), which was programmed using the MiniProg3 device from Cypress. It was suitable for the project because:

- Obviously, the amount of GPIOs was enough to drive all the required signals (including 16 LEDs).
- The chip is quite versatile, in the sense that it has commonly used peripherals already integrated on it, for instance, an analog-to-digital converter (ADC) and comparators, and also all the GPIOs can be independently triggered with an interrupt. This is a key point for the project design, particularly in companies in which the hardware and firmware designs are done by different employees (which is the case of Flex).

## Human interface

Four LEDs were connected to the input signals of the microcontroller (the four counter outputs), in order to be able to see the output in binary code. Sixteen other LEDs were driven by the microcontroller, and were used to show the outputs of the counters in decimal code. In the end, only 8 out of 16 LEDs were used (4 per each two-bit counter, only one of them is turned at a time), see figure 3.6.

A push button (event trigger) was added for making the test chip to count forward each time it's pressed. Also, a slide switch for selecting the mode (manual vs. automatic triggering) was used. An RC debouncing filter for the button signals was implemented, which time constant was  $\tau \approx 10 \mu\text{s}$ .

### 3.1.2 PCB layout

Figure 3.6 shows the main board layout, with some of their respective components or modules highlighted. The board layout was designed by Marco Ferrari at Flex. The fixture or breakout board (figure 3.7) only has traces for connecting each of the pads in the printed circuit to the corresponding pins of four male headers. Those headers are put into the female sockets that can be seen in figure 3.6 (green region), as shown in figure 3.1.

The connection between the test chip and the fixture was done by using a conductive glue, in particular the CircuitWorks<sup>®</sup> CW2400 epoxy from Chemtronics ([datasheet](#): [48]). Then, the circuit was encapsulated by using a rigid 2 mm-thick glass, at both sides. This encapsulation is necessary for making the circuit more robust to ambient conditions.

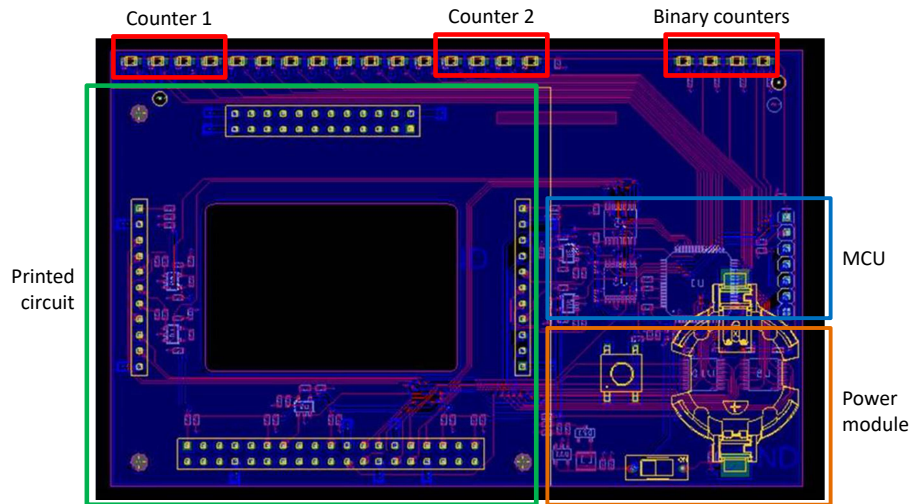


Figure 3.6: Main board layout.

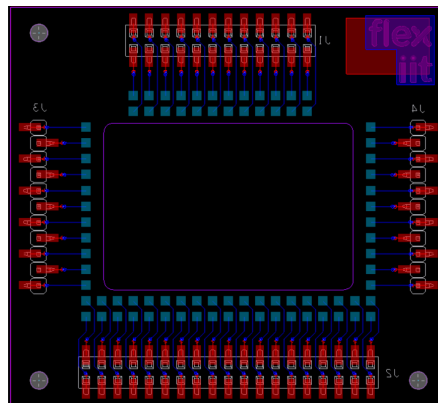


Figure 3.7: Breakout board layout.

## 3.2 Current measurement tests

Measuring the current consumption in one of the boards gave important information about the components that consume more power (thus, the ones in which to focus for reducing the power consumption in the next version of the board).

### Setup

- All the current tests were done at room temperature and 3 V supply voltage.
- The board was powered by using the Keysight 34465A power supply.
- The multimeter used was the Agilent E3648A.

## Procedure

The overall current consumption was measured several times. For identifying the current consumption of each component (at the battery side), some of them were disconnected, and the overall current was measured again.

Therefore, some assumptions were implicitly made in the process (e.g. the efficiency of the DC converter doesn't change that much when changing the load current), which **are not true in general**. As a result, the error is difficult to determine, and all the measurements provided are given just as a rough reference.

## Results

- When 6 LEDs are turned ON (i.e. the maximum: one decimal LED per each counter, and all the 4 binary LEDs), the current consumption of the board is about 19 mA.
- The average current consumption of each LED is approximately 1.5 mA.
- The board has five comparators, and each one consumes about 1.25 mA (equivalent at the battery side).
- The current consumption of the MCU was found to be 2.3 mA, at an operating frequency of 6 MHz.
- For the other components (i.e. level shifter, quiescent current of the DC converter), the current consumption wasn't characterized individually.

With this data, the pie chart shown in figure 3.8 is obtained. It can be seen that the most critical component (apart from the LEDs) is the comparator. Hence, it's really crucial to replace it with another component in order to reduce the current consumption.

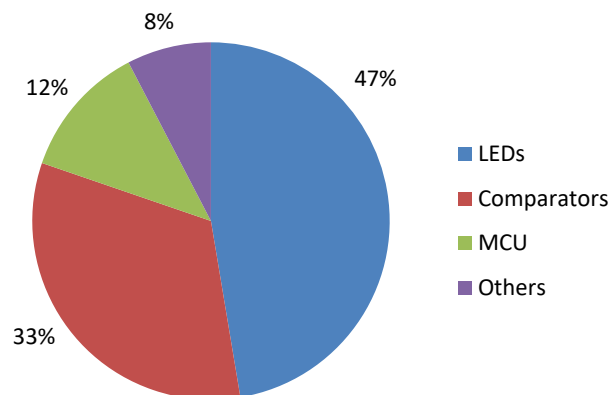


Figure 3.8: Current consumption distribution. 100% = 19 mA.

**Improvable aspects**

The main improvable aspects of this board that were identified are:

- The test chip consists on 2-bit counters (2 units), which is still too simple for any practical application.
- The operating voltage ranges from 6 V to 10 V, making it not practical for testing the printed circuit at lower voltage levels.
- The encapsulation and boards are all rigid, so it's difficult to illustrate the potential of printed electronics for enabling new form factor designs.
- Conventional LEDs and a coin cell battery are used, while other flexible electronic components could be placed instead.
- The current consumption is high to be integrated in a flexible label.

## Chapter 4

# Non-form factor board design

Before doing a flexible demonstrator, a non-form factor (NFF) board was developed. The objectives of this intermediate step were:

- Optimize the design (compared to the previous board), in terms of current consumption.
- Provide a wide amount of test points and headers in order to characterize the new components (especially if a fail should occur).
- Evaluate the integration of possible additional features into the flexible demo.
- Provide an interface to which both the previous PEC (see figure 3.2) and the new one can be connected<sup>1</sup>.

### 4.1 Requirements

#### 4.1.1 Mandatory

At the beginning of the actual project phase, most requirements were stated as qualitative rather than quantitative. In fact, they are:

- Enough low power consumption to be powered by a flexible battery<sup>2</sup>.
- Usage of electrochromic displays instead of LEDs.
- Different PEC: a single 4-bit counter, and a ring oscillator.
- The board must be able to power up the printed electronic circuit at 3 V.

#### 4.1.2 Desirable features

The following are additional features that were implemented in the NFF board, in order to test them and then decide to include them in the flexible demo or not.

---

<sup>1</sup>This means that the external layout of the fixture must be identical, so that both versions of the printed counter can be connected either to the previous board or to the new NFF board.

<sup>2</sup>The nominal capacity of printed batteries on the market is in the order of 10 mAh. However, some of them have problems with delivering high current peaks (see section 2.2).

- MCU-controlled test chip supply voltage, by the means of a digital potentiometer.
- Inclusion of NFC for exchanging data with a cellphone, and also possibly harvesting some energy from the electromagnetic field.

## 4.2 Design process

### 4.2.1 Components benchmark

A benchmark of different components was done, and the chosen ones were selected based on the following criteria:

- Power consumption (i.e. supply current, quiescent current, efficiency, etc.).
- Pertinent operating conditions (e.g. the supply voltage range).
- Size: the smaller, the better. This is important not only for aesthetic purposes, but also for the final demo board to be flexible (despite having rigid silicon circuits).

### Updated components

#### 1. Comparator<sup>3</sup>

The chosen comparator was the TLV7041 from Texas Instruments ([datasheet: \[49\]](#)). It's quiescent supply current is 335 nA, which represents a huge improvement (comparison on table 4.1). Besides, it's an open collector comparator, so a simple pull-up resistor can be used instead of an additional level shifter for lowering the voltage domain. Finally, it's available in an ultra-small package (0.8 mm × 0.8 mm).

Nevertheless, the main drawback is that the maximum supply voltage is only 6.5 V, and this is actually the component that limits the maximum operating voltage of the printed electronics in the NFF board. However, since the technology had already been proven to be reliable at 6 V, this wasn't considered a huge problem.

#### 2. DC converters and level shifters

The ideal conditions that the step-up DC converter should satisfy to be suitable for this project are:

- Output voltage from 3 V to 6.5 V.
- Efficiency: 80% or higher.
- Quiescent current in the order of 1  $\mu$ A.
- Size: 3 mm × 3 mm or smaller.

---

<sup>3</sup>The comparator in the old board was replaced by this component, but the rest of the Schmitt trigger circuit remained exactly the same.

- Suitable for light-load applications.

Unfortunately, no DC converter satisfying all of the above requirements was found. In particular, the voltage range criterion was difficult to obtain without violating one or more of the other requirements. But, as a workaround, two quite suitable DC converters were found and, together, they cover the full voltage range: the TPS61069A from Texas Instruments ([datasheet: \[50\]](#)) and the MAX17220 from Maxim Integrated ([datasheet: \[51\]](#)).

- TPS61069A

It's quiescent current is at most  $2.5\ \mu\text{A}$  at the input side, and  $0.2\ \mu\text{A}$  at the output side. The efficiency logically depends on load conditions, but it's usually above 70%. And it's available in a  $3\ \text{mm} \times 2\ \text{mm}$  package. The drawback is that the **minimum output voltage is 4.5 V**.

A nice feature of this converter is that it incorporates a two-channels level shifter. Hence, **no external level shifter** needs to be added to translate from the MCU voltage domain to the printed electronics one.

- MAX17220

The quiescent current is  $100\ \text{nA}$  at the input side, and  $900\ \text{nA}$  at the output side, at most. The efficiency is higher than the former converter's, being over 90% at the expected load conditions. Its **maximum output value is 5 V**. From the footprint point of view, it measures  $2\ \text{mm} \times 2\ \text{mm}$ , and the power choke's (imperial) dimensions can be 0603, thus minimizing the area of the step-up circuit.

A level shifter needs to be added if this converter is used. The chosen level shifter was the SN74LVC2T45 from Texas Instruments ([datasheet: \[52\]](#)), which quiescent current is at most  $3\ \mu\text{A}$ , at both supply voltages.

As it can be noticed, both alternatives have advantages and disadvantages, and together they cover the full 3 V to 6.5 V range. It would be ideal to use the MAX17220 due to increased efficiency, but when the NFF board was designed, it was difficult to tell if the printed electronics would reliably work at 5 V. On that account, **both converters** were put in the board, in order to test the printed electronics at the full voltage range. Later, depending on its performance, one of the DC converter configurations would be chosen.

### 3. Microcontroller

In order to maintain the same integrated development environment (IDE) as in the previous board (to be able to use the existing firmware as a base for migrating to the new one), a PSoC from the same family was used: CY8C4246AZI-M443 from Cypress ([datasheet: \[47\]](#)). The only substantial difference (pertinent to the

project) with the previous CY8C4247AZI-M485 is that it's a bit smaller ( $7 \times 7 \text{ mm}^2$  instead of  $9 \times 9 \text{ mm}^2$ ).

Regarding the power consumption, according to the datasheet (specifications SID6 and SID31),

- At 6 MHz system clock frequency, the supply current is 2.2 mA typical / 2.8 mA maximum. Logically, if the frequency is slower, the consumption is expected to be reduced as well, but smaller frequencies are not listed in the datasheet.
- In deep sleep mode, the supply current is 1.35  $\mu\text{A}$  typical / 15  $\mu\text{A}$  maximum.

Table 4.1 illustrates the comparison between different components, regarding their consumption. That is, the supply current or quiescent current ( $I_Q$ ), and the efficiency of the converters. As the table shows, all the updated components consume less than the ones in the former board. The most important current reduction is in two orders of magnitude, and corresponds to the replacement of the comparator.

	Component	Measurement	Typ	Max	Unit	Conditions
Comp.	TS391*	Supply current	0.2	0.5	mA	Supply voltage 5V, no load.
	TLV7041	Supply current	335	900	nA	Supply voltage 1.8V, no load, output low.
DC converter	LT1615*	$I_Q$ into IN	20	30	$\mu\text{A}$	Not switching.
		Efficiency	70%	-	-	Input 1.5V, output 3.3V, load current 1.5mA.
		Efficiency	76%	-	-	Input 3.3V, output 20V, load current 1mA.
	MAX17220	$I_Q$ into OUT	300	900	nA	EN pin open after startup.
		Total input $I_Q$	0.5	100	nA	EN pin open after startup.
		Efficiency	89%	-	-	Input 1.5V, output 3.3V, load current 1.5mA.
	TPS61096A	$I_Q$ into OUT	-	0.2	$\mu\text{A}$	Device enabled, 20V output.
		$I_Q$ into IN	1.2	2.5	$\mu\text{A}$	Device enabled, no load, no switching.
		Efficiency	79%	-	-	Input 3.6V, output 18V, load current 1mA.
Level shifter	CD4504B*	$I_Q$ , each side	0.02	1.5	mA	$V_{CC}=V_{DD}=5\text{V}$ , $V_{IN}=0.5\text{V}$ , all 6 channels.
	SN74LVC2T45	$I_Q$ , each side	-	3	$\mu\text{A}$	$V_{CCA}$ , $V_{CCB}$ in range 1.65 to 5.5V; $V_{IN}$ high or low, both channels.
	TPS61096A	$I_Q$ , OUT side	1.5	3	$\mu\text{A}$	Both channels enabled, inputs=HIGH.

Table 4.1: Components' current consumption.

\*Used in the former board.

Of course, these parameters depend on the test conditions, which are not always equal for the different components. Therefore, the data in table 4.1 should be taken only as a general reference (in particular, concerning the efficiency of the converters).

The better efficiency of the converters can be explained by looking at their working principle and block diagram (figures 4.1 and 4.2). First, notice that both converters use the same approach: pulse-frequency-modulation (PFM) control scheme, based on charging an inductor. And, in particular, compared to the converter in the former board (figure 3.4), they reduce the feedback branch current.

- The **TPS61096A** reduces such current by only measuring the FB pin when it's needed. In fact, the VOSNS pin can be disconnected from VOUT through a transistor managed by the control logic.
- The **MAX17220** only uses one resistor (RSEL) to define the desired output voltage, which value is measured at start-up. The feedback resistors are internal to the chip and, judging by its high efficiency, must waste very little current.

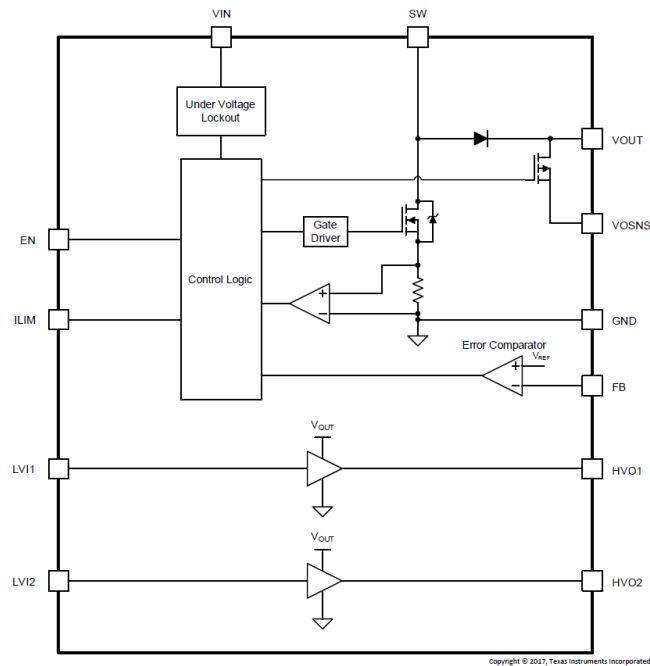


Figure 4.1: TPS61096A, block diagram. Source: datasheet [50].

### Additional components

The NFF board also included some components that were not present in the former board. Thus, this section is dedicated to the digital potentiometers and NFC. The chosen components use the inter-integrated circuit (I2C) protocol, which allows to connect all of them to the MCU using only two signals: SDA and SCL.

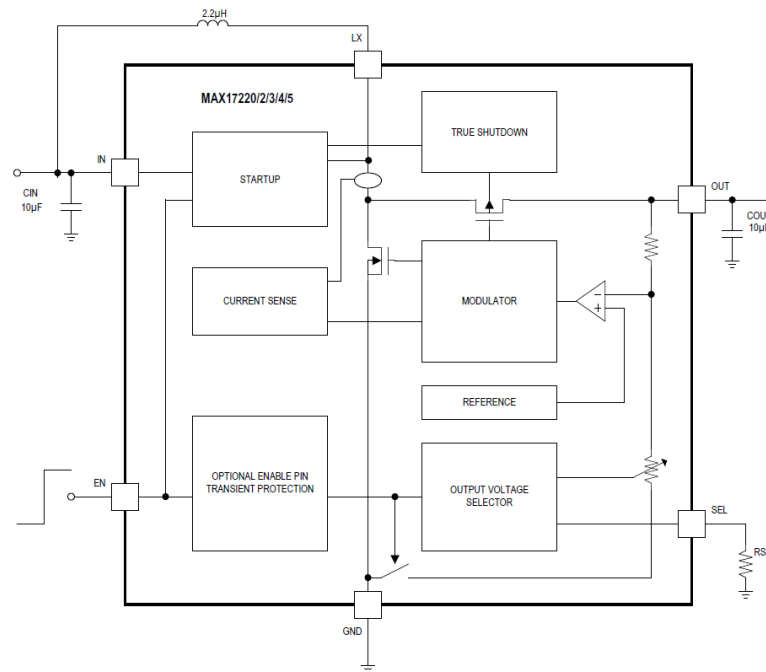


Figure 4.2: MAX17220, block diagram. Source: datasheet [51].

### 1. Digital potentiometer

The digital potentiometers are intended to select the output voltage of the DC converters, i.e. the printed electronics operating voltage. Since two DC converters were chosen, and the selection of their output voltage is consequently done in two different ways, two digital potentiometers were used as well.

- MAX5419, from Maxim Integrated ([datasheet](#): [53]).

A 256-tap, 200 k $\Omega$  potentiometer, which has a standby current of 1  $\mu$ A at maximum. This resistance value is suitable for the MAX17220 DC converter, i.e. the maximum 5 V option.

- MCP4017, from Microchip ([datasheet](#): [54]).

A 128-tap, 50 k $\Omega$  potentiometer. The standby current is 5  $\mu$ A at maximum. This potentiometer is intended for the TPS61096A converter output selection, that is, the minimum 4.5 V option.

Table 4.2 illustrates the consumption of these potentiometers, when they are being programmed and in standby mode. Even though the supply current of the MAX5419 is quite high when the I2C interface is active, it's only programmed during the very first milliseconds, while configuring the DC converter output, so this is not an issue (as long as the battery is able to deliver the required peak).

### 2. NFC

The NFC that was used is the NT3H1101 NFC tag (NTAG) I2C, from NXP ([datasheet](#): [55]). It was appropriate because it satisfies the criteria to be an NFC

	Supply current (active interface)		Standby current		Unit
	Typ	Max	Typ	Max	
MCP4017	45	80	2.5	5	$\mu\text{A}$
MAX5419	200	400	0.5	1	

Table 4.2: Digital potentiometers' consumption.

forum type 2 tag (so the coding process is easier, as the protocol is standard) and has a reasonable supply current of  $155\ \mu\text{A}$ .

It also supports energy harvesting, being able to supply itself from the electromagnetic field generated by a phone, as well as powering light load devices. This could allow it to help the battery to power up the microcontroller. Besides, its field detection pin can trigger an MCU interrupt each time a phone is approaching.

#### 4.2.2 Schematics

In the former board, the MCU was directly connected to a coin cell battery. However, since the series resistance of flexible batteries in the market is higher than conventional lithium batteries, an additional DC converter was added in the NFF board, to generate a stable microcontroller voltage. This converter was the MAX17220 described before.

To summarize, the NFF board has three DC converters:

1. A MAX17220 for generating the MCU supply voltage.
2. A MAX17220 to generate the printed electronics voltage (maximum 5 V output).
3. A TPS61096A, an alternative to the previous, which output goes from 4.5 V to  $28\ \text{V}^4$ .

A general diagram of the circuit of the NFF board is shown in figure 4.3, while the full schematic can be found in the appendix A. The main differences with the diagram of the previous board (figure 3.3) are the addition of the NFC, the digital potentiometers, and two DC converters (as well as replacing all the components by their optimized versions).

In addition, quite a lot of test points and headers were included in the NFF board. The headers were intended not only for current measurement, but also for choosing between different components (for instance, between the two DC converter alternatives).

Figure 4.4 shows a diagram of the power flow, so that the different power configurations of the board are easy to understand. The labeled voltages are:

- VDD: the output of the battery.

<sup>4</sup>Recall: the maximum PEC voltage is 6.5 V, limited by the comparator.

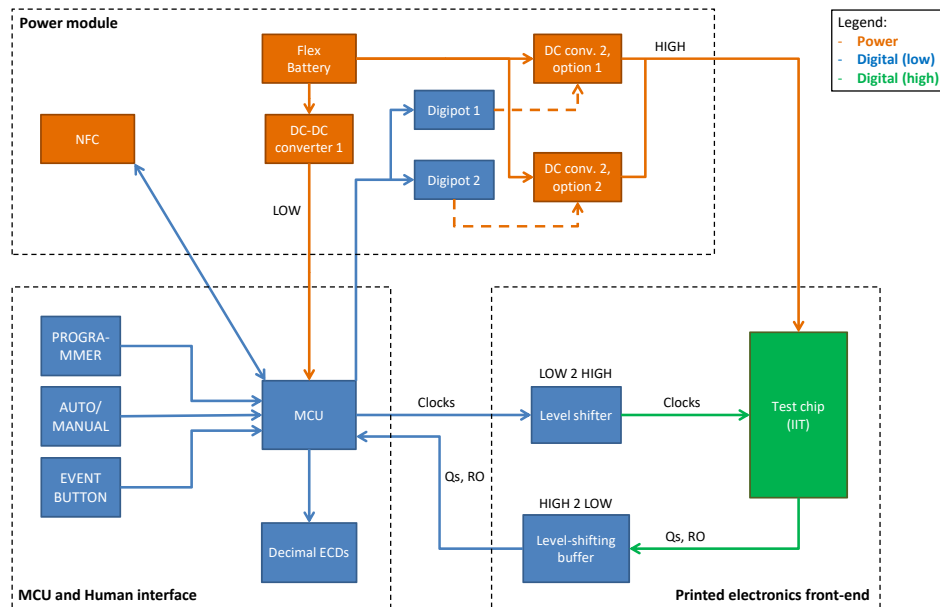
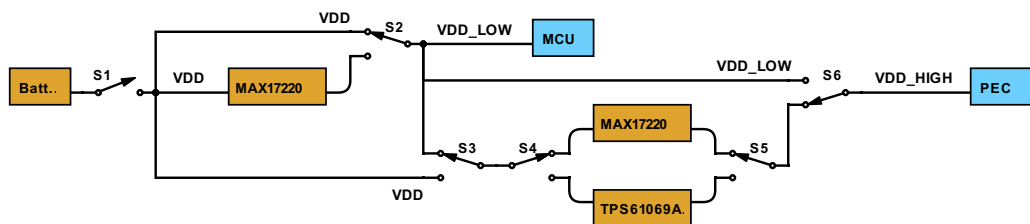


Figure 4.3: NFF Board Block Diagram.

- VDD\_LOW: which powers the MCU and all the same voltage domain components (digipots, NFC, etc.).
- VDD\_HIGH: powers the PEC, and the comparators.

Figure 4.4: NFF Board Power Diagram.  
Done with SchemIt, by Digkey.

All the switches (except the power switch, S1) were truly implemented by using simple headers. The switches allow the following functionalities:

- S1: power switch. Disconnects the battery from the board.
- S2: allows to bypass the first MAX17220 converter. This feature is important, since in this way, two different flexible battery cells can be connected in series (and supply the MCU directly by the battery) or in parallel (the converter steps

up the voltage). There's a trade-off between stable supply voltage level (obtained by using the DC converter) and lower power consumption (by bypassing it).

- **S3**: chooses the input to the second DC converter. It can be either `VDD` ("parallel" DC converter configuration) or `VDD_LOW` ("series" configuration). Logically, if the first `MAX17220` is not bypassed, the best efficiency is got by tying `S3` to the battery. Nevertheless, since the `TPS61069A` has the level shifter already incorporated, its input voltage needs to be equal to `VDD_LOW`, and this was the reason for including `S3`.
- **S4** and **S5**: define the DC converter to be used: `MAX17220` or `TPS61096A`. As a recall, this choice depends on the resulting operating voltage range of the printed electronics (see section 4.2.1).
- **S6**: select the source of `VDD_HIGH`. Normally, it will be tied to the output of the DC converter, but it can also be connected to `VDD_LOW`. This allows to directly connect the microcontroller to the printed electronics<sup>5</sup>, without the need of a level shifter.

For instance, for the configuration presented in the figure, when closing the switch `S1`, the MCU will be fed by the battery voltage, while the printed electronics circuit will be supplied by the `MAX17220`, which input is tied to the battery too.

### **Important: connection mode for the TPS61096A**

Since the `TPS61096A` works also as level shifter (no external level shifter needed), its input voltage must be equal to `VDD_LOW`. That is, whenever `S4` and `S5` are connected to the `TPS61096A`, `S3` must be tied to `VDD_LOW`. As a consequence, the connection mode in which both DC converters are directly connected to the battery ("parallel" configuration) is not possible when using the `TPS61096A`.

### **4.2.3 PCB layout**

The PCB layout was designed by Marco Ferrari (figure 4.5). To be able to connect both the old 2-bits counter and the new 4-bits circuit to the NFF board, the same approach as in the former board was adopted. That is, two boards were designed: a fixture/breakout board, and the main board (see section 3). The interface between them was maintained exactly as it was, so that both fixtures were compatible with the NFF board.

The main components are:

- At the upper-left corner, the interface for connecting the fixture containing the PEC.

---

<sup>5</sup>Additional headers were included in the schematic design, in order to choose between the level shifters. They also allow to bypass the level shifter and tie each low logic-level signal to the corresponding high logic-level net.

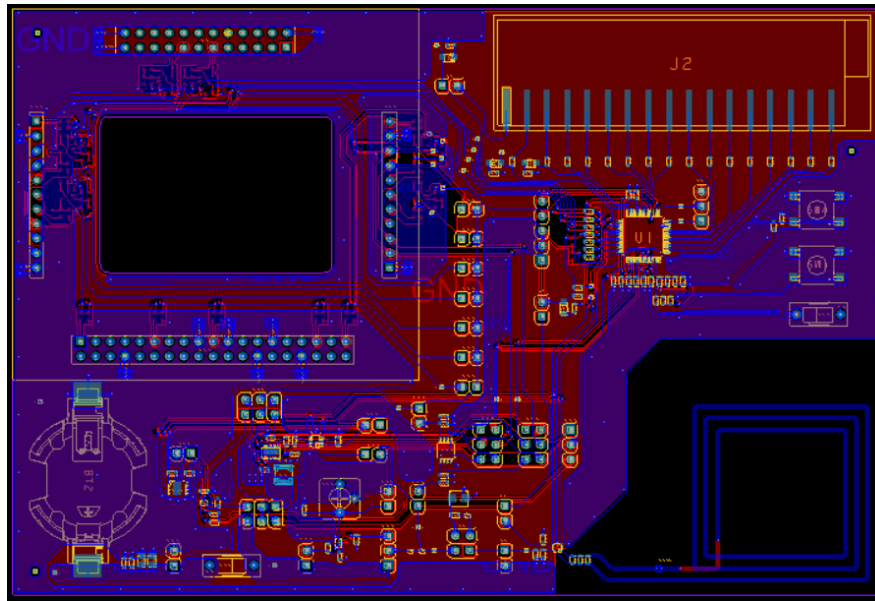


Figure 4.5: NFF Main Board Layout.

- At the upper-right corner, the electrochromic display, as well as the microcontroller and input buttons.
- At the lower-right corner, the NFC.
- At the lower-left corner, the power module: different DC converters, a level shifter, the digital potentiometers, and headers for choosing between them.
- Note that the battery is a coin cell. When the NFF board was designed, the flexible battery supplier wasn't defined yet. Hence, a CR2032 cell was left by default, with the possibility to power up the board with another external source (through a 2-pin header in parallel).

The breakout board, on the other side (figure 4.6), is just a board that ties the used pads of the test chip to the corresponding pins of the headers, for proper connection with the main board.

#### 4.2.4 Firmware

The firmware, that is, the code loaded into the MCU, was based in the former version, which was coded by Emanuele Pozzi. Some extra features (or changes intended for reducing the power consumption of the microcontroller) added by the author during this design of the non-form factor were:

- An extra output pin, for enabling the DC converter that generates VDD\_HIGH.
- I2C driver, and functions for modifying the output voltage of the DC converter (through the digital potentiometer) or storing data into the NFC.

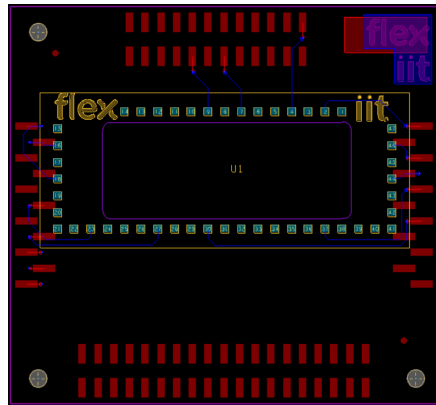


Figure 4.6: NFF Breakout Board Layout.

- An ECD driver, for managing the display.
- Reduction of the system clock frequency to 187.5 kHz (when the I2C module is not used).
- Usage of external (and higher) pull-up resistors, instead of the ones at each GPIO. This was done because the internal ones were too low (typically 5.6 k $\Omega$  according to the specification SID63 present in the datasheet [47]), so the currents flowing through them even reached some milliamperes.
- Modifications to the program flow and hardware components used. First, the program was state-machine-based, and the debounce of the switches was done by using a timer interrupt (implemented in hardware, so it consumed extra current). The timer was removed and a more linear program flow was adopted instead.
- The delays were implemented in a low-power mode: that is, the MCU was set to deep sleep mode each time it had to wait. For waking up, the internal low-speed oscillator (ILO) was set up to generate a watchdog interrupt that wakes up the microcontroller. Even though the ILO clock source is not very precise at all<sup>6</sup>, the current consumption is significantly reduced with this approach.
- Improved modularity and configuration. For instance, working with macros that disable entire modules (in order to load only a particular part of the code), and choose between coding alternatives (e.g. different digital potentiometer, 2-bits or 4-bits PEC, ECD or LEDs driver).

Figure 4.7 illustrates (a simplification of) the program that was adopted. In the case of NFC functionality, the microcontroller stores the counter value into the NFC memory, just before updating the ECD. If the digital potentiometer driver is present, the VDD\_HIGH setup is done inside the `Init` function.

<sup>6</sup> $\pm 60\%$ , but its accuracy can be improved to  $\pm 10\%$  by comparing it with a more precise clock at the beginning of the program.

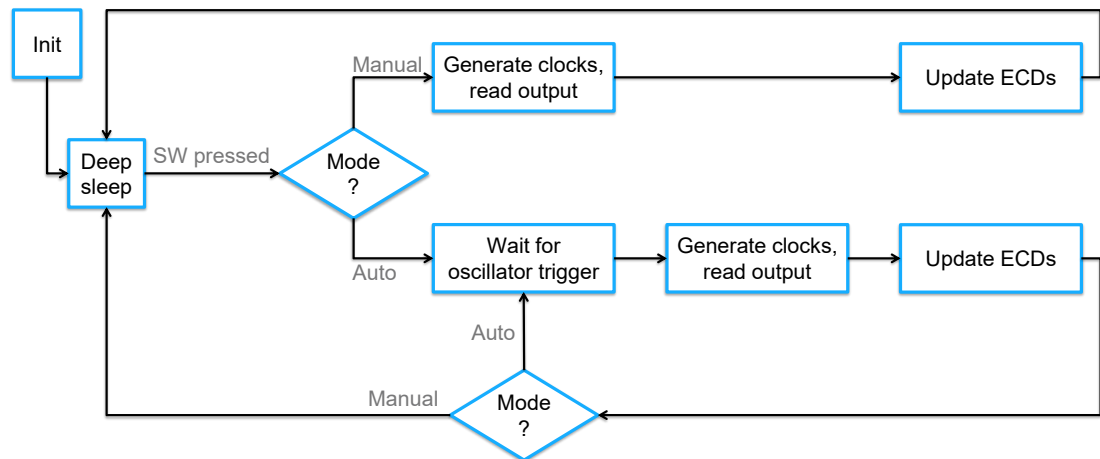


Figure 4.7: Firmware Block Diagram.

The firmware is quite simple. There are two different modes: Auto and Manual<sup>7</sup>.

- In Manual mode, the functionality of the 4-bit counter is tested. The MCU generates the clock and then updates the ECD, displaying the output of the counter.
- In Auto mode, the both oscillator and the 4-bit counter are used. The microcontroller waits for a rising edge on the oscillator output (or a certain amount of them, configurable by firmware if the frequency of the oscillator is too high) before generating the counter clocks, and consequently update the ECD.

No additional details about firmware are given (besides some comments in the next chapter), as the developed code is property to Flex.

<sup>7</sup>The user can change the mode by the means of a slide switch.

## Chapter 5

# NFF board characterization

After the design phase of the NFF board, a benchmark of different electrochromic displays and printed batteries was done. Some of them were acquired, tested separately, and then connected to the NFF board. This chapter describes the most important tests done to this components and the NFF board itself.

### 5.1 Electrochromic display

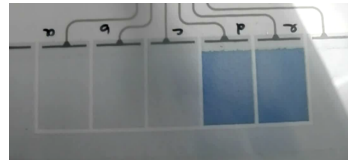
Two ECDs from different companies were tested:

- A 7 segments,  $7.9 \text{ mm} \times 2.3 \text{ mm}$  display from RISE Acreo (figure 5.1a).
- A 5 segments,  $1.5 \text{ cm} \times 1 \text{ cm}$  display from Ynvisible (figure 5.1b).

The aim of this comparison was to define which supplier would manufacture a custom version of the display, consisting on fifteen  $5 \text{ mm} \times 2 \text{ mm}$  segments.



(a) RISE Acreo.



(b) Ynvisible.

Figure 5.1: Electrochromic display samples.

#### 5.1.1 RISE Acreo

Based on PEDOT:PSS, these reversible displays alternate between gray state (off) and blue (on). The display has 7 segments and 8 pins (one extra pin for the common electrode). As stated in the Driver's license [56], the driving protocol is as follows:

1. To turn on a specific segment, drive it high, while maintaining the common electrode low.
2. To turn it off, simply invert the polarity. Be careful, since a too long pulse length in this direction will degrade the display (especially at high voltage<sup>1</sup>).

---

<sup>1</sup>Acreo tests their displays at maximum 3 V.

These displays are almost bi-stable: once a segment has been turned on, it remains turned on for some minutes, (even if the contacts were short-circuited). A refresh pulse can be applied, for example, every 10 minutes, to avoid a too high loss of contrast.

When testing the displays (driving them with the MCU in the previous board), a bit of cross-talk effect was observed (i.e., turning on a segment also slightly turned on the others, especially if they had just been turned off). Adding a series resistance at the common electrode (in the range from 1 k $\Omega$  to 10 k $\Omega$ ) helped to reduce this effect.

### 5.1.2 Ynvisible

Unlike the previous display, the maximum contrast is weaker, and the idle state is transparent. Also, in order to turn off a specific segment, both the segment electrode and the common electrode must be short-circuited (no reverse voltage is ever applied). This may be considered as an advantage, because:

- The common electrode doesn't change its value, so the MCU drives one less signal.
- The driver is simpler: each of the pins are managed independently.

A kind of cross-talk effect was also observed in Ynvisible displays, but of a different kind: when a segment A, adjacent to another one B that is already turned on, was set to blue state, the segment B lost contrast in the neighborhood of the segment A. That is, some of the current needed to turn on segment A is extracted from segment B, instead of the common electrode.

### 5.1.3 ECD Comparison

Table 5.1 illustrates the pros and cons of both displays. The main drawback of the Ynvisible display, for this application, was the bleaching time. Since they're turned off by short-circuiting the electrodes, the ion transfer rate is slower, and the bleaching time depends on the contact resistance.

Considering that the display was going to be pasted with a conductive glue (which resistance is in the order of 30  $\Omega$ , according to [3]), the RISE Acreo display was preferred instead. However, the Ynvisible display may be a good option for other applications in which the contacts are known to have a low parasitic resistance.

### 5.1.4 Custom display

Having decided to use the RISE Acreo option, a custom display sample was requested. The design is illustrated in figure 5.2, and consists on 15 segments (for counting from 0 to 15) of 2 mm  $\times$  5 mm. Figure 5.3 shows images of the physical display.

Upon arrival of the display, different series resistance values connected at the common electrode were tested, in order to limit the peak current consumption of the display and reduce the cross-talking, without affecting too much the switching time. Just by trial and error, a 1 k $\Omega$  resistor was considered effective for a 2.7 V microcontroller supply

Item	RISE Acreo	Ynvisible
Voltage range	At least 2.2 V for minimum contrast. Tested safely at 3 V.	Usually tested at 3 V. 2.5 V is suitable as well.
Turn on time	$\approx 300$ ms at 2.5 V, for a $0.18 \text{ cm}^2$ segment.	1 s at 2.5 V, $1.5 \text{ cm}^2$ segment.
Turn off time	Similar to the turn on time.	Higher than the turn on time, and highly dependent on contact resistance.
Driver	More complex: requires 1 more signal, and three-state control logic.	Simpler: each pin is managed independently.
Idle current	Theoretically zero (high impedance state).	Small, in the order of $10 \mu\text{A}$ ( $1.5 \text{ cm}^2$ segment).
Peak current	Higher, some $\text{mA}/\text{cm}^2$ .	Lower, a couple of $\text{mA}/\text{cm}^2$ .
Color	Greater contrast.	Weaker, but somehow modern due to transparent idle state.
"Cross-talking"	Small, if the pins are turned to high-Z state when not being driven.	Higher (can draw current from other segments instead of common electrode).

Table 5.1: ECD comparison.

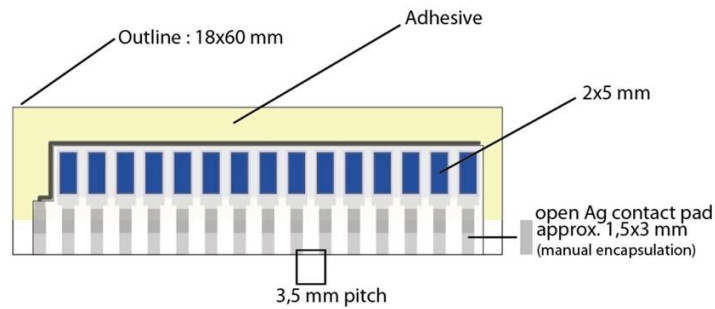


Figure 5.2: RISE Acreo display design layout\*.

\*Finally the pads were  $1.5 \text{ mm} \times 5 \text{ mm}$ , instead of  $1.5 \text{ mm} \times 3 \text{ mm}$ .

voltage. With this value, the peak current of the ECDs is limited to 2.7 mA, but it can be reduced by increasing the series resistance, if necessary.



Figure 5.3: Acereo display: custom version.

## 5.2 NFF board

### 5.2.1 Power budget

#### Theoretical considerations

After the design of the NFF board, a power budget was developed. The parameters used for the calculations are:

- $I_{MCU}$ , the current of the microcontroller and also other low-voltage MCU-interfaced peripherals: includes the NFC, digital potentiometers, and I2C bus current if applicable.
- The efficiency of the DC converters  $\eta_{DC}$ , as well as their supply current into both input and output  $I_{DC}^i, I_{DC}^o$  (with  $DC$  corresponding to  $TPS$  and/or  $MAX$ ). In the  $TPS61096A$  case,  $I_{DC}^o$  considers also the current into the feedback branch.
- Input and output supply currents of the level shifters,  $I_{LS}^i$  and  $I_{LS}^o$ .
- The supply current of the comparators  $I_{comp}$  (per channel), which includes the current across the resistors of the Schmitt trigger configuration<sup>2</sup>. Also, the amount of channels to be read by the microcontroller ( $N_{ch}$ ), and the value of the pull-up resistors  $R_{pull-up}$  connected at the output of the comparators.
- The consumption requested by the display,  $I_{ECD}$ .
- The current consumed by the printed electronics,  $I_{PEC}$ .

At the same time, the result depends on the voltage domains, i.e.  $VDD$  ( $V_{DD}$ ),  $VDD\_LOW$  ( $V_{DD}^L$ ) and  $VDD\_HIGH$  ( $V_{DD}^H$ ), and also on the configuration of the DC converters (is the first one bypassed? If not, are they both connected to the battery, or connected in cascade?).

For instance, let's suppose that: the  $MAX17220$  for generating the MCU voltage is **not** bypassed, the  $TPS61096A$  converter is the one generating the printed electronics supply voltage, and its input is  $VDD\_LOW$  (i.e. the "series" configuration described in

<sup>2</sup>In the worst case scenario, i.e. when the output of the comparator is low

section 4.2.2). Then, the total current consumption  $I_T$  can be recursively calculated as:

$$\begin{aligned} I_H &= I_{TPS}^o + I_{LS}^o + N_{ch} \cdot I_{comp} + I_{PEC} \\ I_L &= I_{MAX}^o + I_{TPS}^i + I_{LS}^i + I_{MCU} + I_{ECD} + N_{ch} \cdot \frac{V_{DD}^L}{R_{pull-up}} + \frac{V_{DD}^H}{V_{DD}^L \cdot \eta_{TPS}} \cdot I_H \\ I_T &= I_{MAX}^i + \frac{V_{DD}^L}{V_{DD} \cdot \eta_{MAX}} \cdot I_L \end{aligned}$$

As another example, if the first MAX17220 is bypassed (so, the MCU is directly connected to the battery), and the printed electronics is fed by the MAX17220 option, the above equations become:

$$\begin{aligned} I_H &= I_{MAX}^o + I_{LS}^o + I_{comp} + I_{PEC} \\ I_T = I_L &= I_{MAX}^i + I_{LS}^i + I_{MCU} + I_{ECD} + N_{ch} \cdot \frac{V_{DD}^L}{R_{pull-up}} + \frac{V_{DD}^H}{V_{DD}^L \cdot \eta_{MAX}} \cdot I_H \end{aligned}$$

with  $V_{DD}^L = V_{DD}$ .

Notice that if no external  $R_{pull-up}$  is connected, since the internal resistor of each GPIO is in the range from 3.5 k $\Omega$  to 8.5 k $\Omega$ , up to 850  $\mu$ A can be drained from VDD\_LOW, per channel. Multiplying this by at least 5 outputs of the PEC<sup>3</sup>, that is up to 4.2 mA, only for reading those signals. It is therefore desirable to add an external resistor, possibly in the order of magnitude of  $R_{pull-up} = 1$  M $\Omega$ .

Also note that, for evaluating the current consumption in deep sleep mode (assuming that no big variation in the efficiency of the DC converters is obtained at lighter load), it's sufficient to remove  $I_{ECD}$  from the above calculations, and replace  $I_{MCU}$  by the deep sleep current.

### Power budget evaluation

The power budget was evaluated at the worst case scenario, using always the maximum consumption of each component (overestimation). Moreover, 2.8 mA were considered for the MCU (which is its maximum at 6 MHz), even though much less consumption is expected while working at lower frequencies.

That being said, the following were the worst case scenario parameters:

- $I_{MCU} = 2.8$  mA in operation, 15  $\mu$ A in deep sleep<sup>4</sup>.
- $\eta_{TPS} = 70\%$ ,  $I_{TPS}^i = 2.5$   $\mu$ A,  $I_{TPS}^o = 0.2$   $\mu$ A +  $V_{DD}^H/R_{fb}$  where the smallest possible value for the feedback branch equivalent resistance is 186 k $\Omega$ <sup>5</sup>.

<sup>3</sup>Four counter signals, and the ring oscillator output.

<sup>4</sup>The current of the digital potentiometer (table 4.2), NFC (155  $\mu$ A) and I2C bus ( $2 \cdot V_{DD}^L/R_{i2c}$ ) shall be added to  $I_{MCU}$ , when applicable.

<sup>5</sup>In section 4.2.1, we said that the feedback branch current of the TPS61096A is reduced due to the fact that the FB pin is not always being measured. For the power budget overestimation, this effect was neglected.

- $\eta_{MAX} = 80\%$ ,  $I_{MAX}^i = 0.1 \mu\text{A}$ ,  $I_{MAX}^o = 0.6 \mu\text{A}$ .
- $I_{LS}^i = 1 \mu\text{A}$  in the case of the TPS61096A;  $9 \mu\text{A}$  in the case of the SN74LVC2T45.  
 $I_{LS}^o = 3 \mu\text{A}$  in both cases.
- $I_{comp} = 0.9 \mu\text{A} + V_{DD}^H/R_{eq}$ , with  $R_{eq} = 1.84 \text{M}\Omega$  the equivalent resistance of the Schmitt trigger circuit from  $V_{DD}^H$  to ground. Also,  $R_{pull-up} = 1 \text{M}\Omega$  and  $N_{ch} = 5$ .
- $I_{ECD} = 2 \text{mA}$ , an assumption made on the base that the maximum current may be limited by putting a series resistor, as described in section 5.1.4.
- $I_{PEC} = 10 \mu\text{A}$  when updating the counter value, and  $1 \mu\text{A}$  in idle state. This is a conservative estimation based on the data owned by the IIT.

Table 5.2 illustrates the current consumption at the above mentioned conditions (worst case scenario). The voltage  $V_{DD}^H$  was set close to its maximum value (6.5 V for the TPS61096A, 5 V for the MAX17220) because at higher supply voltages the power consumption arises.

Voltages [V]			Converters configuration			Peak		Deep sleep	
$V_{DD}$	$V_{DD}^L$	$V_{DD}^H$	1st DC	2nd DC	Conn.	Value	Unit	Value	Unit
3	3	6.2	Bypassed	TPS61096A	-	5.02	mA	207	$\mu\text{A}$
			MAX17220		Series*	6.27		260	
3	3	4.7	Bypassed	TPS61069A	-	4.94	mA	138	$\mu\text{A}$
			MAX17220		Series*	6.18		174	
			Bypassed	MAX17220	-	4.88		82	
			MAX17220		Parallel	6.09		93	
				Series	6.11	103			

Table 5.2: Power budget, worst case scenario.

\*The TPS61096A must be connected in "series" configuration, see section 4.2.2.

Some conclusions that can be obtained from the power budget are:

- Even in the worst case scenario, the highest theoretical current consumption at 3 V is always below 6.5 mA.
- For the peak current calculation, the currents directly drained from  $V_{DD}^H$  (i.e.,  $I_{comp}$ ,  $I_{LS}^o$  and  $I_{TPS}^o$  or  $I_{MAX}^o$ ) are low compared to  $I_{MCU}$  and  $I_{ECD}$ . Hence, modifying the  $V_{DD}^H$  level doesn't affect the peak current consumption that much.
- Another consequence of the previous effect is that the difference when connecting both MAX17220 converters in "series" or "parallel" configuration is not critical for the peak power consumption (6.09 mA vs. 6.11 mA).
- However, in deep sleep state, the ECD current is not present and  $I_{MCU}$  is much smaller. Thus, the deep sleep current is more affected by  $V_{DD}^H$ .

- The trade-off between having a stable MCU voltage and reducing the power consumption (bypassing the first DC converter) becomes more evident, as the current is reduced by about 1.25 mA whenever the first DC is bypassed.

Also, some parameters of the power budget were modified, in order to obtain a more realistic result that still should be an overestimation (table 5.3). First, a linear regression was calculated to extrapolate the maximum supply current of the MCU at a lower frequency of 187.5 MHz. A maximum value of 1.13 mA was obtained with this method, so  $I_{MCU}$  was set to 1.3 mA to be conservative.

Finally, the fact that the feedback branch in the TPS61096A is not always powered was considered. As an assumption, a 10% of duty cycle was supposed, that is, the feedback branch current only is present 10% of the time. Hence, the required deep sleep current is expected to be reduced whenever the TPS61096A is used, as table 5.3 illustrates.

Voltages [V]			Converters configuration			Peak		Deep sleep	
$V_{DD}$	$V_{DD}^L$	$V_{DD}^H$	1st DC	2nd DC	Conn.	Value	Unit	Value	Unit
3	3	6.2	Bypassed	TPS61096A	-	3.52	mA	119	uA
			MAX17220		Series*	4.40		149	
3	3	4.7	Bypassed	TPS61096A	-	3.44	mA	87	uA
			MAX17220		Series*	4.30		110	
		Bypassed	MAX17220	-	3.38	82			
		MAX17220		Parallel	4.22	93			
		MAX17220		Series	4.23	103			
		MAX17220		Series	4.23	103			

Table 5.3: Power budget, more realistic scenario.

\*The TPS61096A must be connected in "series" configuration, see section 4.2.2.

Some additional conclusions comparing tables 5.2 and 5.3:

- The  $I_{MCU}$  current reduction makes the peak current more similar between the different power configurations. In fact, the peak current consumption should always be below 4.4 mA, and bypassing the first converter now only lowers it by 0.9 mA at most (instead of approx. 1.25 mA in table 5.2).
- The deep sleep current when using the TPS61096A was significantly reduced in table 5.3. Moreover, at the same output voltage of  $V_{DD}^H = 4.7$  V, the theoretical deep sleep current is affected by less than 10  $\mu$ A if the second DC converter is changed.

### 5.2.2 Initial tests

Upon arrival of the NFF board, simple tests on some components were done:

- Bring-up of the board, checking that there weren't any shortcircuits.
- Individual test of the DC converters, at no load condition.

- For the MAX17220, the output voltage was a little bit higher than expected: for instance, when the selection resistance was shortcircuited, the output was meant to be 5 V, but was around 5.1 V. This was attributed to low load condition.
- The TPS61096A converter worked well too. With a  $158\text{ k}\Omega$  /  $30\text{ k}\Omega$  feedback branch, the theoretical output should be 6.27 V, and when measuring it with a multimeter, it always was in the 6.25 V to 6.3 V range indeed.

The enable pin feature of the converters was checked as well.

- The MCU was successfully programmed, and able to drive the ECDs which allowed to check the correct mapping of the GPIO nets.
- Individual test of the level shifters, both worked properly.

### 5.2.3 Tests with previous 2-bit printed counter

Before testing the NFF board with a new version of the printed electronics circuit (i.e. the 4-bits counter), initial tests with the previous 2-bit counter were performed (see figure 5.4). The printed circuit worked properly when powered by the NFF board. The power configuration was:

- First MAX17220 bypassed: MCU directly connected to the coin cell battery.
- The TPS61096A converter was chosen, with nominal output 6.27 V<sup>6</sup>.



Figure 5.4: NFF board with previous printed circuit.

Some current measurements were performed, for initial characterization. Of course, these measurements were done only for having an order of magnitude, since this is not

<sup>6</sup>Recall: this circuit worked at 6 V.

the final circuit, nor the ECD. In fact, a multimeter was used, so no information of the time dependency is available. However, these tests allowed to identify some countermeasures for reducing the power consumption. For instance:

- The deep sleep current absorbed by the microcontroller was too high, and this was because the debugging pins were not configured as GPIO.
- 187.5 MHz is a good operating frequency. The current consumption of the MCU at this frequency is about 1.2 mA (quite close to the regression estimation of 1.13 mA). If the frequency is reduced, the power consumption does not drop significantly.
- Connecting 1 M $\Omega$  pull-up resistors at the inputs of the MCU that read the printed electronics outputs is an effective measure for reducing the power consumption. Even though the resistance is quite high, the circuit still works properly, without a significant increase in the delay.

The overall current consumption was found to be less than 100  $\mu$ A in deep sleep, and at most 4 mA while updating the electrochromic display. Note that, since the multimeter does a moving average before displaying the output, the true peak current is higher, but is expected to be present only for a very short time. These values are consistent with the results presented in tables 5.2 and 5.3.

#### 5.2.4 Tests with new 4-bit printed counter

Then, the board was tested with the 4-bit counter, and the custom ECD (described in section 5.1), as shown in figure 5.5. The first test was done at 6.27 V nominal printed electronics supply voltage, and the counter worked properly.

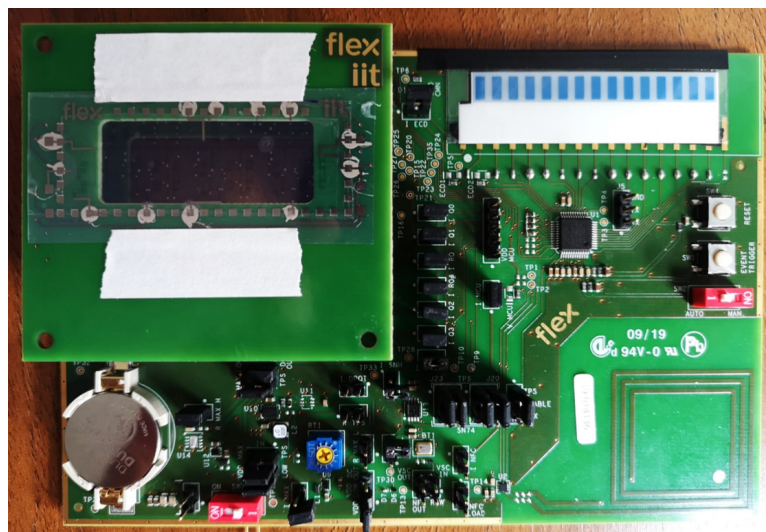


Figure 5.5: NFF board with new 4-bits counter.

Additionally, the overall delay (from the point in which the MCU modifies the clock pins to the moment in which the GPIOs for reading the counter outputs had changed) was measured as well. This includes delays in the level-shifter, the PEC itself, and the comparator. Several measures were performed in different counters at 6.27 V supply voltage, and said delay never exceeded 200 ms. The MCU was configured to wait 500 ms before reading the counter outputs, just to be conservative.

### 5.2.5 Oscillator output

In one of the tested PEC, the on-chip oscillator was a ring oscillator of 7 stages. It was measured, showing a period of approximately 60 ms, with a stage delay of about 8.5 ms at nominal 6.27 V operation (figure 5.6).

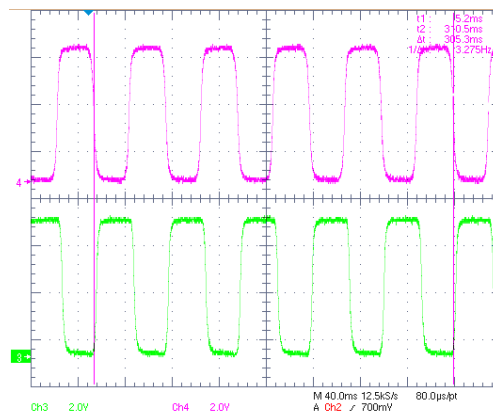


Figure 5.6: Oscillator outputs: original and inverted signals.

This frequency is just too fast for updating the displays, which switching time is in the order of seconds. There are two possible workarounds for this situation:

- Implement a modification in firmware, so that the automatic mode display update is triggered each a certain number of oscillations (for instance, 30 cycles for an updating period of 1.8 s).
- The IIT has been able to produce a slower relaxation oscillator, which period is in the order of 4 s. The final demonstrator could incorporate this oscillator instead of the ring one.

The first approach was later implemented by firmware, with a configurable number of clock divisions, and was properly tested in the NFF board. The IIT, at the same time, also produced oscillators with periods of about 500 ms, which is low enough to trigger the counter. An interesting test was done in one of the NFF boards: a header was soldered, which allowed to directly connect the oscillator outputs to the clocks of the counter. Then, the microcontroller updated the ECD accordingly. This shows that the printed oscillator is capable of driving the counter.

### 5.2.6 Digital potentiometers

The I2C driver worked properly with both digital potentiometers, and their resistance changed as expected.

- The MAX17220 output was correctly tested for the range 2.8 V to 5 V, with a 100 mV step. The output load consumes only some tens of  $\mu\text{A}$ , so the output of the converter was always found a bit higher (around 50 mV to 100 mV), in order to prevent a huge voltage drop if the load current increases (the same kind of result commented on section 5.2.2).
- The TPS61096A output regulation failed, due to a schematic error. The digital potentiometer had different resistance options, and the Flex's database component was 5 k $\Omega$ , while it was supposed to be 50 k $\Omega$ . The output of the converter always saturated at the high level (around 28 V), as expected given this error.

Since the voltage regulation was only an extra feature, the last item wasn't fixed. As a result, the NFF allows to power up the printed circuit with:

- Firmware-controlled voltage from 2.8 V to 5 V, using the MAX17220.
- Fixed voltage, nominal 6.27 V, using the TPS61096A. The nominal output can be modified by replacing a resistor.

Four printed counters were tested for different supply voltages. All of them worked at 6.27 V, and two even worked down to 3 V. Testing them at 4 V generally gave positive results, but sometimes the counter was slower, so that the third and fourth bits were still changing when the MCU read the output, resulting in a logic fail.

### 5.2.7 NFC

#### I2C interface

As with the digital potentiometers, a driver for the I2C commands of the NFC was coded. All the following commands (as indicated in the datasheet [55]) were developed and successfully tested:

- **Read:** receives the address of a 16-bytes page, and returns the data in said page.
- **Write:** stores a page of 16 bytes in the NFC. Depending on the specified address, the page can be stored into volatile (SRAM) or non-volatile (EEPROM) memory, and it can be a configuration register.
- **Read register:** gets a single register from the session registers, which are the parameters used in the current communication session (i.e. volatile parameters).
- **Write register:** modifies one of the session registers.

The main difference between the configuration registers and the session registers is that the last ones contain the effective parameters within the current communication session, while the former are the default parameters after power on reset (POR). On reset, the configuration registers are loaded into the session registers.

The most useful register for this project are: the `NC_REG`, which controls, for instance, when to turn on and off the field detection pin, and the `LAST_NDEF_BLOCK`, that indicates the I2C address in which the NFC Data Exchange Format (NDEF) message ends. The FD pin is an input to the MCU, and is able to trigger an interrupt.

### Antenna tuning

From the point of the radio frequency (RF) interface, the NFC standard works at 13.56 MHz. The matching network used was a simple capacitance in parallel with the antenna (figure 5.7). The capacitors were set as not mounted in order to tune the antenna once the NFF was received.

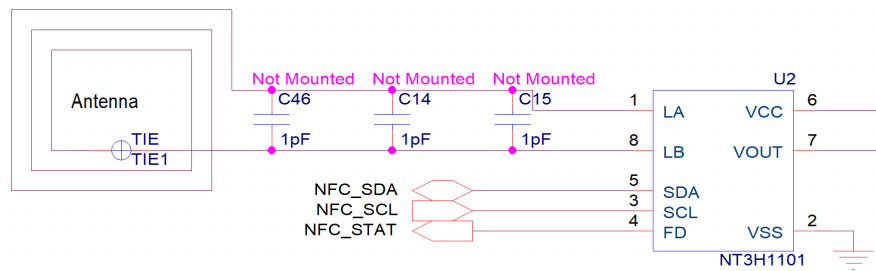


Figure 5.7: NFC matching network schematic.

The theoretical resonance frequency of the antenna circuit is given by:

$$f_{res} = \frac{1}{2\pi\sqrt{L \cdot C_{eq}}}$$

where  $L$  is the inductance of the antenna (at the operating frequency) and  $C_{eq}$  is the equivalent capacitance, that is: the total external capacitance, plus the internal capacitance of the NFC, illustrated in table 5.4.

	Min	Typ	Max	Unit
$C_{IN}$	44	50	56	pF

Table 5.4: Internal capacitance of the NFC.

The physical characteristics of the antenna are:

- Shape: 31 mm square, 3 turns.
- Trace width of 1 mm, with 1 mm spacing.
- Simulated inductance: 450 nH, done with an STMicroelectronics toolbox [57].

According to the recommendations present in [58], the target frequency was set to 13.7 MHz. Hence, the external capacitance to be connected (assuming the NFC internal capacitance is its typical value: 50 pF) is theoretically 256 pF.

Three C0G capacitors, of values: 220 pF, 15 pF and 15 pF were soldered in parallel, making a total capacitance of 250 pF, in six different boards. The resonance frequency was then measured with a network analyzer, and it was around 13.59 MHz<sup>7</sup>.

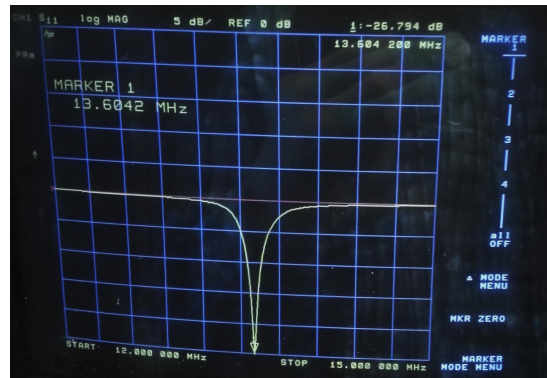


Figure 5.8: NFC resonance frequency. Taken with an HP8753D network analyzer.

The difference with respect to the theoretical 13.7 MHz value can be explained by a combination of the following factors:

- An error in the estimation of the inductance. Since all the measured resonance frequencies were below 13.7 MHz, most probably the real inductance value was higher than 450 nH (and it may even be depending on the board itself).
- Tolerance of the external capacitors connected.
- Different values of the input capacitance of the NFC.

Despite the above considerations, the obtained resonance frequencies are good enough: all the the tags were able to be detected by a GoToTags NFC reader. Hence, the antenna was considered as successfully tuned on all boards.

### Communication with a cellphone

A function for writing an NDEF message into the NFC was coded and tested. The MCU was configured to write the message: “Smart Data Label demo. The counter value is: XY.” where XY denotes the current count. Each time the ECD is updated with a new value, said value is stored into the NFC memory for future communication with a phone.

The function implementation was successful, and an Android phone was able to read the NDEF message from the different NFF boards (despite the differences in resonance

<sup>7</sup>The values obtained were: 13.51 MHz, 13.52 MHz, 13.58 MHz, 13.60 MHz (figure 5.8), 13.64 MHz and 13.66 MHz.

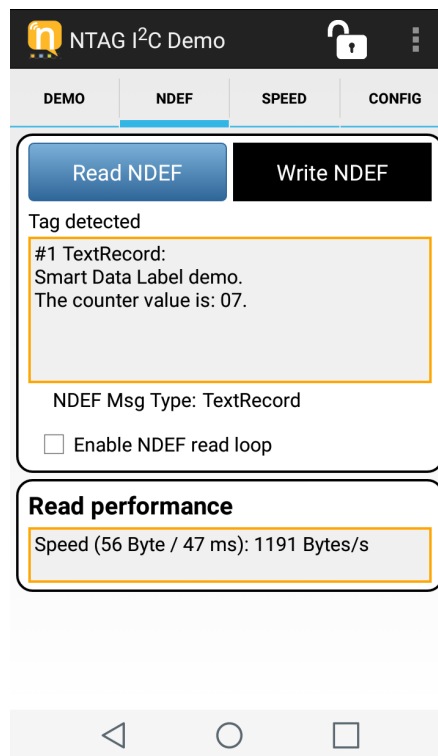


Figure 5.9: NTAG I2C Demo app.

frequency already commented). This test was done by downloading the NTAG I2C Demo app (figure 5.9), developed by NXP, on an LG phone<sup>8</sup>.

### Energy harvesting capability

The NT3H1101 NFC supports energy harvesting, e.g. extracts energy from the electromagnetic field generated by the NFC reader (or in this case, the phone), that can be used to energize a low-power circuit.

According to the datasheet [55], typically the chip can provide 5 mA at 2 V output powered with a phone<sup>9</sup>, but logically the power delivery depends on the inductive coupling, that is:

- The strength of the RF field.
- The shape of the tag antenna (the size used was not standard, but its area is between a class 3 and a class 4 antenna).
- The distance from the NFC phone.

Since the consumption of the circuit is about 4 mA at 3 V, which is higher than the typical 10 mW exposed in the datasheet, the board was powered by the NFC without

<sup>8</sup>The same test was also tried with a Huawei P8 Lite, but the power transmitted to the NFC wasn't high enough to enable the communication.

<sup>9</sup>For more details in the energy harvesting documentation, see the Application Note AN11578 [59].

any expectations. Surprisingly, the electromagnetic field was able to power up the whole board, even if: the MCU frequency was 6 MHz, the MAX5419 digital potentiometer was enabled, and an extra red LED indicating that the MCU is powered up was present.

When powering the board with the NFC, the NTAG output was directly tied to VDD\_LOW (passing through a diode), so the first DC converter was not needed (recall figure 4.4). The output of the NTAG was equal to 2.97 V, and after the diode drop, the supply voltage to the MCU was  $VDD\_LOW = 2.74$  V, which doesn't stress that much the ECDs.

### 5.3 Flexible battery

The chosen flexible batteries were purchased from Imprint Energy. Some of the advantages are that they are fully printed, low thickness ( $< 0.6$  mm) and their proprietary *ZincPoly*<sup>™</sup> technology allows the production of rechargeable batteries (even though the ones acquired are primary cells).

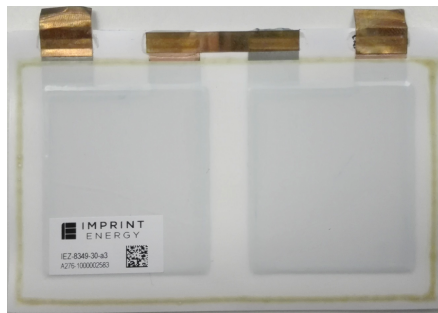


Figure 5.10: Flexible battery from Imprint Energy.

Moreover, they have been successfully tested at 400 ms pulses of 45 mA. Since the circuit uses DC converters and the current absorbed from the battery will always be extracted in the form of quick pulses, this was a huge advantage. Also, they're two nominal 1.5 V cells already connected in series (see figure 5.10), so they could be directly used to power up the MCU without the need of the first DC converter.

Upon arrival of the batteries, the open circuit voltage was measured in one of them, and it was 2.88 V. Then, said battery was connected both to the NFF with the 2-bits counter, and the one with the 4-bits counter. In all the measurements, a few seconds after disconnecting the battery from the circuit, it's voltage had dropped by 50 mV at most, and was slowly recovering the original open-circuit voltage.

The battery was tested for all the possible power configurations in which the PEC worked (without active I2C interface), and it was always able to power up the circuit. This shows that the implementation in a flexible board is feasible for any combination of DC converters. An even further reduction of the power consumption will therefore only affect the duration of the demonstrator, but it's not critical for its functional behaviour.

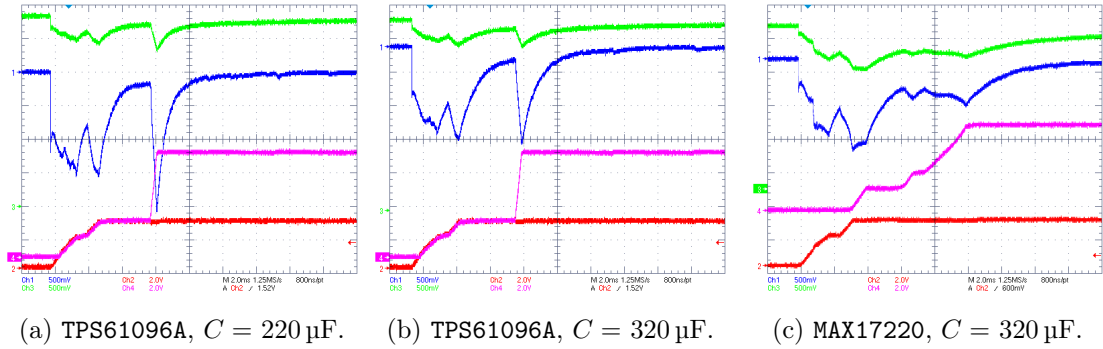


Figure 5.11: Startup current. CH1: supply current (scale: 35 mV/mA). CH2: 1st DC converter output. CH3: battery voltage. CH4: 2nd DC converter output.

### 5.3.1 Current extracted from the battery

#### Startup current

Originally, the bypass capacitance for maintaining the battery voltage was set to  $220 \mu\text{F}$  (two  $100 \mu\text{F}$  and two  $10 \mu\text{F}$  capacitors in parallel). The current extracted from the flexible battery was measured in the worst case scenario: 1st DC converter not bypassed, 2nd DC converter corresponding to the TPS61096A, with nominal output of 6.27 V. In this conditions, the startup current reached  $60.7 \text{ mA}^{10}$  (see figure 5.11a).

Since the battery datasheet only contained information up to 45 mA pulses, an extra  $100 \mu\text{F}$  capacitor was connected in parallel, in order to reduce the peak current. With this modification, the startup current was reduced to  $44.7 \text{ mA}^{11}$ , as figure 5.11b shows. In both cases (figures 5.11a and 5.11b), the startup phase lasts about 10 ms, and the peak current occurs when the 2nd DC converter is turned on.

Then, the current with the MAX17220 option for the second converter (with nominal output 5 V) was measured. As it can be seen in figure 5.11c, the MAX17220 is slower than the TPS61096A, in fact the startup phase lasts longer: around 15 ms. There's no significant reduction in peak startup current, it is  $41.5 \text{ mA}^{12}$ .

Finally, a last check that was done when measuring the startup current was the calculation of the battery series resistance, which was found to be  $8.5 \Omega$ . This value is consistent with the measurements performed at Imprint Energy. Note that in order to measure the current, a  $1 \Omega$  resistor was connected in series with the battery, so the results obtained are not totally accurate compared to the case in which said resistance is not present.

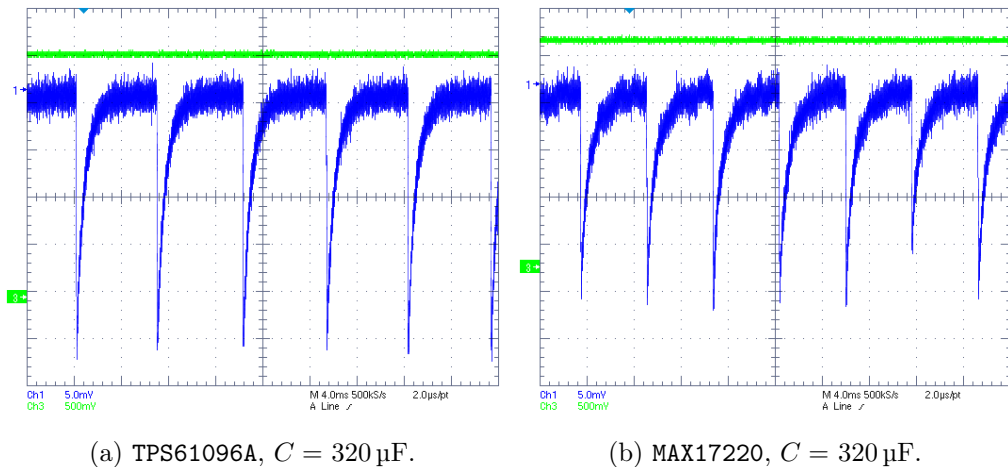
<sup>10</sup>Five measurements were performed. The average was 60.68 mA, with a 4.43 mA standard deviation.

<sup>11</sup>Again, 5 measurements were done: average 44.73 mA, standard deviation of 3.20 mA.

<sup>12</sup>Average: 41.52 mA. Standard deviation: 1.30 mA. Note that the variance is significantly smaller, which means that the MAX17220 option is more reliable in terms of consistent power consumption.

### Deep sleep current

As expected, the deep sleep current required from the battery consists on peaks, due to the presence of the DC converters (see figure 5.12). Comparing the two DC converter options, the peak current of the MAX17220 is lower (at most  $750\ \mu\text{A}$ , compared to  $900\ \mu\text{A}$  for the TPS61096A), but the frequency of the signal peaks is higher (approximately  $180\ \text{Hz}$  instead of  $142\ \text{Hz}$ ). As a result, the average current consumption is similar, in the order of  $100\ \mu\text{A}$ <sup>13</sup>.



(a) TPS61096A,  $C = 320\ \mu\text{F}$ .

(b) MAX17220,  $C = 320\ \mu\text{F}$ .

Figure 5.12: Deep sleep current.

CH1: supply current (scale:  $35\ \text{mV}/\text{mA}$ ). CH3: battery voltage.

### ECD update

Figure 5.13 shows the total current of the board when the ECD is being updated. Logically, that screen capture doesn't allow to do any precise calculation, but it can be used to identify the general shape of the current curve. Small peaks are seen when each of the segments is turned on (every  $\approx 1.75\ \text{ms}$ ), and a higher peak occurs when all of them are turned off. The signal seems to be noisy, because all the current is proportioned in the form of peaks absorbed by the 1st DC converter's input.

<sup>13</sup>The average current in the MAX17220 case is  $106\ \mu\text{A}$ , and in the TPS61096A is  $95\ \mu\text{A}$

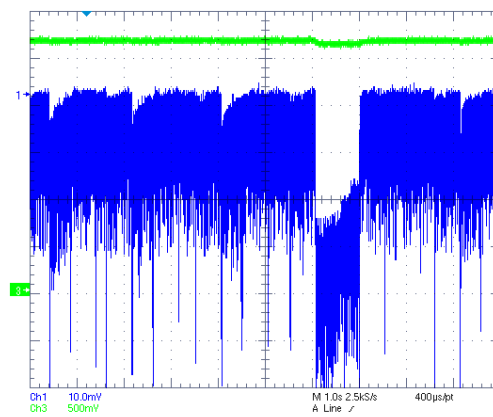


Figure 5.13: ECD update current.  
CH1: supply current (scale: 35 mV/mA). CH3: battery voltage.

## Chapter 6

# Flexible board

### 6.1 Implications of the NFF tests

In this section, the some results from the previous chapter<sup>1</sup> are summarized. These are the key aspects which affect the design decisions taken for the flexible board, or provide additional requirements for it.

- The overall current measurement tests show that the two alternatives: TPS61096A y MAX17220 are not so different in terms of power consumption, especially during the deep sleep state. This encourages to choose the most reliable alternative, i.e. the one that ensures the PEC will work in the flexible board.
- The possibility to test the PEC at lower voltages was indeed useful, as some printed circuits even worked down to 3 V supply voltage. However, the 6 V operation is still more reliable.
- Similarly, the 1.5 V parallel or 3 V series battery (almost) doesn't affect the power consumption (even though it obviously affects the current consumption). The fact that the acquired battery is already in series configuration is a reason for preferring the 3 V alternative.
- The NFC is capable of delivering the current to power up the whole circuit. If the NFC is used, the clock frequency of the MCU can't be 187.5 kHz, and it must be increased (6 MHz was used for the tests).
- A 1 k $\Omega$  resistor in series with the common electrode of the custom display sample didn't present a significative increase in switching time, while being effective for reducing the peak current across the display.
- Connecting external pull-up resistors of value 1 M $\Omega$  for the input signals<sup>2</sup> didn't make the signal changes too slow (so that a reading problem could occur). Therefore, they provide a good trade-off between low power consumption and correct behaviour of the circuit.

---

<sup>1</sup>And also from other tests who weren't included in the thesis, for simplicity.

<sup>2</sup>Basically, the printed electronic circuit outputs.

- The start-up current test showed that an additional 100  $\mu\text{F}$  capacitor effectively reduces the initial current. However, the default bypass capacitance of 220  $\mu\text{F}$  was already high enough for the flexible battery to power up the circuit. There's not enough data to ensure that lowering the start-up current will significantly increase the duration of the battery, nor that the 100  $\mu\text{F}$  capacitor is the optimal solution.

## 6.2 Design process

### 6.2.1 Design decisions

#### NFC

Although the NFC was capable of powering the NFF board, it was removed from the flexible board, because:

- According to the ultimate aim of the project (a fully printed label for an MDI), having to touch the device with a phone each time the inhaler is sprayed is not user-friendly, so an always present power supply is more comfortable.
- Besides, the flexible battery was preferred in order to highlight the usage of printed electronics technologies (one of the goals presented in section 1.3).
- It occupies space.
- Both the communication with a phone and the energy harvesting capability can be shown in the NFF board.

However, in future projects (e.g. smart labels not focused on MDI applications) it's always possible to power-up the circuit only with an NFC instead of a printed battery, if desired.

#### Power module

- The TPS61096A DC converter was preferred for generating the PEC supply voltage, taking into consideration what was said in section 6.1, and that the printed technology has been reliably tested at 6 V for more time.
- Similarly, the nominal voltage chosen as output of the TPS61096A was 6.27 V, just to be cautious. It can be changed by replacing a single resistor.
- The batteries were connected as Imprint Energy provided them: in series 3 V configuration.
- In order to have a stable MCU voltage, the first DC converter (MAX17220) was **not** bypassed, and its target output was set to 2.7 V in the flexible board in order to avoid stressing the ECDs.

- Nevertheless, given that the duration of the demonstrator is not yet known and bypassing the previous DC converter could help to improve it, a not mounted resistor was added, which connects the input and output of the converter. If further tests determine that it's better to reduce the power consumption rather than having a stable ECD operating voltage, the MAX17220 can be removed<sup>3</sup>.
- Due to the considerations made in section 6.1, the default 220  $\mu$ F bypass capacitance was left, but an additional not mounted capacitor was connected in parallel in order to increase it if required.

### Digital potentiometers

The digital potentiometer was removed because:

- It's an unnecessary power consumption waste. Not only because it requires current to operate, but also since the MCU needs to be clocked at higher frequency in order to manage the I2C module.
- The MCP4017 potentiometer, the one for the TPS61096A, wasn't successfully tested (see section 5.2.6).
- The NFF board already allows to demonstrate the integration of a digital potentiometer (the MAX5419).

### Other minor open points

- The series resistance of the display, and the pull-up resistors were updated according to the values present in section 6.1.
- In order to program the microcontroller, the 5-pin header approach was maintained. The header can be desoldered after programming and, if needed, the MCU can be re-programmed by contacting the programmer via test points.

### 6.2.2 Schematic

The following modifications were made to the NFF board schematic in order to migrate to the FPC version:

- Replacement of components with a smaller footprint version: DC converters, level shifter, comparators, slide switches and push button, and the microcontroller.
- Many components were removed. As already said, the digital potentiometers and NFC. But also an UART connector that was in the NFF for debugging purposes, multiple test points and all the current measurement headers.

---

<sup>3</sup>However, there are other methods for reducing the power consumption of the flexible board. Certainly, the most effective one is updating the firmware: currently, the loaded fw turns on all the segments up to the counter value (e.g. if the count is 6, 6 segments are turned on), which generates a high current peak when an overflow occurs (figure 5.13). By turning on one segment at a time, this is avoided.

- The already commented design decisions, in particular the ones concerning the power module, were implemented.

With this done, the final block diagram of the flexible board is shown in figure 6.1. The DC converter and level shifter were intentionally merged into a single big block, in order to emphasize that both functions are done by the same IC: the TPS61096A. The schematic can be found in appendix B.

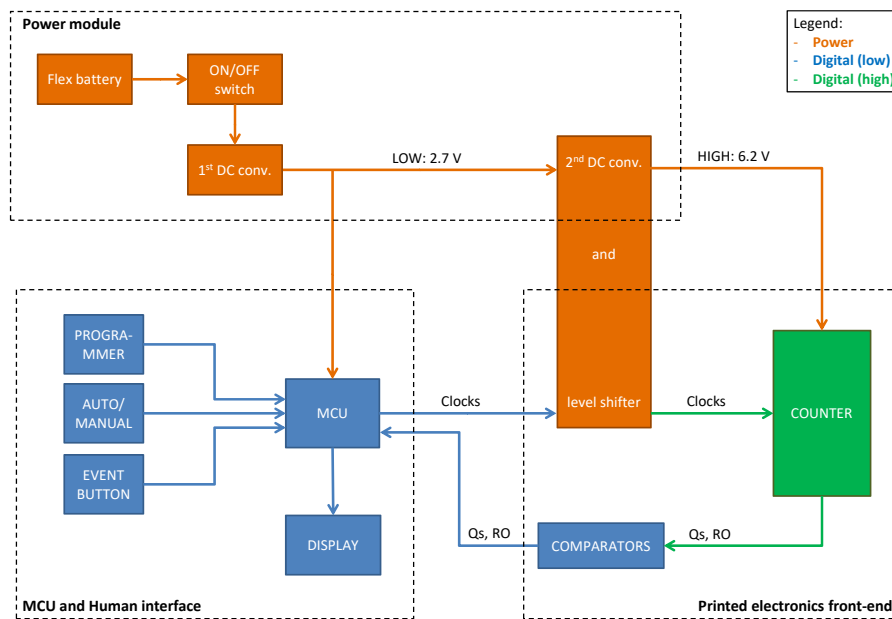


Figure 6.1: Flexible board Block diagram.

### 6.2.3 PCB layout

The PCB layout was developed by Ennio Bandera at Flex. The spatial arrangement was done in collaboration with the Industrial Design department. Note that, for the final flexible board, no fixture board was needed. That is, all the components were directly integrated into a single main board.

The final layout is shown in figure 6.2. On the uppermost part, top side, there's the battery, which surpasses the outline of the board itself. Right below the battery, comes the ECD<sup>4</sup>. Finally, at the nethermost (but always on the top side), there's the test chip. All the other components, except the switches and the programming header, were located at the bottom side of the board.

<sup>4</sup>Not mounted LEDs and their corresponding series resistors were added as well, in order to display the count by using them instead of the ECD, if desired.

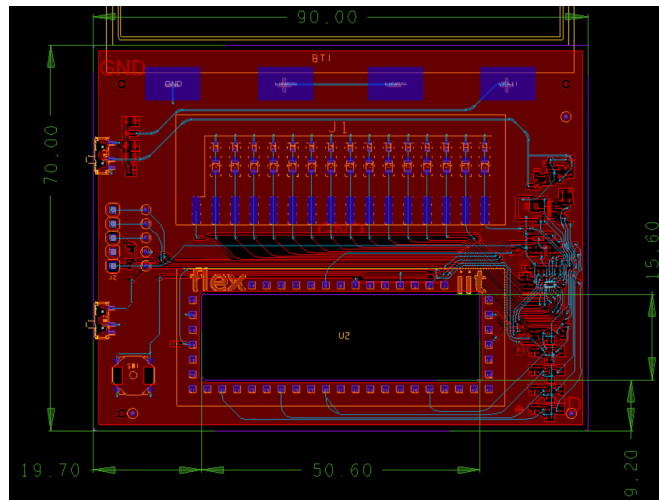


Figure 6.2: Flexible board layout.

### 6.2.4 Demonstrator Showcase

The Industrial Design department at Flex developed a showcase for mounting the board. The FPC is wrapped around a cylinder, in order to show its flexibility (figure 6.3). The material used was PMMA, so the overall weight of the showcase is estimated as approximately 830 g considering a density of  $1.18 \text{ g/cm}^3$ .

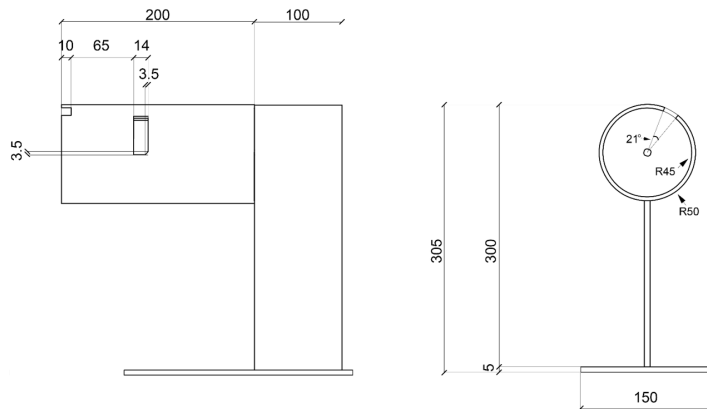


Figure 6.3: Demonstrator showcase. Only some of the quotes are present in this image. All lengths are in mm.

This showcase also was designed in order to leave a space for explaining labels, which briefly describe the three printed electronics technologies: the flexible battery, the electrochromic display and the printed circuit (obviously emphasizing the latter).

## 6.3 Testing and results

Upon arrival of the flexible boards, the following procedure was performed:

- Bring-up: visual inspection and continuity tests.

- Check that the MCU was able to be programmed. This was a major concern, since the board had some "vias in pad" that could encumber its soldering process (figure 6.4).
- After uploading the firmware, the supply voltage of the printed electronics, as well as the transient behaviour of the clock pads, were checked. This showed that the level shifter inside the TPS61096A was working correctly.
- Finally, the board was fed with a power supply at 2V, and the MCU voltage was measured. As expected, the VDD\_LOW voltage level was between 2.7V and 2.8V for all the tested boards, which confirms that the MAX17220 DC converter was working properly.

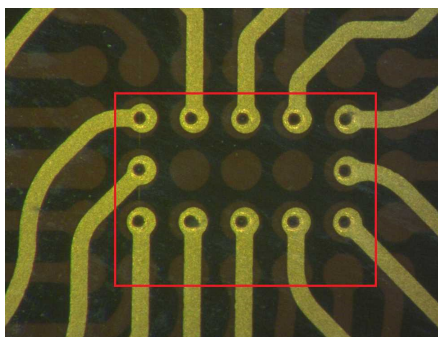


Figure 6.4: Vias in pad.

Later, the ECDs were pasted. Three different pasting methods were tested:

1. The same isotropic glue that had been used in the past: the CW2400 [48].
2. An anisotropic glue: the 124-19A/B2713 from Creative Materials [60].
3. A Z-axis conducting adhesive.

The CW2400 worked, but since it's isotropic (i.e. conducts electricity in all directions) it was quite easy to short different pins of the electrochromic display, so that two segments turned on when only one of them was supposed to<sup>5</sup>. Nevertheless, since the printed electronic circuit was designed in such a way that the used pads are never consecutive, this method was considered suitable for fixing the PEC.

On the other hand, the 124-19 is anisotropic, which means that after curing, it only conducts in the Z direction (orthogonal to the board plane). This is a very interesting feature, since it would allow to avoid the above mentioned problem. However, using this glue resulted in the following problems:

- With room temperature curing for 24 hours, only some of the pads were electrically connected. Currently Flex is in contact with Creative Materials in order to understand why this happened.

<sup>5</sup>The very same problem also occurred with another silver epoxy: the 8330S-21G from MG Chemicals (datasheet: [61])

- The mixing ratio of both parts is 100:58, which is difficult to measure precisely.
- The bond strength is so high that is hard to remove a display without delaminating it (see figure 6.5).



Figure 6.5: Delaminated display.

Due to these reasons, the anisotropic epoxy adhesive was considered risky, and the other options were preferred. The Z-axis adhesive was found to be the most practical solution in terms of correct application. But, since the bond strength is not so tight, it tends to detach with time, increasing its internal equivalent resistance. As a consequence, the display segments don't turn on properly (they require a higher switching time). Therefore, the final demonstrators were approached in two different ways:

- Using the CW2400, and leaving some pins shorted, or pasting the displays a couple of times until there aren't any short circuits.
- Attaching them with the Z-axis conducting adhesive, and pressing the contact area before showing the functionality of the demonstrator, in order to reduce the series resistance.

Another observed issue is that the vertical 5-pin header for programming the MCU tended to break the tracks when the programmer was taken out. As a result, in some boards the header was replaced by a 90-degree alternative, and further copper wires were soldered from the header pins to the test points, as figure 6.6 illustrates.

Even though some electrical connections (programmer and FPC) are not very practical, the battery can be perfectly soldered, with no connection issues, and the CW2400 works well for attaching the PEC. Moreover, the electronic design of the FPC was successful, so this board was able to fulfill its main objective: being a flexible demonstrator that integrates three different printed electronics technologies.

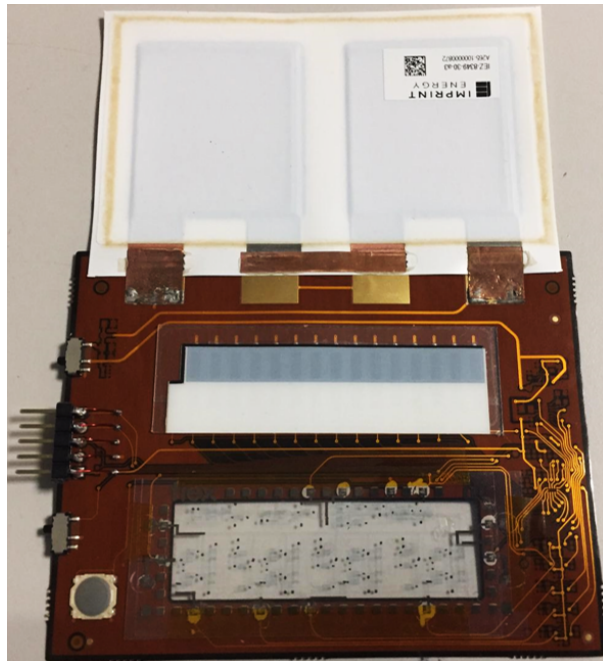


Figure 6.6: Flexible demonstrator.

## Chapter 7

# Conclusion and remarks

During this phase of the project, a flexible demonstrator integrating three different printed electronics technologies (a flexible battery, an electrochromic display and a printed digital circuit) was successfully developed. Even though this project is intended for usage in the context of Smart Labels for metered-dose inhalers, the incorporated technologies promise a wide range of applications.

The design process was quite linear:

- The end of the first phase of the project established three short term improvements, which included testing the PEC at lower voltages, and designing a flexible board. Additional goals were proposed by Flex: usage of a printed battery and electrochromic display, as well as including optional MCU-controlled voltage, and NFC with energy harvesting capabilities.
- A non-form-factor board was designed in order to fulfill the above mentioned goals (listed in section 4.1). The NFF board also included different power supply options, in order to test the PEC in the full 3 V to 6 V supply range, and measure the current consumption. All the features were successfully tested<sup>1</sup>.
- Based on the tests performed in the NFF board, a flexible printed circuit (which schematic was basically a subset of the NFF one) was designed and manufactured. The flexible battery was simply soldered to the board, while the ECD and the PEC were attached using conductive adhesives. Apart from unpractical attachment of the ECD, the flexible board was considered a success.

It's also important to notice that even though the main objective of the project was to just design a flexible board, the development of an NFF board allowed not only to mitigate the risk, but also to end up with two demonstrators, which offer different purposes:

1. The NFF board, with expanded functionality:
  - NFC with incorporated energy harvesting, which is able to power up the whole board, as well as showing connectivity with an external cellphone.
  - Variable PEC operating voltage: firmware-controlled 2.8 V to 5 V, or fixed 6.27 V nominal output.

---

<sup>1</sup>Apart from the MCU-regulated TPS61096A output, as explained in section 5.2.6.

- It's compatible with the previous 2-bit version of the counter.
  - Simple hardware modifications on the board allow to show that the oscillator is able to drive the counter, by directly connecting the oscillator outputs to the clocks. This was successfully tested in one of the boards (at 6.27 V nominal voltage).
2. The FPC board, with limited functionality, but is a more user-friendly demonstrator which also integrates a flexible battery. It can also be mounted into the designed showcase, for illustration of the flexibility of its components, and a brief description the printed electronics technologies involved.

Since this is an intrinsically interdisciplinary project concerning different parties, only saying that the author was the main developer from the Flex point of view is not precise enough. Just to clarify, a summary of the most important contributions of the author is given below:

- For both the NFF and the FPC boards:
  - Schematic design and consumption estimation.
  - Firmware development, including all the required drivers.
  - Due to Flex's policy, the layout was not designed by the author, but obviously he participated in the layout review, i.e. in an active collaboration with Flex's "layoutists".
  - Board bring-up and testing.
  - Integration of the ECD and PEC, trying different conductive adhesives. In particular, this item was always performed in collaboration with Paolo Colpani, from the IIT.
- Characterization of RISE Acreo and Ynvisible electrochromic displays, as well as identifying Pros and Cons.
- Benchmark and acquisition of displays and batteries.
- The showcase was not designed by the author, but by Ruben Gandus, from the industrial design department of Flex. As occurred with the layouts, the author did participate in design reviews, since the design of the showcase is strictly related to the flexible board layout.

It's also worth mentioning that even though this is a Research & Development project, the "research" part was mostly done by the Italian Institute of Technology, while the author's work was limited to an almost pure "development" contribution. However, the author maintained a very close relation with the IIT during his internship at Flex, and managed to understand their internal processes (to a basic level), but this thesis doesn't include too many details on this topic due to confidentiality issues.

Finally, a list of the future steps for this project (which are the author's comments, and don't necessarily represent the direction Flex is going to take) is detailed:

- From the IIT side, further work in increasing the process reliability is required. In particular, concerning the device yield, the reduction of the operating voltage and the accuracy of the printed oscillators. To the date, devices from the same printing run are still presenting some differences in performance.
- From the Flex side, the goals of the next phase of the project shall be defined. Possible objectives include the development of a prototype in which a low-to-high level shifter is not anymore required<sup>2</sup>, or designing the electrochromic display at either Flex or the IIT, instead of depending on an external supplier.
- From a practical point of view, the flexible board can still be improved, by finding a better conductive adhesive solution. Moreover, it would be useful to measure the duration of the battery for better characterization. It's also an option to acquire rechargeable batteries<sup>3</sup>, so that the measurement of said duration doesn't require an irreversible discharge that would make the battery useless after the test.

---

<sup>2</sup>The NFF allows to try this configuration, but unfortunately, it didn't work properly for any of the devices under test.

<sup>3</sup>Recall Imprint Energy's proprietary ZincPoly™ technology allows the manufacturing of secondary cells.

# Bibliography

- [1] T. Borghi, “Smart data logger technology scouting report (company confidential)”, Flex Milan, Tech. Rep., 2015.
- [2] Food and Drug Administration. (2003). Integration of Dose-Counting Mechanisms into MDI Drug Products, [Online]. Available: <https://www.fda.gov/media/71073/download>. (accessed: 09.07.2019).
- [3] Printed and Molecular Electronics team, “Smart data label: End project report (confidential)”, Istituto Italiano di Tecnologia, Tech. Rep., 2018.
- [4] H. Shirakawa, E. J. Louis, A. G. MacDiarmid, C. K. Chiang, and A. J. Heeger, “Synthesis of electrically conducting organic polymers: Halogen derivatives of polyacetylene, (ch)<sub>x</sub>”, *J. Chem. Soc., Chem. Commun.*, pp. 578–580, 16 1977. DOI: [10.1039/C39770000578](https://doi.org/10.1039/C39770000578).
- [5] K.-J. Baeg, M. Caironi, and Y.-Y. Noh, “Toward printed integrated circuits based on unipolar or ambipolar polymer semiconductors”, *Advanced Materials*, vol. 25, no. 31, pp. 4210–4244, 2013. DOI: [10.1002/adma.201205361](https://doi.org/10.1002/adma.201205361).
- [6] J. D. MacKenzie and C. Ho, “Perspectives on energy storage for flexible electronic systems”, *Proceedings of the IEEE*, vol. 103, no. 4, pp. 535–553, Apr. 2015, ISSN: 0018-9219. DOI: [10.1109/JPROC.2015.2406340](https://doi.org/10.1109/JPROC.2015.2406340).
- [7] S. D. Jones and J. R. Akridge, “A thin film solid state microbattery”, *Solid State Ionics*, vol. 53-56, pp. 628–634, 1992, ISSN: 0167-2738. DOI: [10.1016/0167-2738\(92\)90439-V](https://doi.org/10.1016/0167-2738(92)90439-V).
- [8] H. Cha, J. Kim, Y. Lee, J. Cho, and M. Park, “Issues and challenges facing flexible lithium-ion batteries for practical application”, *Small*, vol. 14, p. 1702989, Dec. 2017. DOI: [10.1002/smll.201702989](https://doi.org/10.1002/smll.201702989).
- [9] Y. H. Kwon, S.-W. Woo, H.-R. Jung, H. K. Yu, K. Kim, B. H. Oh, S. Ahn, S.-Y. Lee, S.-W. Song, J. Cho, H.-C. Shin, and J. Y. Kim, “Cable-type flexible lithium ion battery based on hollow multi-helix electrodes”, *Advanced Materials*, vol. 24, no. 38, pp. 5192–5197, 2012. DOI: [10.1002/adma.201202196](https://doi.org/10.1002/adma.201202196).
- [10] Y. Yang, S. Jeong, L. Hu, H. Wu, S. W. Lee, and Y. Cui, “Transparent lithium-ion batteries”, *Proceedings of the National Academy of Sciences*, vol. 108, no. 32, pp. 13013–13018, 2011. DOI: [10.1073/pnas.1102873108](https://doi.org/10.1073/pnas.1102873108).

- [11] A. M. Gaikwad, A. M. Zamarayeva, J. Rousseau, H. Chu, I. Derin, and D. A. Steingart, “Highly stretchable alkaline batteries based on an embedded conductive fabric”, *Advanced Materials*, vol. 24, no. 37, pp. 5071–5076, 2012. DOI: [10.1002/adma.201201329](https://doi.org/10.1002/adma.201201329).
- [12] G. Kettlgruber, M. Kaltenbrunner, C. M. Siket, R. Moser, I. M. Graz, R. Schwödiauer, and S. Bauer, “Intrinsically stretchable and rechargeable batteries for self-powered stretchable electronics”, *J. Mater. Chem. A*, vol. 1, pp. 5505–5508, 18 2013. DOI: [10.1039/C3TA00019B](https://doi.org/10.1039/C3TA00019B).
- [13] D. Wei, D. Cotton, and T. Ryhänen, “All-solid-state textile batteries made from nano-emulsion conducting polymer inks for wearable electronics”, *Nanomaterials (Basel, Switzerland)*, vol. 2, no. 3, pp. 268–274, Aug. 2012, ISSN: 2079-4991. DOI: [10.3390/nano2030268](https://doi.org/10.3390/nano2030268).
- [14] S. Pang, Y. Gao, and S. Choi, “Flexible and stretchable biobatteries: Monolithic integration of membrane-free microbial fuel cells in a single textile layer”, *Advanced Energy Materials*, vol. 8, no. 7, p. 1702261, 2018. DOI: [10.1002/aenm.201702261](https://doi.org/10.1002/aenm.201702261).
- [15] V. L. Pushparaj, M. M. Shaijumon, A. Kumar, S. Murugesan, L. Ci, R. Vajtai, R. J. Linhardt, O. Nalamasu, and P. M. Ajayan, “Flexible energy storage devices based on nanocomposite paper”, *Proceedings of the National Academy of Sciences*, vol. 104, no. 34, pp. 13574–13577, 2007, ISSN: 0027-8424. DOI: [10.1073/pnas.0706508104](https://doi.org/10.1073/pnas.0706508104).
- [16] N. Singh, C. Galande, A. Miranda, A. Mathkar, W. Gao, A. L. M. Reddy, A. Vlad, and P. M. Ajayan, “Paintable battery”, *Scientific Reports*, vol. 2, p. 481, Jun. 2012. DOI: [10.1038/srep00481](https://doi.org/10.1038/srep00481).
- [17] A. M. Gaikwad, D. A. Steingart, T. Nga Ng, D. E. Schwartz, and G. L. Whiting, “A flexible high potential printed battery for powering printed electronics”, *Applied Physics Letters*, vol. 102, no. 23, p. 233302, 2013. DOI: [10.1063/1.4810974](https://doi.org/10.1063/1.4810974).
- [18] M. Tatsumisago, F. Mizuno, and A. Hayashi, “All-solid-state lithium secondary batteries using sulfide-based glass–ceramic electrolytes”, *Journal of Power Sources*, vol. 159, no. 1, pp. 193–199, 2006, Special issue including selected papers from the 3rd International Conference on Materials for Advanced Technologies (ICMAT 2005, Singapore, Malaysia) and the Summer School on Synthesis of Nanostructured Materials for Polymer Batteries (Augustów, Poland) together with regular papers, ISSN: 0378-7753. DOI: [10.1016/j.jpowsour.2006.04.037](https://doi.org/10.1016/j.jpowsour.2006.04.037).
- [19] A. M. Gaikwad, G. L. Whiting, D. A. Steingart, and A. C. Arias, “Highly flexible, printed alkaline batteries based on mesh-embedded electrodes”, *Advanced Materials*, vol. 23, no. 29, pp. 3251–3255, 2011. DOI: [10.1002/adma.201100894](https://doi.org/10.1002/adma.201100894).

- [20] C. C. Ho, J. W. Evans, and P. K. Wright, “Direct write dispenser printing of a zinc microbattery with an ionic liquid gel electrolyte”, *Journal of Micromechanics and Microengineering*, vol. 20, no. 10, p. 104 009, Sep. 2010. DOI: [10.1088/0960-1317/20/10/104009](https://doi.org/10.1088/0960-1317/20/10/104009).
- [21] N. Guan, X. Dai, A. V. Babichev, F. H. Julien, and M. Tchernycheva, “Flexible inorganic light emitting diodes based on semiconductor nanowires”, *Chem. Sci.*, vol. 8, pp. 7904–7911, 12 2017. DOI: [10.1039/C7SC02573D](https://doi.org/10.1039/C7SC02573D).
- [22] P. A. Ersman, J. Kawahara, and M. Berggren, “Printed passive matrix addressed electrochromic displays”, *Organic Electronics*, vol. 14, no. 12, pp. 3371–3378, 2013, ISSN: 1566-1199. DOI: [10.1016/j.orgel.2013.10.008](https://doi.org/10.1016/j.orgel.2013.10.008).
- [23] D. K. Nguyen, Q.-V. Bach, J.-H. L. 3, and I.-T. Kim, “Synthesis and irreversible thermochromic sensor applications of manganese violet”, *Materials*, vol. 11, no. 9, p. 1693, 2018. DOI: [10.3390/ma11091693](https://doi.org/10.3390/ma11091693).
- [24] L. Liu, S. Peng, W. Wen, and P. Sheng, “Paperlike thermochromic display”, *Applied Physics Letters*, vol. 90, pp. 213 508–213 508, Jun. 2007. DOI: [10.1063/1.2742781](https://doi.org/10.1063/1.2742781).
- [25] A. C. Siegel, S. T. Phillips, B. J. Wiley, and G. M. Whitesides, “Thin, lightweight, foldable thermochromic displays on paper”, *Lab Chip*, vol. 9, pp. 2775–2781, 19 2009. DOI: [10.1039/B905832J](https://doi.org/10.1039/B905832J).
- [26] K. Itaya, K. Shibayama, H. Akahoshi, and S. Toshima, “Prussian-blue-modified electrodes: An application for a stable electrochromic display device”, *Journal of Applied Physics*, vol. 53, no. 1, pp. 804–805, 1982. DOI: [10.1063/1.329997](https://doi.org/10.1063/1.329997).
- [27] J. Kawahara, P. A. Ersman, I. Engquist, and M. Berggren, “Improving the color switch contrast in pedot:pss-based electrochromic displays”, *Organic Electronics*, vol. 13, no. 3, pp. 469–474, 2012, ISSN: 1566-1199. DOI: [10.1016/j.orgel.2011.12.007](https://doi.org/10.1016/j.orgel.2011.12.007).
- [28] D. Levasseur, I. Mjejri, T. Rolland, and A. Rougier, “Color tuning by oxide addition in pedot:pss-based electrochromic devices”, *Polymers*, vol. 11, no. 1, p. 179, 2019. DOI: [10.3390/polym11010179](https://doi.org/10.3390/polym11010179).
- [29] K. Myny, “The development of flexible integrated circuits based on thin-film transistors”, *Nature Electronics*, vol. 1, no. 1, pp. 30–39, 2018, ISSN: 2520-1131. DOI: [10.1038/s41928-017-0008-6](https://doi.org/10.1038/s41928-017-0008-6).
- [30] A. Tsumura, H. Koezuka, and T. Ando, “Macromolecular electronic device: Field-effect transistor with a polythiophene thin film”, *Applied Physics Letters*, vol. 49, no. 18, pp. 1210–1212, 1986. DOI: [10.1063/1.97417](https://doi.org/10.1063/1.97417).
- [31] A. F. Paterson, S. Singh, K. J. Fallon, T. Hodsdon, Y. Han, B. C. Schroeder, H. Bronstein, M. Heeney, I. McCulloch, and T. D. Anthopoulos, “Recent progress in high-mobility organic transistors: A reality check”, *Advanced Materials*, vol. 30, no. 36, p. 1 801 079, 2018. DOI: [10.1002/adma.201801079](https://doi.org/10.1002/adma.201801079).

- [32] M. Katsuhara, I. Yagi, A. Yumoto, M. Noda, N. Hirai, R. Yasuda, T. Moriwaki, S. Ushikura, A. Imaoka, T. Sasaoka, and K. Nomoto, “An flexible oled driven by otft backplane manufactured using a scalable process”, *Proc. of SPIE*, vol. 7417, Aug. 2009. DOI: [10.1117/12.828846](https://doi.org/10.1117/12.828846).
- [33] B. Crone, A. Dodabalapur, Y.-Y. Lin, R. W. Filas, Z. Bao, A. LaDuca, R. Sarpeshkar, H. E. Katz, and W. Li, “Large-scale complementary integrated circuits based on organic transistors”, *Nature*, vol. 403, no. 6769, pp. 521–523, 2000, ISSN: 1476-4687. DOI: [10.1038/35000530](https://doi.org/10.1038/35000530).
- [34] K. Myny, E. van Veenendaal, G. H. Gelinck, J. Genoe, W. Dehaene, and P. Heremans, “An 8-bit, 40-instructions-per-second organic microprocessor on plastic foil”, *IEEE Journal of Solid-State Circuits*, vol. 47, no. 1, pp. 284–291, Jan. 2012, ISSN: 0018-9200. DOI: [10.1109/JSSC.2011.2170635](https://doi.org/10.1109/JSSC.2011.2170635).
- [35] K. Myny, S. Smout, M. Rockelé, A. Bhoolokam, T. H. Ke, S. Steudel, B. Cobb, A. Gulati, F. G. Rodriguez, K. Obata, M. Marinkovic, D.-V. Pham, A. Hoppe, G. H. Gelinck, J. Genoe, W. Dehaene, and P. Heremans, “A thin-film microprocessor with inkjet print-programmable memory”, *Scientific Reports*, vol. 4, p. 7398, Dec. 2014, Article. DOI: [10.1038/srep07398](https://doi.org/10.1038/srep07398).
- [36] S. Kergoat, B. Piro, M. Berggren, G. Horowitz, and M.-C. Pham, “Advances in organic transistor-based biosensors: From organic electrochemical transistors to electrolyte-gated organic field-effect transistors”, *Analytical and Bioanalytical chemistry*, vol. 402, no. 5, pp. 1813–1826, 2012. DOI: [10.1007/s00216-011-5363-y](https://doi.org/10.1007/s00216-011-5363-y).
- [37] H. Sun, M. Vagin, S. Wang, X. Crispin, R. Forchheimer, M. Berggren, and S. Fabiano, “Complementary logic circuits based on high-performance n-type organic electrochemical transistors”, *Advanced Materials*, vol. 30, no. 9, p. 1704916, 2018. DOI: [10.1002/adma.201704916](https://doi.org/10.1002/adma.201704916).
- [38] S. Wachter, D. K. Polyushkin, O. Bethge, and T. Mueller, “A microprocessor based on a two-dimensional semiconductor”, *Nature Communications*, vol. 8, p. 14948, Apr. 2017. DOI: [10.1038/ncomms14948](https://doi.org/10.1038/ncomms14948).
- [39] S. Mandal, G. Dell’Erba, A. Luzio, S. G. Bucella, A. Perinot, A. Calloni, G. Berti, G. Bussetti, L. Duò, A. Facchetti, Y.-Y. Noh, and M. Caironi, “Fully-printed, all-polymer, bendable and highly transparent complementary logic circuits”, *Organic Electronics*, vol. 20, pp. 132–141, 2015, ISSN: 1566-1199. DOI: [10.1016/j.orgel.2015.02.006](https://doi.org/10.1016/j.orgel.2015.02.006).
- [40] E. Stucchi, G. Dell’Erba, P. Colpani, Y.-H. Kim, and M. Caironi, “Low-voltage, printed, all-polymer integrated circuits employing a low-leakage and high-yield polymer dielectric”, *Advanced Electronic Materials*, vol. 4, no. 12, p. 1800340, 2018. DOI: [10.1002/aelm.201800340](https://doi.org/10.1002/aelm.201800340).

# Datasheets

- [41] Thenergy. (2012). MEC202 Solid-State, Flexible, Rechargeable Thin-Film Micro-Energy Cell, [Online]. Available: <https://media.digikey.com/pdf/Data%20Sheets/Infinite%20Power%20Solutions%20PDFs/MEC202.pdf>. (accessed: 29.06.2019).
- [42] Blue Spark. (2012). UT Series Printed Batteries, [Online]. Available: [www.bluesparktechnologies.com/images/PDFs/Blue\\_Spark\\_UT\\_Series\\_Batteries\\_Jan\\_14\\_1.pdf](http://www.bluesparktechnologies.com/images/PDFs/Blue_Spark_UT_Series_Batteries_Jan_14_1.pdf). (accessed: 30.06.2019).
- [43] Enfucell. (). Technical specifications for SoftBattery<sup>®</sup>, [Online]. Available: [https://asiakas.kotisivukone.com/files/enfucell.kotisivukone.com/Dokumentit/Enfucell\\_SoftBattery\\_specifications\\_2019-05-15.pdf](https://asiakas.kotisivukone.com/files/enfucell.kotisivukone.com/Dokumentit/Enfucell_SoftBattery_specifications_2019-05-15.pdf). (accessed: 30.06.2019).
- [44] Linear Technology. (1998). LT1615/LT1615-1 - Micropower Step-Up DC/DC Converters in ThinSOT, [Online]. Available: <https://www.analog.com/media/en/technical-documentation/data-sheets/16151fas.pdf>. (accessed: 07.03.2019).
- [45] STMicroelectronics. (2017). TS391, TS391A - Low-power single voltage comparator, [Online]. Available: <https://www.st.com/resource/en/datasheet/cd00001660.pdf>. (accessed: 07.03.2019).
- [46] Texas Instruments. (2004). CMOS Hex Voltage-Level shifter for TTL-to-CMOS or CMOS-to-CMOS operation, [Online]. Available: <http://www.ti.com/lit/ds/symlink/cd4504b.pdf>. (accessed: 11.03.2019).
- [47] Cypress. (2018). PSoC<sup>®</sup> 4: PSoC 4200M Datasheet, [Online]. Available: <https://www.cypress.com/file/377971/download>. (accessed: 15.03.2019).
- [48] Chemtronics. (2018). CircuitWorks<sup>®</sup> Conductive Epoxy, [Online]. Available: [https://www.chemtronics.com/content/msds/TDS\\_CW2400.pdf](https://www.chemtronics.com/content/msds/TDS_CW2400.pdf). (accessed: 27.03.2019).
- [49] Texas Instruments. (2018). TLV7031 and TLV7041 Small Size, nanoPower, Low-Voltage Comparators, [Online]. Available: <http://www.ti.com/lit/ds/symlink/tlv7031.pdf>. (accessed: 27.03.2019).
- [50] Texas instruments. (2017). TPS61096A 28-V Output Voltage Boost Converter with Ultra-Low Quiescent Current, [Online]. Available: <http://www.ti.com/lit/ds/symlink/tps61096a.pdf>. (accessed: 27.03.2019).

- [51] Maxim Integrated. (2017). MAX17220 - MAX17225. 400mV to 5.5V Input, nanoPower Synchronous Boost Converter with True Shutdown, [Online]. Available: <https://datasheets.maximintegrated.com/en/ds/MAX17220-MAX17225.pdf>. (accessed: 27.03.2019).
- [52] Texas Instruments. (2017). SN74LVC2T45 Dual-Bit Dual-Supply Bus Transceiver With Configurable Voltage Translation, [Online]. Available: <http://www.ti.com/lit/ds/symlink/sn74lvc2t45.pdf>. (accessed: 27.03.2019).
- [53] Maxim Integrated. (2010). 256-Tap, Nonvolatile, I2C-Interface, Digital Potentiometers, [Online]. Available: <https://datasheets.maximintegrated.com/en/ds/MAX5417-MAX5419.pdf>. (accessed: 27.03.2019).
- [54] Microchip. (2009). 7-Bit Single I2C™ Digital POT with Volatile Memory in SC70, [Online]. Available: <http://ww1.microchip.com/downloads/en/devicedoc/22147a.pdf>. (accessed: 27.03.2019).
- [55] NXP. (2015). NT3H1101/NT3H1201 NTAG I2C - Energy harvesting NFC Forum Type 2 Tag with field detection pin and I2C interface, [Online]. Available: [https://www.mouser.com/ds/2/302/NT3H1101\\_1201-1127167.pdf](https://www.mouser.com/ds/2/302/NT3H1101_1201-1127167.pdf). (accessed: 27.03.2019).
- [56] RISE Acreo. (). Acreo Display: Driver's license, [Online]. Available: [https://www.acreo.se/sites/default/files/pub/acreo.se/EXPERTISE/printed-electronics/Acreo-Display/acreodisplay\\_driverslicense\\_1.7.pdf](https://www.acreo.se/sites/default/files/pub/acreo.se/EXPERTISE/printed-electronics/Acreo-Display/acreodisplay_driverslicense_1.7.pdf). (accessed: 03.06.2019).
- [57] STMicroelectronics. (2019). eDesign Antenna simulator, [Online]. Available: [https://my.st.com/analogsimulator/html\\_app/antenna/#/](https://my.st.com/analogsimulator/html_app/antenna/#/). (accessed: 22.05.2019).
- [58] Texas Instruments. (2014). RF430CL330H Practical Antenna Design Guide, [Online]. Available: <http://www.ti.com/lit/an/sloa197/sloa197.pdf>. (accessed: 22.05.2019).
- [59] NXP. (2016). AN11578. Energy Harvesting with the NTAG I2C and NTAG I2C *plus*, [Online]. Available: <https://www.nxp.com/docs/en/application-note/AN11578.pdf>. (accessed: 04.06.2019).
- [60] Creative Materials. (2016). Anisotropic conductive epoxy adhesive, [Online]. Available: [https://server.creativematerials.com/datasheets/DS\\_124\\_19.pdf](https://server.creativematerials.com/datasheets/DS_124_19.pdf). (accessed: 25.06.2019).
- [61] MG Chemicals. (2017). Silver Conductive Epoxy Adhesive, [Online]. Available: [http://www.farnell.com/datasheets/2547505.pdf?\\_ga=2.56567403.1740764972.1561461998-757106934.1561461998](http://www.farnell.com/datasheets/2547505.pdf?_ga=2.56567403.1740764972.1561461998-757106934.1561461998). (accessed: 25.06.2019).

## News and other online resources

- [62] American Semiconductors. (). FleX-ICs: Silicon-on-Polymer Products, [Online]. Available: <https://www.americansemi.com/flex-ics.html>. (accessed: 26.06.2019).
- [63] NextFlex. (2018). NextFlex Proves Manufacturability of Flexible Hybrid Electronics Process, Creating First Flexible Arduino System Ideal for Bringing New IoT/Sensor Products to Market Fruition, [Online]. Available: <https://www.nextflex.us/news-events/news/nextflex-proves-manufacturability-flexible-hybrid-electronics-process-creating-first-flexible-arduino-system-ideal-bringing-new-iot-sensor-products-market-fruition/>. (accessed: 24.06.2019).
- [64] Blue Spark Technologies. (2018). TempTraq Wearable Wireless Thermometer, [Online]. Available: <http://bluesparktechnologies.com/index.php/products-and-services/temptraq>. (accessed: 30.06.2019).
- [65] Digital Trends. (2017). Spyder's NFC-enabled ski jacket provides real-time snow reports and local trail maps, [Online]. Available: <https://www.digitaltrends.com/outdoors/spyder-nfc-ski-jacket/>. (accessed: 30.06.2019).
- [66] Vogue Business. (2019). Loomia's electronic jacket heats up the e-textile market, [Online]. Available: <https://www.voguebusiness.com/technology/loomia-heated-electronic-jacket-e-textiles>. (accessed: 30.06.2019).
- [67] Printed Electronics Now. (2018). ASI Launches World's First Smart Wine Bottle, [Online]. Available: [https://www.printedelectronicsnow.com/contents/view\\_breaking-news/2018-11-19/asi-launches-worlds-first-smart-wine-bottle/](https://www.printedelectronicsnow.com/contents/view_breaking-news/2018-11-19/asi-launches-worlds-first-smart-wine-bottle/). (accessed: 30.06.2019).
- [68] Organic and Printed Electronics Association. (2019). Take off with printed electronics - Interview with Airbus, [Online]. Available: <https://oe-a.org/viewer/-/v2article/render/29260873>. (accessed: 30.06.2019).
- [69] IDTechEx. (2018). Flexible, Printed and Thin Film Batteries 2019-2029 (sample pages), [Online]. Available: <https://www.idtechex.com/de/research-report/flexible-printed-and-thin-film-batteries-2019-2029/634>. (accessed: 29.06.2019).
- [70] Update Market Research Reports. (2018). ThermoChromic materials market: application, share, scope, manufacturing, analysis and forecasts 2025, [Online]. Available: <http://update-market-research.over-blog.com/2018/09/>

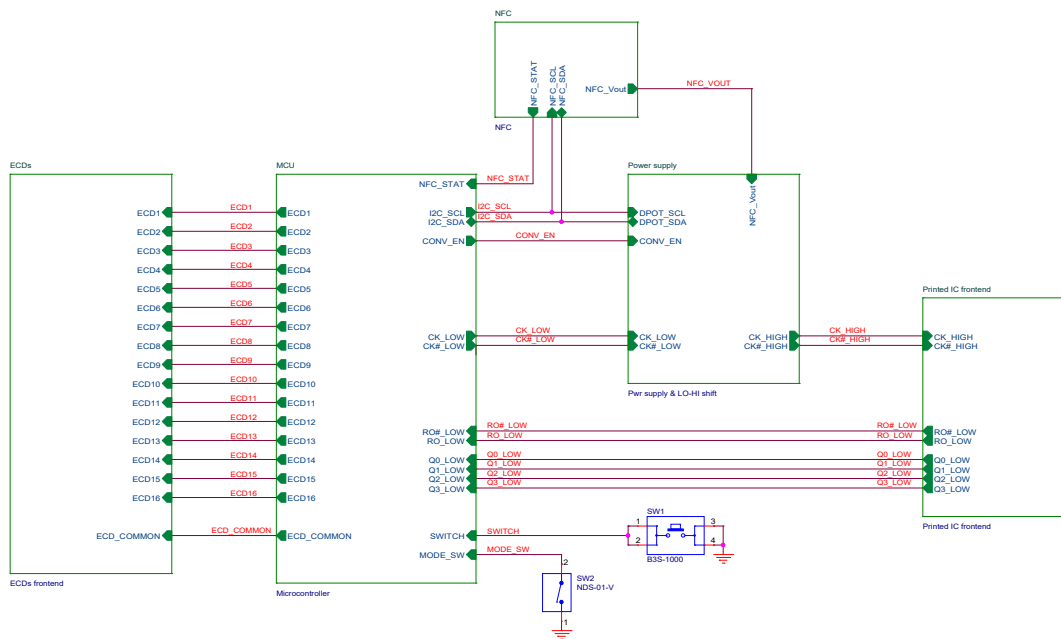
[thermochromic-materials-market-application-share-scope-manufacturing-analysis-and-forecasts-2025.html](#). (accessed: 27.06.2019).

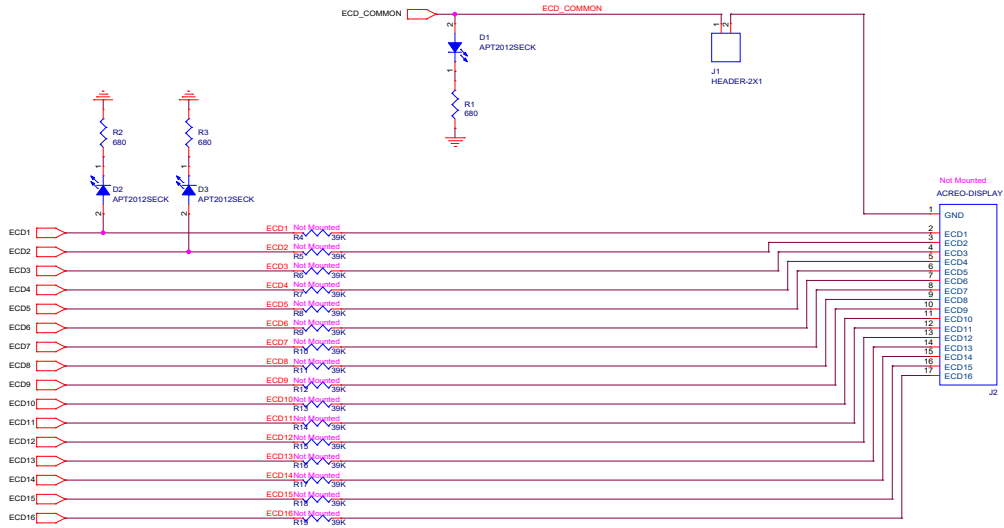
- [71] ThinFilm. (2014). Affordable scaling of Sensor Manufacturing with Printed Electronics, [Online]. Available: <https://www.thinfilmnfc.com/wp-content/uploads/2014/09/Thinfilm-Tsensors-Munich-presentation.pdf>. (accessed: 01.07.2019).

## Appendix A

### NFF main schematic

The schematic of the rigid non-form factor main board (without including the fixture board), which was developed by the author during his internship at Flex. This schematic is described in chapter 4.

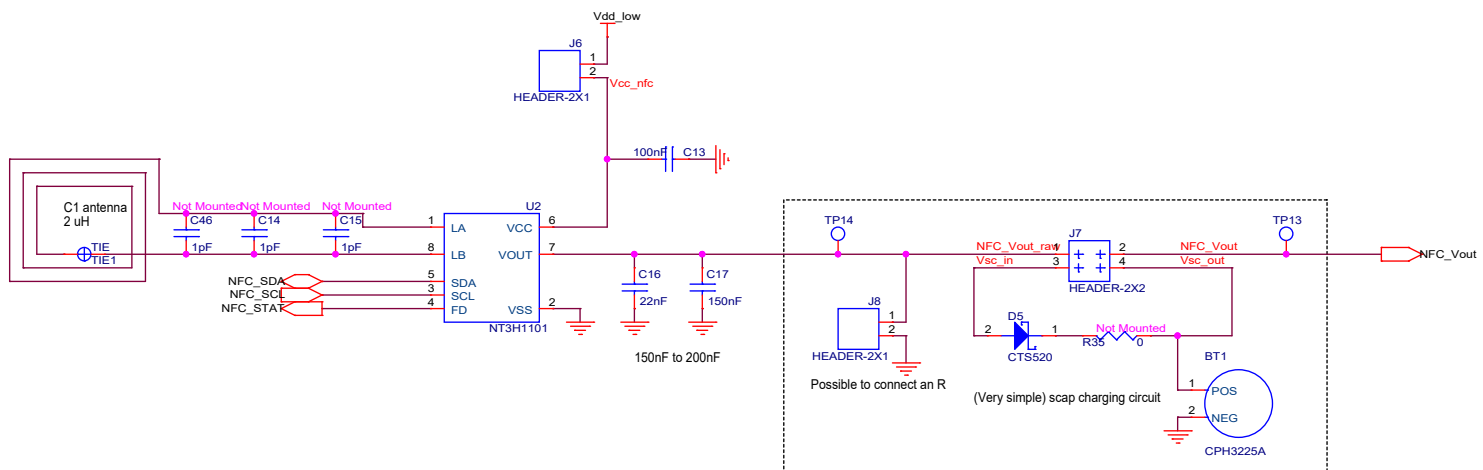




The resistors can be changed according to the results of the ECD tests. These values guarantee a current of max 75uA per each ECD @ 3V

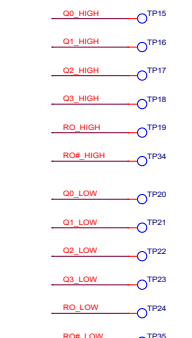
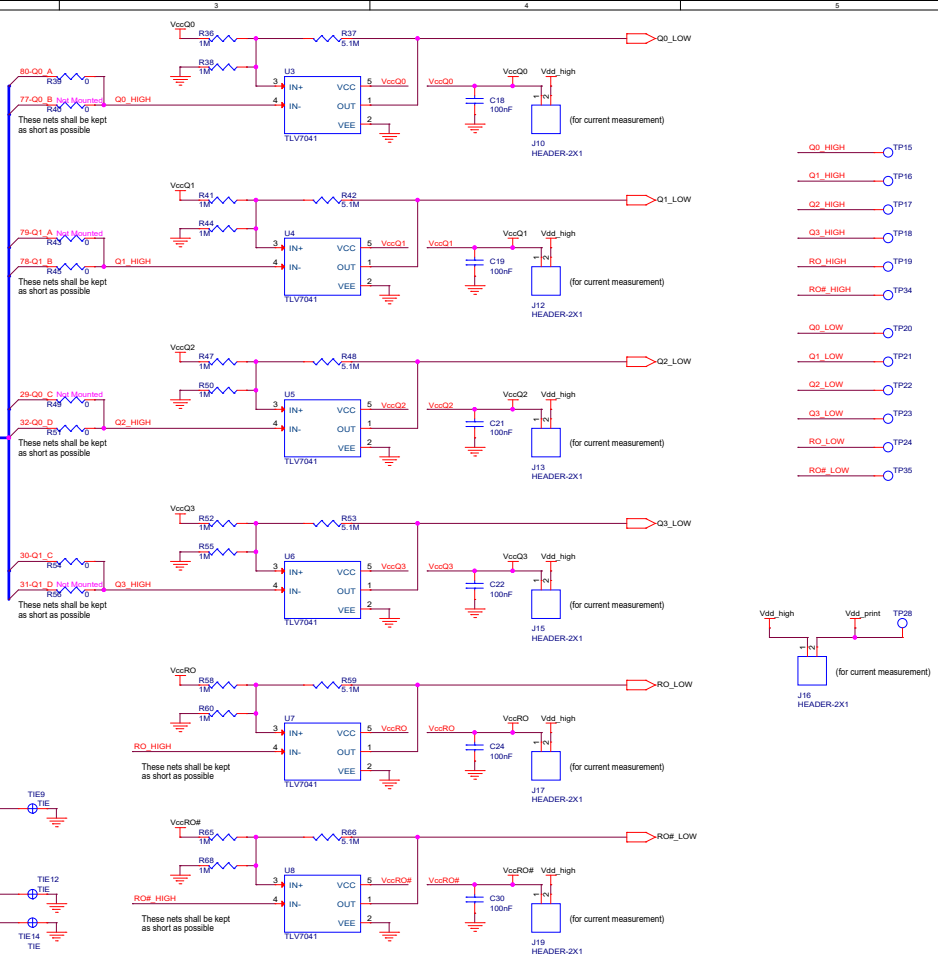
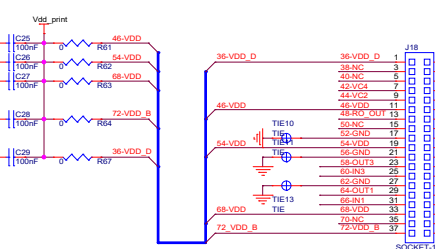
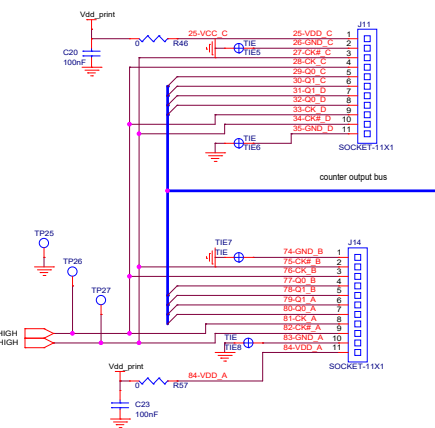
<b>flex</b>		Design Title: <b>Smart Data Label Demo</b>	
Via E. Breda, 176 20126 - Milano (MI) ITALY		Page Title: <b>ECDs frontend</b>	
Author: <b>Artel Seisdedos</b>	Approved by: <b>&lt;Approved&gt;</b>		Rev: <b>A01</b>
Size: <b>A3</b>	Doc. Number: <b>&lt;DocNumber&gt;</b>	Date: <b>Friday, January 18, 2019</b>	Sheet <b>3</b> of <b>7</b>



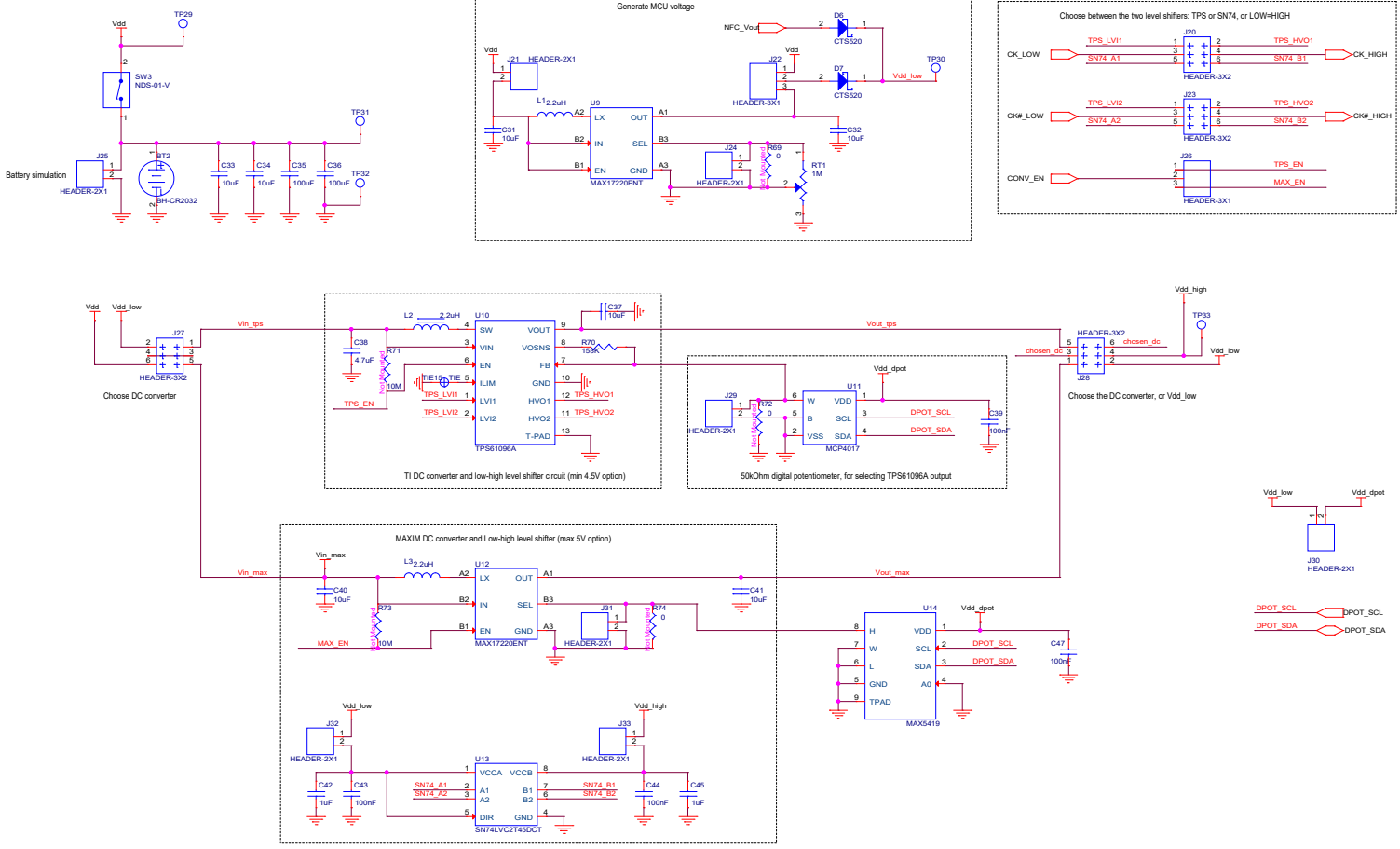


 Via E. Breda, 176 20126 - Milano (MI) ITALY	Design Title <b>Smart Data Label</b>	
	Page Title <b>NFC NXP</b>	
	Author: <b>Ariel Seisdedos</b>	Approved by: <b>&lt;Approved&gt;</b>
	Size: <b>A4</b>	Doc. Number: <b>&lt;DocNumber&gt;</b>
	Date: <b>Friday, January 18, 2019</b>	Rev: <b>&lt;RevC&gt;</b>
		Sheet <b>5</b> of <b>7</b>

[REMINDER] 4 2-bit counters part: PPS00041545-100



<p>Via E. Breda, 176 20126 - Milano (MI) ITALY</p>	<p>Design Title: <b>Smart Data Label Demo</b></p>
	<p>Page Title: <b>Printed IC frontend</b></p>
	<p>Author: <b>Arnel Seisdedos</b>   Approved by: <b>&lt;Approved&gt;</b></p>
	<p>Size: <b>A3</b>   Doc. Number: <b>&lt;DocNumber&gt;</b>   Rev: <b>A01</b></p>
<p>Date: <b>Friday, January 18, 2019</b>   Sheet <b>6</b> of <b>7</b></p>	

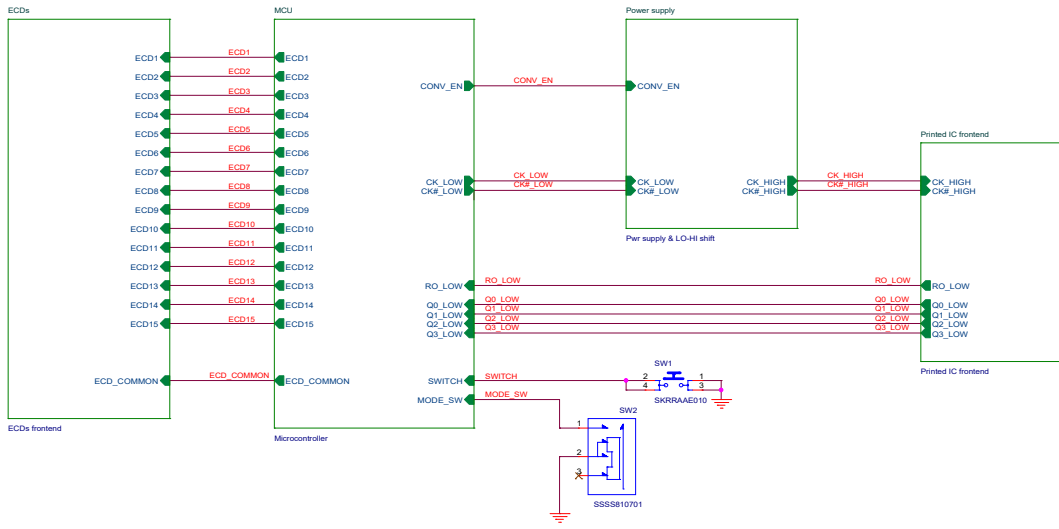


<b>flex</b>		Design Title: <b>Smart Data Label Demo</b>	
Via E. Breda, 176 20126 - Milano (MI) ITALY		Page Title: <b>Power supply and LO-HI level shifting</b>	
Author: <b>Ariel Seisdedos</b>	Doc. Number: <b>&lt;DocNumber&gt;</b>	Approved by: <b>&lt;Approved&gt;</b>	Rev: <b>A01</b>
Date: <b>Friday, January 18, 2019</b>	Sheet: <b>7</b>	of: <b>7</b>	

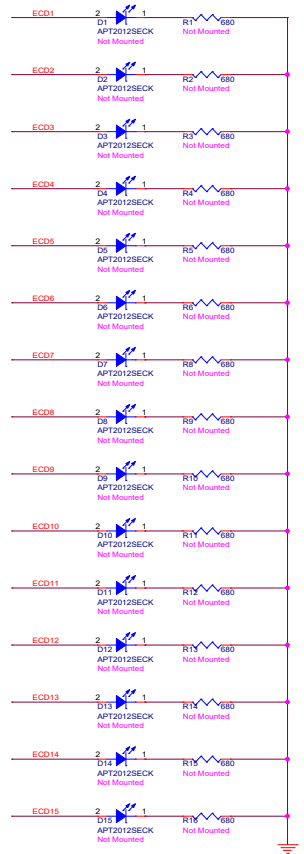
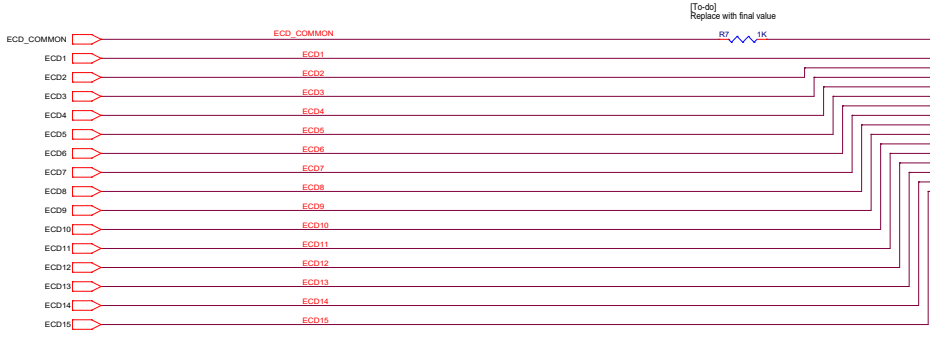
## Appendix B

### FPC schematic

The schematic of the flexible board, which was developed by the author during his internship at Flex. This schematic is described in chapter 6.

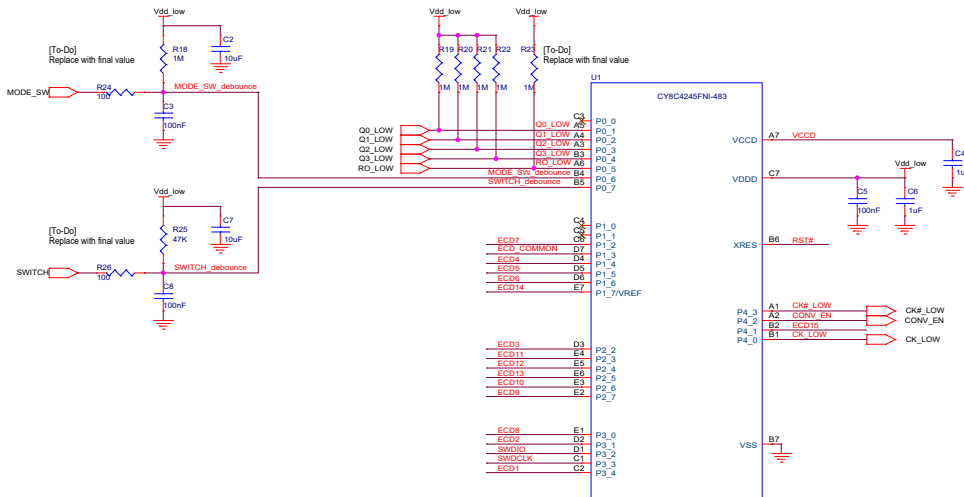
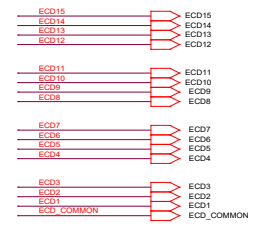
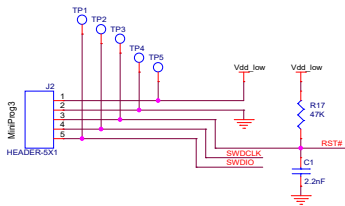


		Design Title: <b>Smart Data Label Demo</b>	
		Page Title: <b>High level connections</b>	
Via E. Breda, 176 20126 - Milano (MI) ITALY		Author: <b>Arnel Alvarado</b>	Approved by: <b>&lt;Approved&gt;</b>
Size: <b>A3</b>	Doc. Number: <b>&lt;DocNumber&gt;</b>	Rev: <b>A01</b>	
Date: <b>Thursday, May 02, 2019</b>	Sheet <b>2</b> of <b>6</b>		



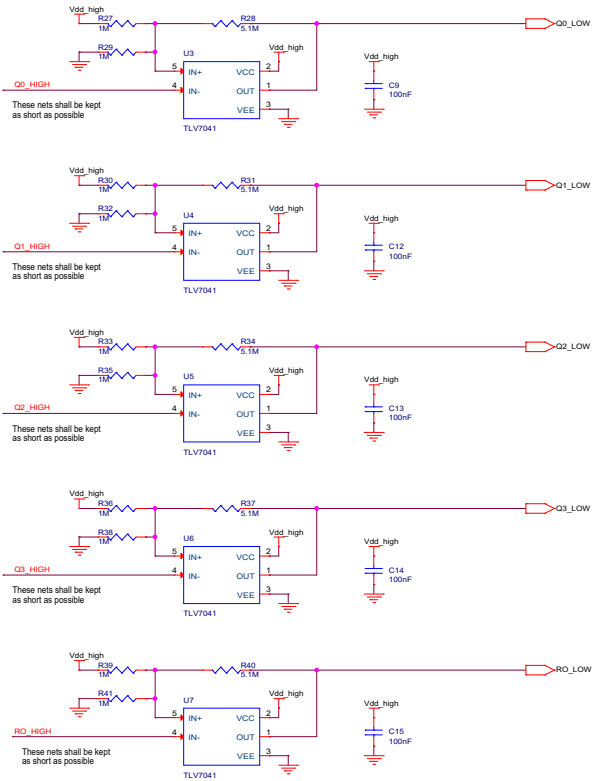
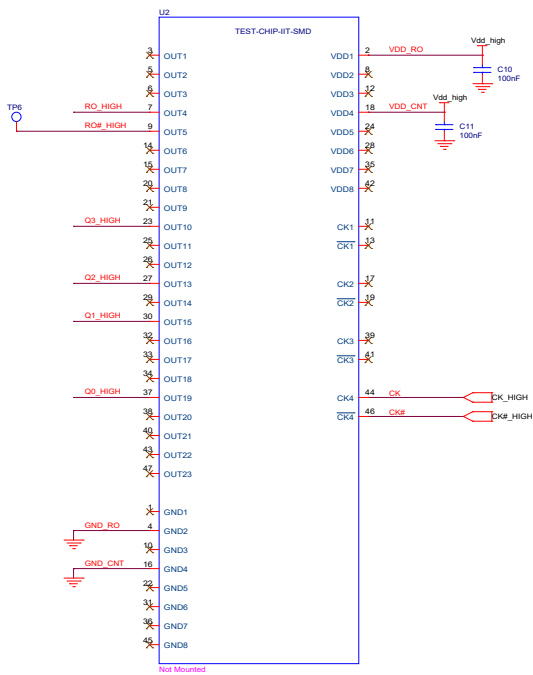
		Design Title: <b>Smart Data Label Demo</b>	
		Page Title: <b>ECDs frontend</b>	
Author: <b>Arnel Alvarado</b>		Approved by: <b>&lt;Approved&gt;</b>	
Size: <b>A3</b>	Doc. Number: <b>&lt;DocNumber&gt;</b>	Rev: <b>A01</b>	
Date: <b>Monday, April 29, 2019</b>		Sheet: <b>3</b>	of <b>6</b>

These testpoints need to be spaced at the SAME pitch as the header (2.54mm).  
They're going to be used for reprogramming the MCU after the header is unsoldered

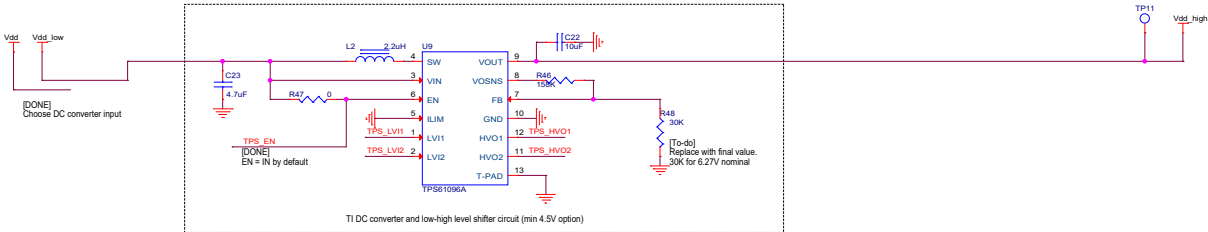
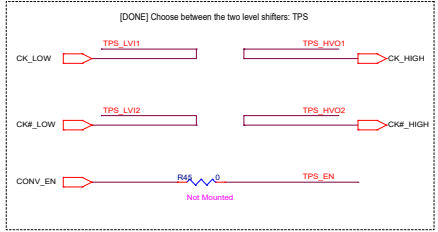
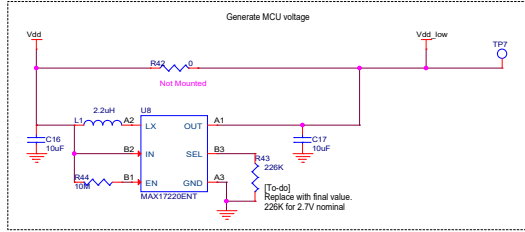
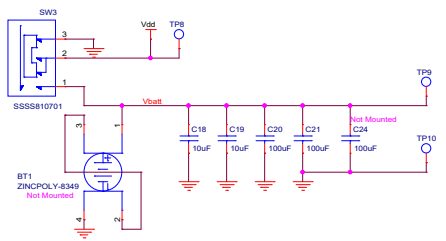


The signal pins can be changed in order to simplify the routing process.  
The rules are:  
- Maintain SWDIO and SWDCK at P3\_2 and P3\_3 respectively.  
- Don't connect anything at pins: C3 (P0\_0), C4 (P1\_0), C5 (P1\_1).  
- Don't connect the MODE switch, the EVENT switch, nor the RO\_LOW signals at port 4 or higher.  
Also, preferably (but not mandatory).  
- The Q signals should be consecutive pins belonging to the same port.

Design Title: <b>Smart Data Label Demo</b>	
Page Title: <b>Microcontroller</b>	Approved by: <b>&lt;Approved&gt;</b>
Author: <b>Artel Alvarado</b>	Rev: <b>A01</b>
Size: <b>A3</b>	Doc. Number: <b>&lt;DocNumber&gt;</b>
Date: <b>Monday, April 29, 2019</b>	Sheet <b>4</b> of <b>6</b>



		Design Title: <b>Smart Data Label Demo</b>	
		Page Title: <b>Printed IC frontend</b>	
Author: <b>Arlei Alvarado</b>	Approved by: <b>&lt;Approved&gt;</b>		Rev: <b>A01</b>
Size: <b>A3</b>	Doc. Number: <b>&lt;DocNumber&gt;</b>		Date: <b>Monday, April 29, 2019</b>
Sheet <b>5</b> of <b>6</b>			



Design Title: <b>Smart Data Label Demo</b>	
Page Title: <b>Power supply and LO-HI level shifting</b>	Approved by: <Approved>
Author: <b>Arnel Alvarado</b>	Rev: <b>A01</b>
Size: <b>A3</b>	Doc. Number: <DocNumber>
Date: <b>Monday, April 29, 2019</b>	Sheet <b>6</b> of <b>6</b>

# Index

## Companies

American Semiconductors, 4, 7  
Analog Devices, 21  
Blue Spark, 7, 11  
BrightVolt, 11  
Chemtronics, 24  
Creative Materials, 63  
Cypress, 24, 30  
Digikey, 35  
Duracell, 13  
Enfucell, 11  
Fleep Technologies, 17  
Flex Milan, ii, 21  
FlexEnable, 17  
GoToTags, 52  
Imprint Energy, ii, 54, 55  
LG, 53  
Linear Technology, 21

LionRock, 9  
Loomia, 7  
Maxim Integrated, 30, 33  
MG Chemicals, 63  
Microchip, 33  
NXP, 33, 53  
PragmatIC, 17  
Preionic Technologies, 15  
rdot, 15  
RICOH, 15  
RISE Acreo, ii, 15, 40  
Siemens, 15  
STMicroelectronics, 23, 51  
Texas Instruments, 23, 29, 30  
Thinergy, 11  
ThinFilm, 17  
Ynvisible, 7, 15, 40